UC Berkeley
UC Berkeley Electronic Theses and Dissertations

Title
Neural Effects of Beta Amyloid in Normal Aging

Permalink
https://escholarship.org/uc/item/7gz2v2w6

Author
Mormino, Elizabeth Charlotte

Publication Date
2011

Peer reviewed|Thesis/dissertation

eScholarship.org Powered by the California Digital Library
University of California

Neural Effects of Beta Amyloid in Normal Aging

By

Elizabeth Charlotte Mormino

A dissertation submitted in partial satisfaction of the

requirements for the degree of

Doctor of Philosophy

in

Neuroscience

in the

Graduate Division

of the

University of California, Berkeley

Committee in charge:

Professor William J. Jagust, Chair
Professor Mark D'Esposito
Professor William A. Satariano
Professor Arthur P. Shimamura

Spring 2011

Neural Effects of Beta Amyloid in Normal Aging

Copyright 2011

By

Elizabeth Charlotte Mormino

Abstract

Neural Effects of Beta Amyloid in Normal Aging

By

Elizabeth Charlotte Mormino

Doctor of Philosophy in Neuroscience

University of California, Berkeley

Professor William J. Jagust, Chair

In this dissertation, I examine neural effects of beta-amyloid (Aβ) deposition, a primary pathological feature of Alzheimer's disease (AD), that also appears in cognitively "normal" elderly controls. This work represents a conjunction between the fields of AD research and the cognitive neuroscience of aging. Whereas the former strives to understand early disease mechanisms and potential treatment approaches, the latter aims to characterize neural changes in the aged brain and corresponding effects on cognition. Despite their differences, these fields are interconnected by the fact that Aβ pathology is very common amongst "normal" aged individuals. Therefore, an understanding of the effects of Aβ in aging has important implications for uncovering disease processes, and for providing biological mechanisms for neural changes observed in studies of aging.

The research herein employs a multimodal approach to investigating Aβ in aging. Throughout the experiments, particular emphasis was placed on brain regions subserving episodic memory (EM)—this domain is the first compromised in AD and shows decline in normal aging, therefore it was hypothesized that the earliest effects of Aβ would relate to this cognitive domain. Specifically, PET imaging with 'Pittsburgh Compound-B' (PIB) was used to assess Aβ burden, magnetic resonance imaging was used to assess brain structure (hippocampus volume) and function (functional connectivity during rest and activation during EM encoding), and neuropsychological testing was used to assess cognitive function.

In the first experiment, I provide support for a sequential relationship between Aβ burden, hippocampus volume and EM in stages preceding dementia. This model is consistent with a cascade model of AD, such that Aβ deposition is an early event that initiates downstream neuronal atrophy, which in turn leads to cognitive decline. In the second experiment, I show that brain functional connectivity in the EM subcomponent of the DMN is reduced, whereas functional connectivity in non-EM regions of the DMN is increased in NCs with high Aβ burden. Finally, in experiment 3 I show that NCs with high Aβ burden have increased task-related activation during successful EM encoding. Importantly, these activations were related to better overall memory performance,

suggesting that these increases reflect a beneficial process to elderly individuals with high Aβ burden.

Overall, these experiments support a biological relevance of Aβ in aging. Specifically, these results suggest that Aβ is related to early signs of dysfunction in regions subserving EM. However, it is also shown that NCs with high Aβ burden display a capacity for neuronal compensation in the face of this pathology. Taken together, these results suggest that although Aβ likely reflects the beginning stages of AD development, compensatory mechanisms exists that may enable individuals to cope with this pathology, or at least prolong the period between initial deposition and impending cognitive decline.

Table of Contents

Acknowledgements ..... **iii**

1. Introduction **1**

1.1 General background 1

1.2 Measurements of beta amyloid 2

1.3 Beta amyloid in cognitively normal elderly individuals 3

2. Episodic memory loss is related to hippocampal-mediated beta amyloid deposition in elderly subjects **6**

2.1 Introduction 7

2.2 Methods 8

2.3 Results 13

2.4 Discussion 21

3. Relationships between beta amyloid and functional connectivity in different components of the default mode network in aging **26**

3.1 Introduction 27

3.2 Methods 28

3.3 Results 32

3.4 Discussion 36

4. Beta amyloid deposition in aging is associated with beneficial increases in brain activation during successful memory encoding 41

4.1 Introduction 42

4.2 Methods 44

4.3 Results 48

4.4 Discussion 61

5. Concluding remarks 65

5.1 Summary 65

5.2 Personal opinion 66

5.3 Future directions 66

6. Appendices 68

6.1 Appendix A: chapter 3 supplemental materials 68

6.2 Appendix B: PIB+ classification based on young data 76

7. References 93

Acknowledgements

First and foremost, I would like to thank my advisor Bill Jagust. From the beginning I have felt fortunate to be in his lab, and that feeling has only strengthened over time. Throughout the years, Bill has continuously motivated me in all aspects of my work. He is an ideal role model, a great scientist and a good person. In addition to the support and criticism that have been essential to this process, Bill has shown patience and kindness towards me during a stage in my life that at times was very daunting. I know that the bond I share with Bill will stay with me throughout my life, and I am grateful to have that gift. It saddens me to leave, but am comforted to know our interactions will continue.

The Helen Wills Neuroscience Institute has been an amazing place to learn and perform research. The intelligence of those around me has been humbling, and I feel honored to be apart of this community. In particular I would like to thank my thesis committee members, Mark D'Esposito, Bill Satariano and Art Shimamura, for their time and all that I have learned from them. I would also like to thank Kati Markowitz for watching out for me.

During graduate school I have had the pleasure to work aside a number of gifted colleagues. In particular I would like to acknowledge Suzanne Baker, Beth Kuczynski, Susan Landau, Cindee Madison and Gil Rabinovici. I have greatly benefited from the scientific thoughts we have exchanged, the guidance they have given me, and the friendship that we share.

Old people! I am clearly indebted to the Berkeley Aging Cohort volunteers, to whom allowed me to peer inside their brains with grace and good humor (for the most part). In addition to their time, they often imparted great advice during our interactions, and I am thankful for the opportunity to have worked with these inspirational individuals.

I would like to thank my family—they have greatly impacted my life both before and during graduate school. My mother for sacrificing her own career to take care of me, my father for his strong work ethic, and my sisters Amy and Julie for all the memories and all the memories to come.

I am so lucky to have meet wonderful friends during this time, they have been incredibly supportive and essential to my happiness. Thank you Matar Davis, Adeen Flinker, Amy Gitcho, Libby O'Hare, Amynta Hayenga, Shawn Marks, Henry Schwimmer, Lavi Secundo, Amitai Shenhav and Kirstie Whitaker. And of course, all my summer softball teammates (go Animals!).

And lastly, a very special thank you to my squash partner Charles Cadieu.

Chapter 1

Introduction

1.1 General background

Molecular basis of beta amyloid

The beta-amyloid (Aβ) peptide forms after cleavage of the transmembrane amyloid precursor protein (APP) by β- and γ-secretases. Depending on this cleavage, resulting peptides are 38, 40 or 42 amino acids in length, with $A\beta_{42}$ the most likely to undergo subsequent aggregation. Resulting peptides oligomerize to form different species which are collectively referred to as soluble Aβ. Soluble Aβ oligomers form fibrils, which are the main component of beta-amyloid plaques. There are two main stages of Aβ plaques: diffuse (diffuse deposits lacking dystrophic neurites) and neuritic (dense core surrounded by microglia and dystrophic neurites). Fibrillar forms of Aβ are mainly found in neuritic plaques, but can also be seen in diffuse plaques.

The production of the Aβ peptide occurs under normal circumstances in neuronal and non-neuronal cells throughout life, suggesting this peptide has a normal function or is a normal intermediate step in APP catabolism (Selkoe, 1994). Although the normal function is not established, it is known that Aβ disrupts LTP (Bredesen, 2009; Walsh et al., 2002), decreases synaptic number (Shankar et al., 2007), and shows activity dependent release (Cirrito et al., 2005). Given the fact that Aβ production per se is a normal phenomenon, it is likely that negative consequences of this peptide in the context of Alzheimer's disease are due to abnormal accumulation (via heightened production, insufficient clearance, etc).

The amyloid hypothesis of Alzheimer's disease

Alzheimer's disease (AD) is a progressive neurodegenerative disorder found in ~10% of individuals over age 65 and ~40% of individuals over age 85. AD typically begins with episodic memory impairment, and slowly affects other cognitive domains as the disease progresses. An association between Aβ and AD was first observed by Dr. Alois Alzheimer in postmortem tissue from his patient Auguste D. more than 100 years ago (Alzheimer, 1907). However, evidence for a direct relationship between Aβ and AD has emerged more recently across research spanning multiple fields (Walsh and Selkoe, 2007). For instance, autosomal dominant genetic variants that cause early onset AD involve mutations affecting APP directly or its cleavage (mutations within or near the Aβ portion of APP (Citron et al., 1992); mutations in the catalytic site of γ-secretase (Bentahir et al., 2006); etc), ultimately resulting in an increased production of $A\beta_{42}$ in these mutation carriers. Down syndrome individuals have an extra copy of chromosome 21, the locus of the APP gene, produce high amounts of Aβ and have increased risk of developing AD (Lott et al., 2006). Experimental work in mice has shown a relationship between Aβ and memory that is reversed after passive immunization with an Aβ antibody (Dodart et al., 2002). As stated above, soluble Aβ reduces synaptic strength and number in rodent models

(Shankar et al., 2007; Walsh et al., 2002), consistent with the observation that neurons from AD patients have 15-35% fewer synapses than nondemented controls (Davies et al., 1987). Overall, these observations are consistent with a central role of the Aβ peptide in AD pathogenesis and progression (Hardy and Selkoe, 2002). Furthemore, these findings suggest that forms of Aβ preceding plaque deposition (ie. soluble Aβ oligomers) may be the direct substrate of impairment during the initial stages of AD development by affecting synaptic function.

1.2 Measurements of beta amyloid

Postmortem quantification of Aβ plaques

Aβ plaques have traditionally been studied during postmortem analysis of brain tissue using stains such as thioflavin-T, congo red, and Bielschowsky. Protocols have been developed to characterize plaques based on these staining procedures, and are currently used in the diagnosis of AD (Mirra et al., 1991). By examining the frequency of samples showing deposition across brain regions, postmortem work has suggested stages of Aβ deposition that begins in neocortical heteromodal regions, followed by limbic regions and unimodal sensory cortices, with subcortical structures affected last (Braak and Braak, 1991; Thal et al., 2002).

Although postmortem analysis has expanded our understanding of Aβ, there are many methodological constraints inherent in this approach. Obviously, postmortem confirmation of AD is a sub-optimal diagnostic tool. Furthermore, an accurate assessment of total pathological burden is difficult to attain since sampling is limited to discrete areas of brain tissue. Additionally, there is potentially a large time delay between premortem assessment and brain acquisition, obscuring correlations between pathology and in vivo measures (such as cognition and measures of neuronal integrity via structural and functional neuroimaging). For these reasons, researchers have made extensive efforts towards the development of an in vivo marker of brain Aβ deposition (Klunk et al., 2004).

In vivo quantification of Aβ plaques

The recent development of [^{11}C]PIB ('Pittsburgh Compound-B'), a positron emission tomography (PET) radiotracer, enables in vivo investigation of Aβ plaques (by binding to the fibrillar component of Aβ plaques (Ikonomovic et al., 2008)). Since the initial study investigating tracer uptake in AD (Klunk et al., 2004), this approach to amyloid imaging has been applied to various patient populations, such as mild cognitive impairment (Okello et al., 2009; Wolk et al., 2009), frontotemporal dementia (Rabinovici et al., 2007), primary progressive aphasia (Rabinovici et al., 2008), as well as Parkinson's disease and dementia with lewy bodies (Foster et al., 2010). The presence and pattern of PIB uptake is consistent with postmortem patient studies (Fripp et al., 2008). The consistency of inter-lab findings has increased validation of PIB-PET imaging as a reliable marker of Aβ burden with obvious clinical applications.

The specificity of this tracer for Aβ plaques has also been investigated in subjects that have undergone premortem imaging and postmortem examination. These studies have revealed that PIB readily detects high levels of neuritic Aβ plaques (Bacskai et al., 2007; Ikonomovic et al., 2008). Interestingly, recent data suggests that even low levels of

neuritic Aβ plaques may be detectable by PIB-PET imaging (Sojkova et al., 2011). Detection of sub-AD plaque quantities has important implications for understanding the time course of Aβ deposition.

1.3 Beta amyloid in cognitively normal elderly individuals

Prevalence

Although beta amyloid (Aβ) plaques are a central etiology of AD, this pathology is commonly observed in the brains of normal control (NC) individuals. This observation has consistently been observed in postmortem studies (Bennett et al., 2006; Davis et al., 1999; Hulette et al., 1998; Knopman et al., 2003; Kok et al., 2009; Price and Morris, 1999; Savva et al., 2009; Tomlinson et al., 1968), and replicated with PIB-PET imaging (Rabinovici and Jagust, 2009). As depicted in figure 1 below, there is a strong relationship between age and the percentage of NCs with an Aβ burden comparable to AD patients (around 40% of individuals in their 80's). In addition to these NC subjects with AD-like Aβ burden, a significant number of NC have evidence for slightly elevated quantities of Aβ (Bennett et al., 2006; Kok et al., 2009; Sojkova et al., 2011). Although the age at which Aβ plaque deposition begins is unknown, it is most likely minuscule before age 50 (Braak and Del Tredici, 2011; Kok et al., 2009).

Figure 1: NCs with AD-like Aβ burden

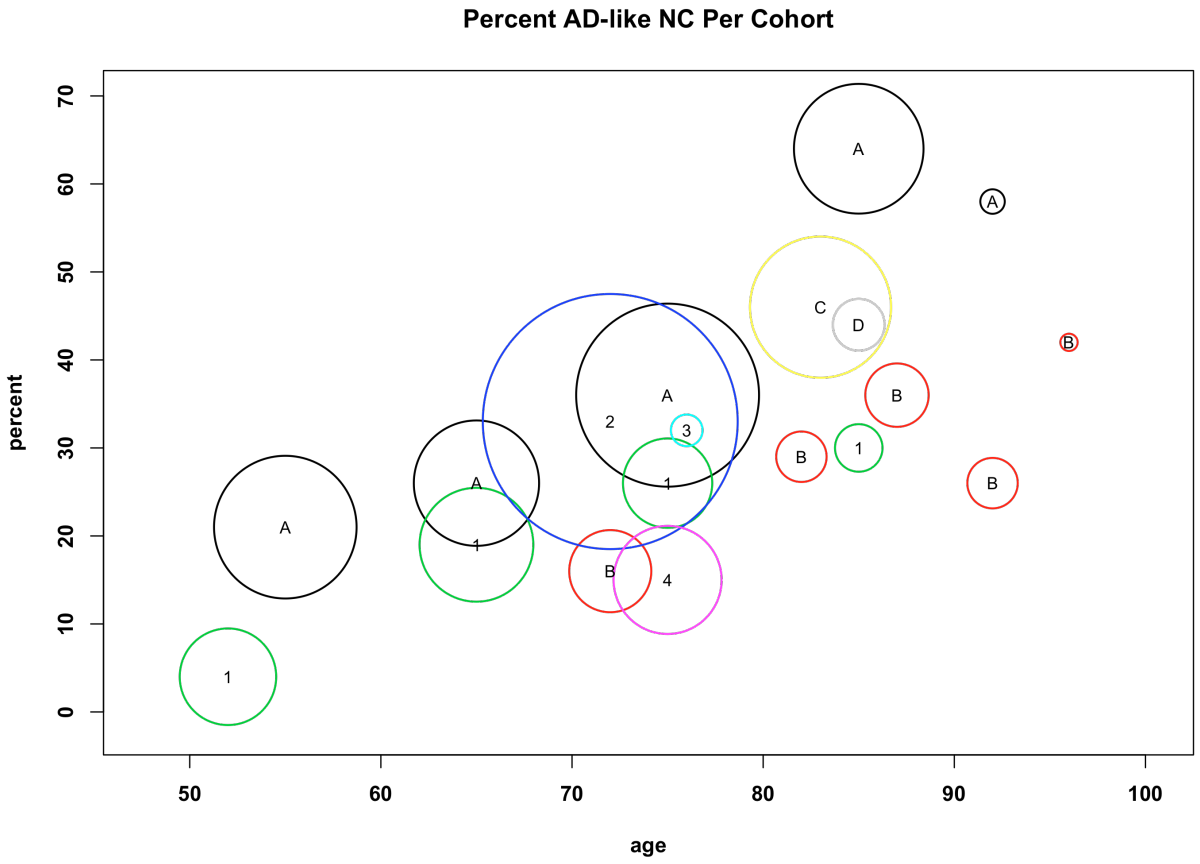

Figure 1: Percent of NC subjects with AD-like Aβ quantities across a subset of postmortem and PIB-PET imaging studies. Mean cohort age is on the x-axis, and the percent of NC subjects with AD-like levels of Aβ is on the y-axis (defined by the concordance of Aβ levels between NC and AD subjects within each particular cohort). Although measurements of Aβ vary across studies, a clear pattern of increased Aβ burden and age is obvious. Studies reporting information separately for different age groups are depicted by multiple bubbles of the same color. Postmortem studies are indicated with letters (A-D) while PIB imaging studies are indicated with numbers (1-4), and bubble size is scaled by the number of individuals comprising each group (range=12-177 NC subjects). A= Tampere Autopsy Study (Kok *et al.*, 2009), B= Medical Research Council Cognitive Function & Ageing Study (Savva *et al.*, 2009), C=Religious Orders Study (Bennett *et al.*, 2006), D=Memory and Aging Project (Bennett *et al.*, 2006), 1=Washington University (Morris et al., 2010), 2=Australian Imaging, Biomarkers and Lifestyle Study of Aging (Rowe et al., 2010), 3=Massachusetts General Hospital (Sperling et al., 2009), 4=Berkeley Aging Cohort Study.

Relevance of Aβ in cognitively normal elderly individuals

It is possible that the presence of this pathology in NCs reflects the earliest stage in AD development, with suspicion of a 10-year delay between initial Aβ deposition and dementia onset. Furthermore, episodic memory (EM) deficits are common in aging (Small et al., 1999), a cognitive domain that is greatly impaired in AD and has been associated with conversion to AD (Grober et al., 2008; Small et al., 2000). In addition to subtle cognitive decline, brain regions implicated in episodic memory processing are compromised in aging. For instance, the hippocampus, which is essential for episodic memory processing (Eichenbaum et al., 2007), atrophies at a rate of 1.7% per year in individuals over age 60 (Raz and Rodrigue, 2006), and predicts AD conversion (Apostolova et al., 2006; de Leon et al., 1996; Jack et al., 1999; Smith et al., 2007). Thus, it is likely that subtle episodic memory-related changes commonly observed in aging are related to underlying Aβ pathology. Therefore, understanding the impact of this pathology in NCs before widespread and profound AD-typical neuronal dysfunction has occurred is of utmost importance to clarify underlying neural effects of Aβ.

Relationships between Aβ burden and cognition

Postmortem work that has focused on the relevance of Aβ in NCs has been inconclusive, with some studies finding an association between subtle antemortem cognitive deficits and others not (Goldman et al., 2001; Hulette *et al.*, 1998; Katzman et al., 1988; Schmitt et al., 2000). It is possible that these inconsistencies are due to the aforementioned methodological constraints inherent in postmortem analyses—these relationships have therefore been heavily interrogated with the advent of in vivo Aβ imaging in NCs (*I address the relationship between Aβ burden and cognition in chapter 2 of the dissertation*).

Downstream neural effects of Aβ

A complication in establishing the relevance of Aβ in NCs is that relationships between Aβ and cognition are likely indirect and separated temporally. This cascade model of AD implies that a relationship between Aβ pathology and cognition is weak or even non-existent in NCs (Jack et al., 2010a). Consistent with this model, it is probable that neuronal intermediates reside between aberrant Aβ accumulation and resulting cognitive deficits, such as synaptic dysfunction and loss (ie. Aβ accumulation→neuronal

dysfunction→cognitive decline; this sequence of events may occur over many years). Therefore, a relationship between Aβ burden and markers of neuronal dysfunction should be present relatively early, but relationships between Aβ burden and cognition should be weak or null in NCs (*I address relationships between Aβ burden and markers of neuronal dysfunction in chapters 1 and 2 of the dissertation*).

Neuronal compensation

Lastly, factors may exist that dampen the detrimental impact of Aβ. These factors have been described as cognitive reserve processes (Stern, 2006). This theory posits that for a given level of pathological burden, an individual with high cognitive reserve will cope more optimally than an individual with low cognitive reserve. Increased brain activation during cognitive tasks may reflect cognitive reserve processes ("neuronal compensation"). Evidence for neuronal compensation has been observed in the context of aging (Cabeza et al., 2002; Park and Reuter-Lorenz, 2009; Rosen et al., 2002) and individuals at risk for developing AD (Bookheimer et al., 2000; Dickerson et al., 2005), but has not been directly related to Aβ burden in NC subjects (*I investigate evidence for neuronal compensation in high Aβ NCs in chapters 2 and 3 of the dissertation*).

Chapter 2

Episodic memory loss is related to hippocampal-mediated beta amyloid deposition in elderly subjects

Abstract

Although beta-amyloid (Aβ) plaques are a primary diagnostic criterion for Alzheimer's disease (AD), this pathology is commonly observed in the brains of nondemented older individuals. To explore the importance of this pathology in the absence of dementia, we compared levels of amyloid deposition [via 'Pittsburgh Compound-B' (PIB) positron emission tomography (PET) imaging] to established markers of AD, specifically hippocampus volume (HV) and episodic memory (EM). These comparisons were examined in 3 nondemented groups: 1) normal controls from the Berkeley Aging Cohort (BAC NC, n=20); 2) normal controls from the Alzheimer's Disease Neuroimaging Initiative (ADNI NC, n=17); and 3) PIB+ mild cognitive impairment subjects from the ADNI (ADNI PIB+ MCI, n=40). Age, gender, and education were controlled for in each statistical model, and HV was adjusted for intracranial volume (aHV). In BAC NC, elevated PIB uptake was significantly associated with smaller aHV ($p= 0.0016$) and worse EM ($p= 0.0086$). Within ADNI NC, elevated PIB uptake was significantly associated with smaller aHV ($p=0.047$) but not EM ($p= 0.60$); within ADNI PIB+ MCI, elevated PIB uptake was significantly associated with both smaller aHV ($p=0.00070$) and worse EM ($p=0.046$). To further understand these relationships, a recursive regression procedure was conducted within all ADNI NC and PIB+ MCI subjects (n=56) to test the hypothesis that HV mediates the relationship between Aβ and EM. Significant correlations were found between PIB index and EM ($p=0.0044$), PIB index and aHV ($p< 0.0001$), as well as between aHV and EM ($p<0.0001$). When both aHV and PIB were included in the same model to predict EM, aHV remained significant ($p=0.0015$) whereas PIB index was no longer significantly associated with EM ($p=0.50$). These results are consistent with a model in which Aβ deposition, hippocampal atrophy, and EM occur sequentially in elderly subjects, with Aβ deposition as the primary event in this cascade. This pattern suggests that declining episodic memory in older individuals may be caused by Aβ-induced hippocampus atrophy.

2.1 Introduction

Although converging evidence across many fields suggests that the beta-amyloid (Aβ) protein is a central etiologic event in the pathogenesis of AD (Hardy and Selkoe, 2002; Walsh and Selkoe, 2007) the role of this pathology in stages preceding AD, especially normal aging, is poorly understood. Postmortem studies have consistently observed Aβ pathology in normal elderly subjects (Bennett et al., 2006; Davis et al., 1999; Hulette et al., 1998; Knopman et al., 2003; Price and Morris, 1999; Tomlinson et al., 1968), and it has been suggested that the presence of this pathology reflects the earliest stage in the development of AD. Proving this hypothesis has been difficult due to limitations inherent in postmortem analysis. The recent development of [^{11}C]PIB ('Pittsburgh Compound-B'), a positron emission tomography (PET) radiotracer that binds to fibrillar Aβ plaques, provides the unique opportunity to quantify this pathology antemortem, while simultaneously testing cognitive status. Studies employing PIB-PET imaging show high tracer uptake in AD (Kemppainen et al., 2006; Klunk et al., 2004; Rowe et al., 2007) and elevated tracer uptake in a subset of normal individuals (Aizenstein et al., 2008; Fotenos et al., 2008; Jack et al., 2008; Mintun et al., 2006; Pike et al., 2007; Rowe et al., 2007). These results are consistent with postmortem studies, validating the application of PIB-PET imaging towards understanding the role of Aβ deposition in nondemented people.

Postmortem studies report Aβ pathology in 25-45% of normal elderly individuals, depending on the age of the cohort and the pathological criteria employed (Bennett et al., 2006; Davis et al., 1999; Hulette et al., 1998; Knopman et al., 2003; Price and Morris, 1999; Tomlinson et al., 1968). Recent PIB-PET studies have found that 10-30% of cognitively normal controls show elevated PIB uptake (Fotenos et al., 2008; Jack et al., 2008; Mintun et al., 2006; Pike et al., 2007; Rowe et al., 2007). These findings are consistent with the postmortem frequencies after considering the younger cohort age in most PIB-PET studies. Although the general trend in postmortem and PIB-PET studies has been to dichotomize normal controls into low- and high-Aβ groups (referred to as "PIB-" and "PIB+" in PIB-PET studies), PIB uptake in published studies of normal older people clearly appears on a continuum, with PIB+ normal subjects usually showing lower levels than AD patients (Jack et al., 2008; Pike et al., 2007; Rowe et al., 2007). This pattern supports the hypothesis that Aβ accumulation is a continuous process that results in clinical AD once a certain threshold is reached. Thus, examining Aβ accumulation as a continuous variable, rather than dichotomizing subjects into PIB+ and PIB- groups, may yield further insights into the contribution of Aβ to cognitive dysfunction in normal older individuals, emphasizing the need to examine early Aβ accumulation as a continuous variable rather than dichotomizing into PIB+ and PIB- groups.

Episodic memory (EM) deficits are common in aging, particularly with respect to encoding new information (Small et al., 1999). Furthermore, EM decline has been associated with conversion to AD (Grober et al., 2008; Small et al., 2000), and the relationship between the presence of Aβ pathology in normal older people and EM needs to be further studied. Postmortem studies examining the relationship between Aβ pathology and EM have yielded inconsistent results, perhaps reflecting methodological limitations such as long delays between antemortem cognitive testing and autopsy (Goldman et al., 2001; Hulette et al., 1998; Katzman et al., 1988; Schmitt et al., 2000). Recent PIB-PET

studies have examined this relationship, with one research group reporting an association between PIB uptake and EM (Pike et al., 2007; Villemagne et al., 2008).

Hippocampus volume (HV) atrophy has been shown to occur at a rate of 1.7% per year in individuals over age 60 (Raz and Rodrigue, 2006), and has also been associated with AD (Apostolova et al., 2006; de Leon et al., 1996; Jack et al., 1999; Smith et al., 2007). It is unclear whether atrophy in this structure is related to Aβ pathology in normal subjects. Jack et al. found an association between PIB uptake and HV when nondemented subjects were combined with AD subjects, as well as a nonsignificant trend for an association between elevated PIB and smaller HV within normal control subjects (Jack et al., 2008).

We hypothesize that if Aβ burden in nondemented populations represents the earliest signs of AD, then this pathology should correlate with putative preclinical markers of AD. Our study addresses this issue by comparing PIB uptake to HV and EM within normal elderly individuals. To determine whether observed relationships generalize to other populations, analyses were replicated in independent samples of normal control and mild cognitive impairment subjects from the Alzheimer's Disease Neuroimaging Initiative (ADNI, http://www.adni-info.org/).

2.2 Methods

Design Overview

The relationships between Aβ burden and preclinical AD markers were examined in two independent groups of normal control (NC) subjects. The primary analysis was performed in cognitively normal subjects from the Berkeley Aging Cohort (BAC NC), and a confirmatory analysis was performed in normal control subjects from the Alzheimer's Disease Neuroimaging Initiative (ADNI NC). Analyses were also conducted in ADNI mild cognitive impairment subjects showing elevated levels of PIB uptake (ADNI PIB+ MCI). Due to study protocol differences, data collection and processing between BAC and ADNI cohorts differ as discussed in detail below.

Subject Recruitment

BAC NC subjects were recruited from the community via newspaper advertisement. Eligibility requirements include age ≥ 60, living independently in the community, normal performance on cognitive tests, absence of neurological or psychiatric illness and lack of major medical illnesses and medications that affect cognition. One hundred nineteen subjects [mean age=72.1(8.1), mean MMSE=29.0(1.5)] are currently enrolled in the BAC. Twenty BAC subjects underwent PIB positron emission tomography (PIB-PET) imaging and magnetic resonance imaging (MRI) for this study. BAC subjects recruited for this study scored above 27 on the MMSE and below 10 on the Geriatric Depression Scale.

PIB-PET data for 20 AD patients recruited from the University of California San Francisco (UCSF) Memory and Aging Center were used for comparison purposes. The diagnosis of AD was based on a comprehensive multi-disciplinary evaluation that includes a clinical history and physical examination, a caregiver interview and a battery of neuropsychological tests (Kramer et al., 2003). All AD subjects meet NINDS criteria for probable AD (McKhann et al., 1984). No other significant co-morbid medical, neurologic or

psychiatric illnesses were present.

The ADNI is a large multi-site collaborative effort launched in 2003 by the National Institute on Aging, the National Institute of Biomedical Imaging and Bioengineering, the Food and Drug Administration, private pharmaceutical companies and non-profit organizations as a public-private partnership aimed at testing whether serial MRI, PET, other biological markers and clinical and neuropsychological assessment can be combined to measure the progression of MCI and early AD. The Principal Investigator of this initiative is Michael Weiner, MD, and ADNI is the result of many co-investigators from a broad range of academic institutions and private corporations, with subjects recruited from over 50 sites across the US and Canada. ADNI NC subjects have MMSE scores between 24-30, have no memory complaints, have normal memory function as documented by performance on the Logical Memory II subscale (delayed paragraph recall) of the Wechsler Memory Scale-Revised (Wechsler, 1987b), and a clinical dementia rating scale score of 0 (Morris, 1993). ADNI MCI subjects have MMSE scores between 24-30, have a memory complaint verified by an informant, documented abnormal memory function on the WMS-R paragraph recall, a CDR score of 0.5 and preservation of general cognition and function that excludes a diagnosis of AD. AD patients were required to meet published criteria for probable AD with MMSE scores of 20-26 and CDR scores of 0.5 or 1. Further information on inclusion and exclusion criteria can be found at http://www.adni-info.org.

Subjects from the ADNI database were included in this study if they had completed PIB-PET imaging, structural MRI imaging, and cognitive testing. PIB uptake was compared to putative preclinical AD markers in ADNI NC and MCI subjects meeting these criteria, whereas AD subjects were used as a comparison group for PIB uptake. Three ADNI subjects meeting these criteria were excluded due to technical factors related to PET intensity normalization. Seventeen normal controls, 52 MCI, and 15 AD subjects from ADNI were included in this study.

Cognitive testing data

BAC subjects undergo a medical evaluation and detailed cognitive testing in multiple domains to assure normal functioning (episodic and working memory, language, visuospatial ability, frontal/executive ability). Cognitive composite scores across various domains were derived by averaging individual z-transformed test scores. Scores were z-transformed using mean and standard deviations from all BAC subjects 60 years and older. When applicable, z-transformed scores were inverted to make positive values correspond to better performance. Test scores within 6 months of PIB-PET imaging were used in statistical analyses. If cognitive testing did not occur within 6 months of PIB-PET imaging, then an interpolated score was derived from testing sessions flanking the PET scanning session (interpolation was performed for 5 subjects, with a median duration between PET and closest cognitive testing date of 235 days).

Episodic memory composite scores were derived from the long delay free recall portion of the California Verbal Learning Test (CVLT) (Delis et al., 2000) and Wechsler Memory Scale (WMS-R) visual reproduction (Wechsler, 1987b). A working memory composite score was derived from the Wechsler Adult Intelligence Scale (WAIS-R) digit span backwards (Wechsler, 1987a) and listening span total recall (Salthouse et al., 1991). A frontal function composite score was derived from the Trails B minus A (Reitan, 1958) and Stroop total correct in 60 seconds (Zec, 1986).

ADNI participants undergo cognitive testing annually. Long delay free recall scores from the Rey Auditory Verbal Learning were used as a measure of episodic memory. Mean and standard deviations from the ADNI NC PIB group were used to z-transform scores for all ADNI subjects (NC, MCI, and AD). ADNI subjects completed cognitive testing within 6 months of PIB-PET scanning (mean time and standard deviation between cognitive testing and PET was 36 ± 40 days).

Radiotracer synthesis and PIB-PET acquisition

BAC NC and UCSF AD subjects underwent PIB-PET scanning at the Lawrence Berkeley National Laboratory (LBNL). PIB was synthesized at this facility using a previously published protocol (Mathis et al., 2003). In brief, high specific activity 11C-carbon dioxide produced on an 11 MeV CTI RDS-111 cyclotron was used to synthesize ^{11}C-CH_3I (Langstrom et al., 1987; Link et al., 1997). The PIB precursor 2-(4'-aminophenyl)-6 methoxymethoxybenzothiazole was prepared and methylated with ^{11}C -CH_3I prior to deprotection to afford the 6-hydroxy compound, ^{11}C -PIB (Mathis et al., 2003). The final compound was purified by semipreparative HPLC and injected at high specific activity. ADNI subjects underwent PIB scanning at 12 sites, using one of two methods to synthesize ^{11}C-PIB: [11C]methyl iodide and a 6-MOM-protected precursor (Mathis et al., 2003) or [11C]methyl triflate and an unprotected precursor (Wilson et al., 2004). The minimum radiochemical purity was 90% and the minimum specific activity of the product at the time of injection was 300 Ci/mmol.

PIB-PET imaging for BAC and UCSF subjects was performed using a Siemens ECAT EXACT HR PET scanner in 3D acquisition mode. PIB (10-15 mCi) was injected into an antecubital vein. Dynamic acquisition frames were obtained as follows: 4 x 15 s, 8 x 30 s, 9 x 60 s, 2 x 180 s, 8 x 300 s and 3 x 600 s (90 minutes total). Ten minute transmission scans for attenuation correction were obtained for each PIB scan. PIB-PET data was reconstructed using an ordered subset expectation maximization algorithm with weighted attenuation. Images were smoothed with a 4mm Gaussian kernel with scatter correction. ADNI PIB-PET images used in this study were collected at 12 different scanning sites. Dynamic acquisition frames were collected 50-70 min post-injection (4 x 5min frames).

MRI acquisition

Structural images for BAC NC subjects were collected at LBNL on a 1.5T Magnetom Avanto System (Siemens Inc., Iselin, NJ) with a 12 channel head coil run in triple mode. Three high-resolution structural T1-weighted volumetric magnetization prepared rapid gradient echo (MP-RAGE) scans were collected axially for each subject (TR/TE/TI=2110/3.58/1100ms, flip angle = 15°, with 1.00x1.00mm^2 in-plane resolution and 1.00mm slice thickness). For 13 UCSF AD subjects, MP-RAGE scans were collected coronally at UCSF on a 1.5T Vision System (Siemens Inc., Iselin, NJ) with a quadrature head coil (TR/TE/T1=10/7/300ms, flip angle = 15°, with 1.00x1.00mm^2 in plane resolution and 1.40mm slice thickness). For 7 UCSF AD subjects, MP-RAGE scans were collected sagittally on a Bruker MedSpec 4T system with an 8 channel head coil (TR/TE/T1=2300/3.37/950ms, flip angle = 7°, with 1.00x1.00mm^2 in-plane resolution and 1.00mm slice thickness).

ADNI MRI scans are collected at multiple sites using either a GE, Siemens, or Philips 1.5T system. Two high-resolution T1-weighted volumetric MP-RAGE scans were collected for each subject. Parameter values vary depending on scanning site and can be found at http://www.loni.ucla.edu/ADNI/Research/Cores/. For this study, we used MP-RAGE scans that had undergone gradient warping correction (raw scans were used for images collected on Philips scanners, since these images do not require gradient warping correction) (Jack et al., 2008).

PIB-PET processing

For BAC NC and UCSF AD subjects, PIB-PET data was preprocessed using the SPM2 software package (http://www.fil.ion.ucl.ac.uk/spm). Realigned PIB frames corresponding to the first 20 minutes of acquisition were averaged and used to guide coregistration between each subject's PIB DVR image and structural MRI scan. A gray matter masked cerebellum reference region for PIB data was derived using the subject's averaged MP-RAGE scan via automated labeling (see section below). Distribution volume ratios (DVRs) for PIB images were created using Logan graphical analysis with frames corresponding to 35-90 min post-injection (Logan et al., 1996; Price et al., 2005).

DVR images underwent partial volume correction to minimize signal washout in voxels adjacent to cerebrospinal fluid (Meltzer et al., 1999; Zaidi et al., 2006). Our partial volume correction procedure convolves a gray/white matter brain matter mask with a scanner-specific point-spread function. The resulting 3D image is used to correct radiotracer counts in the native space PET image by elevating voxels contaminated by cerebrospinal fluid.

In addition to creating partial volume corrected DVR images for BAC NC and UCSF AD PIB data, these data were also analyzed using an standardized uptake value ratio (SUVR) approach (realigned frames corresponding to 50-70 min post injection were averaged and normalized to mean value in cerebellum gray matter). SUVR images were not corrected for partial volume effects and were used to compare PIB values from our cohorts to PIB values derived from ADNI.

For ADNI subjects, all scans were checked for quality (counts, field-of-view, subject movement) and then SUVR images were created using the following processing steps: 50-70 min post injection frames were realigned and averaged, processed to a standard orientation, image and voxel size, smoothed to a common resolution of 8 mm FWHM and intensity normalized to the mean uptake in cerebellum gray matter. Further information about image processing is available at http://www.adni-info.org. These preprocessing steps were completed by the ADNI PET core and were downloaded for use in this study. Partial volume correction was not applied to these data.

ROI Analysis

For all subjects, region of interest (ROI) labeling was implemented using the FreeSurfer software packages (http://surfer.nmr.mgh.harvard.edu/). For BAC NC, three structural T1 scans for each subject were realigned and averaged to yield a single high-resolution image with excellent gray-white contrast. For UCSF AD, a single structural T1 image was processed through FreeSurfer. Structural images were bias field corrected, intensity normalized, and skull stripped using a watershed algorithm (Dale et al., 1999; Segonne et al., 2004). Manual touchup was performed to exclude all non-brain tissue

(resulting in a cleaned mask containing all gray/white matter and cerebrospinal fluid). These images underwent a white matter-based segmentation, gray/white matter and pial surfaces were defined, and topology correction was applied to these reconstructed surfaces (Dale et al., 1999; Fischl et al., 2001; Segonne et al., 2004). A trained operator (ECM) visually confirmed resulting surface output and made additional manual edits when necessary. Subcortical and cortical ROIs spanning the entire brain were defined in each subject's native space (Desikan et al., 2006; Fischl et al., 2002). Hippocampus and caudate ROIs from this step provided volumes for these structures (averaged across the hemispheres) and were used in subsequent regression models. The resulting cerebellum ROI (gray matter only) was used as a reference region to create PIB-DVR and SUVR images for BAC NC and UCSF AD subjects. Additionally, multiple cortical ROIs were collapsed to yield four large ROIs that spanned prefrontal cortex (all cortex anterior to the precentral sulcus), lateral temporal cortex (middle and superior temporal gyri), parietal cortex (supramarginal gyrus, inferior/superior parietal lobules and precuneus), and anterior/posterior cingulate gyrus. A PIB index was the primary variable of interest in this study, and was derived by averaging the mean DVR value from these four ROIs. A PIB index from SUVR images was also extracted for BAC NC and AD UCSF for comparison with ADNI PIB index values.

Gray and white matter components from the cleaned mask were combined and used to partial volume correct BAC and UCSF PIB-DVR images, and total volume of the cleaned mask (gray/white matter and cerebrospinal fluid) were used to adjust brain volumes by total intracranial volume (ICV).

MP-RAGE scans for ADNI subjects were processed through Freesurfer as described above, although only two MP-RAGE scans for ADNI subjects were averaged. In addition, for ADNI cases an estimate of total ICV was derived using an automated atlas scaling method (Buckner et al., 2004), and was used to adjust brain volumes. A PIB index was extracted for all ADNI subjects using SUVR images.

Statistical Models

All analyses were completed using the statistical programming language R, version 2.3 (http://www.r-project.org/). Welch two sample t-tests were used for group comparisons of continuous variables (age, education, MMSE and PIB index). Chi-squared tests were used to compare gender across groups.

A covariance approach was used to adjust HV by total intracranial volume (ICV) (Mathalon et al., 1993). Adjusted HV (aHV) was obtained with the following formula: aHV = raw HV – b (ICV – mean ICV), with b reflecting the regression coefficient when raw HV is regressed against ICV and mean ICV reflects the group mean. Regression coefficients and mean ICV for volume adjustments were calculated separately for each group analysis. Caudate and brain volume (gray/white matter combined) were corrected for ICV using the same covariance approach. Adjusted volumes were used in subsequent regression models.

Hierarchical multiple regression models were used to determine whether PIB index was significantly associated with putative preclinical AD markers, controlling for the effects of age, gender, and education. Two models were examined separately within BAC NC, ADNI NC, and ADNI PIB+ MCI groups: the first model used aHV as the dependent variable and the second model used EM as the dependent variable. Age, gender and education were entered into each model in the first step and PIB index was entered into each model in the second

step. For each model, we report change in R^2 (ΔR^2) to reflect the increase in R^2 before and after PIB index is entered into the model. Partial regression plots were used to visualize the relationships between PIB index and aHV/EM (which displays the residuals of each variable after adjusting for age, gender and education). Using the same hierarchical regression approach, the relationship between aHV and EM was also examined within each group. Furthermore, "control" hierarchical multiple regression models were executed within BAC NC, using caudate volume, brain volume, frontal function, and working memory as dependent variables.

To test whether evidence exists for a sequential relationship between PIB index, aHV, and EM, we implemented a recursive linear regression procedure used previously in a postmortem study (Baron and Kenny, 1986; Bennett et al., 2004). Specifically, we hypothesized that hippocampus atrophy mediates the relationship between Aβ burden and EM deficits in nondemented subjects. ADNI NC and PIB+ MCI were combined in this analysis (n=56). In the first step of this approach, PIB index versus EM, PIB index versus aHV, and aHV versus EM are examined in separate regression models. In the second step, a multivariate model with PIB index and aHV simultaneously predicting EM was examined. Assuming the relationships in the first step are significant, the purposed sequential relationship is supported if aHV significantly predicts EM after controlling for PIB index (and PIB index does not significantly predict EM after controlling for aHV). Age, gender and education are controlled for in each model using the same hierarchical multiple regression approach described above. For this analysis, overall model R^2 values are reported, as well as the ΔR^2 associated with PIB index and aHV during the multivariate step.

2.3 Results

BAC NC and UCSF AD characteristics

Demographics and group PIB index values for BAC NC and UCSF AD are summarized in Table 1. BAC NC and UCSF AD did not significantly differ in education or gender. The UCSF AD group was younger (t= -3.36, p=0.0018) and scored lower on the MMSE (t= -6.02, p= 1.02e-05) than the BAC NC group. Qualitative examination of cortical PIB uptake revealed a varied pattern across BAC NC and UCSF AD subjects. Illustrative data from three individual subjects with AD are shown in Figure 1A-C, and are contrasted with three BAC NC subjects (Figure 1D-F). In AD subjects, high DVR values were typically found throughout cortical association areas, with relative sparing of primary cortical areas (ie. motor/sensory cortex and occipital lobe, Figure 1A-C). A number of subjects showed a more focal pattern, with elevated DVR in medial frontal cortex and precuneus/posterior cingulate (Figure 1C). The BAC NC with the highest PIB uptake showed a pattern similar to a typical AD case, with elevated uptake in the medial frontal cortex, precuneus, cingulate, and lateral temporo-parietal cortex (Figure 1D). The BAC NC with the second highest PIB uptake showed localized deposition in medial frontal cortex and lateral parietal cortex (Figure 1E). There were also NC subjects that did not have any indication of elevated DVR values throughout cortex (Figure 1F). DVR PIB index values were significantly higher in UCSF AD than BAC NC (t= 8.49, p= 3.30e-08, Figure 2).

Table 1: Group characteristics

	BAC NC	UCSF AD	ADNI NC	ADNI PIB- MCI	ADNI PIB+ MCI	ADNI AD
N	20	20	17	13	39	15
Age	72.3 (6.0)	64.3 (8.8)**	78.5 (5.4)	72.7 (7.8)*	75.0 (7.9)	72.6 (8.7)*
Gender	13F, 7M	9F, 11M	7F, 10M	3F, 10M	13F, 26M	5F, 10M
Education	18.3 (2.8)	16.7 (3.1)	14.9 (3.2)	16.8 (2.6)	16.2 (2.9)	14.9 (2.7)
MMSE	29.6 (0.6)	19.7 (6.7)***	28.6 (1.5)	27.1 (2.8)	27.4 (2.0)*	22.7 (2.9)***
PIB Index	SUVR: 1.40 (0.09); DVR: 1.44 (0.10)	SUVR: 2.02 (0.41)***; DVR: 2.13 (0.33)***	SUVR: 1.64 (0.49)	SUVR: 1.30 (0.10)*	SUVR: 2.14 (0.44)**	SUVR: 2.18 (0.45)**
EM	-0.05 (0.85)	NA[+]	0.00 (1.0)	-1.29 (0.79)***	-1.11 (1.14)***	-1.89 (0.29)***

Table 1: Values are listed as mean (standard deviation). In statistical contrasts, UCSF AD are compared to BAC NC; for ADNI groups, MCI and AD are compared to NC ($p<0.05$*, $p<0.01$**, $p<0.001$***). For BAC NC and UCSF AD, PIB index values were computed using both DVR and SUVR approaches (DVR values were used for regression analyses, whereas SUVR values were used for comparison with ADNI values). [+]Comparable EM scores were unavailable for this group. MMSE=Mini Mental State Examination, EM=Episodic memory.

Figure 1: Qualitative examination of PIB-DVR data

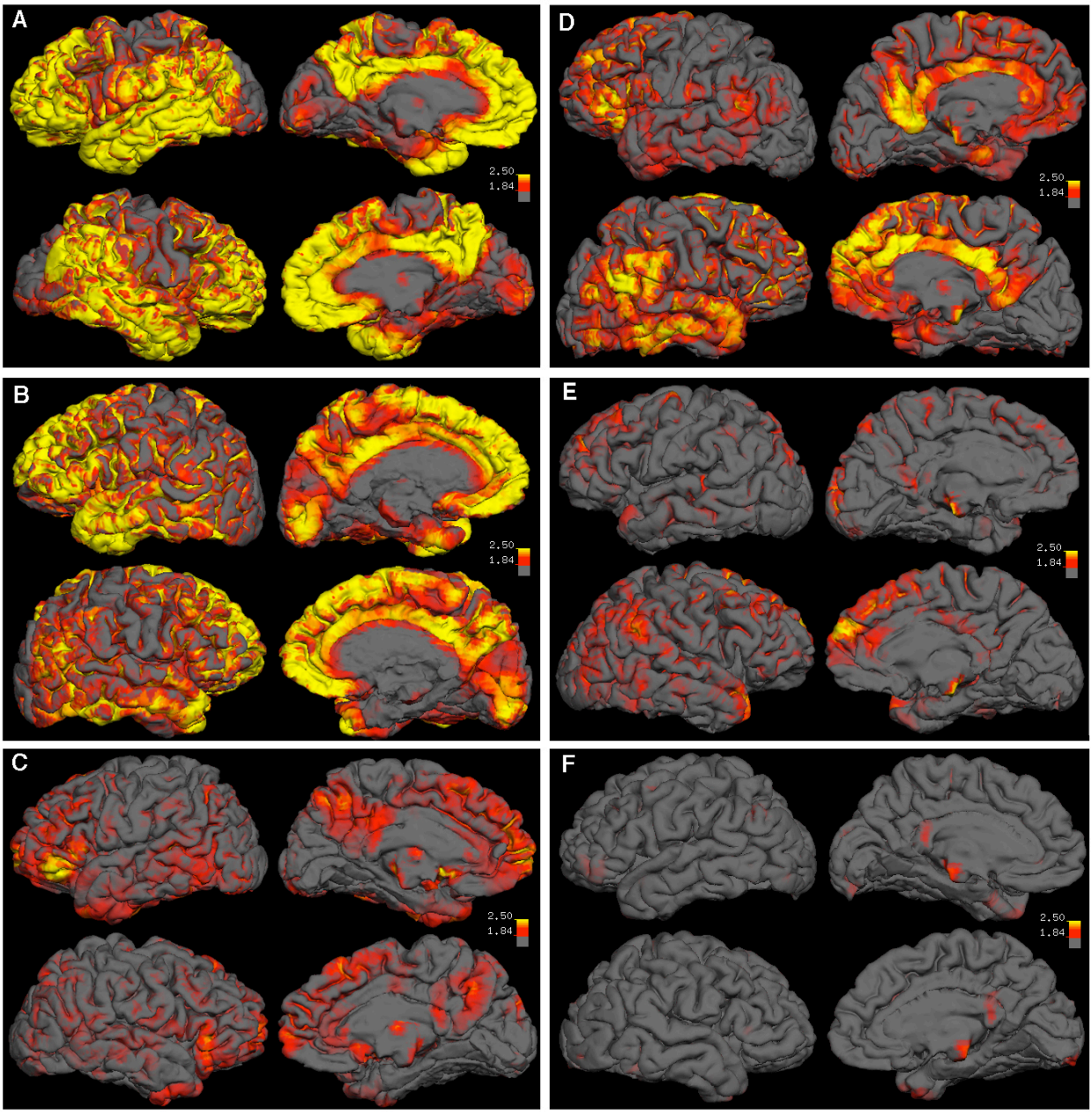

Figure 1: Partial volume corrected PIB-DVR images were overlaid on native space reconstructed surfaces derived from the subject's T1-weighted structural scan for 3 UCSF AD subjects (A-C) and 3 BAC NC subjects (D-F). Each box shows lateral and medial views of PIB distribution for a single subject (left hemisphere is above right hemisphere in each box). All images reflect the same color scale, with yellow indicating high PIB uptake, red indicating medium PIB uptake, and gray indicating low PIB uptake.

Figure 2: Distribution of PIB DVR values in BAC NC and UCSF AD

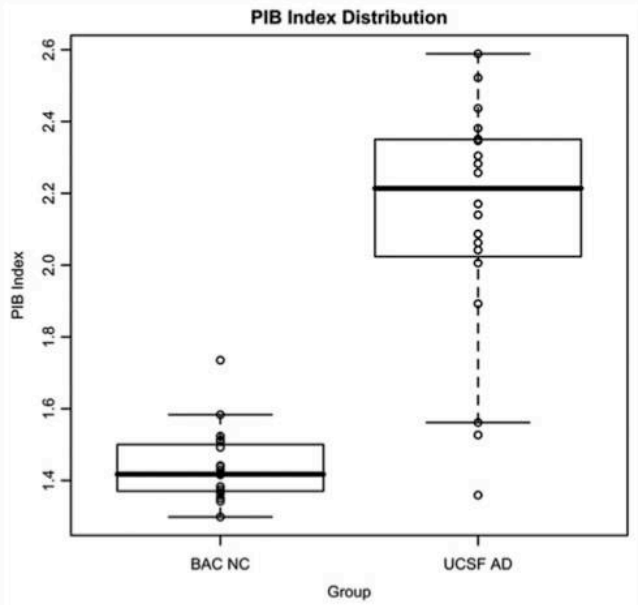

Figure 2: Box and whiskers plot showing the distribution of DVR PIB index values in BAC NC and UCSF AD.

Relationships between PIB index and preclinical AD markers in BAC NC

Age, education and gender were not significantly associated with either aHV or EM in the BAC NC group. PIB index was significantly correlated with aHV (ΔR^2= 0.45, t = -3.84, p= 0.0016) and EM (ΔR^2= 0.35, t= -3.02, p= 0.0086, Figure 3). Furthermore, aHV was significantly associated with EM (ΔR^2= 0.27, t= 2.44, p= 0.028). To examine the extent to which these relationships were influenced by subjects with elevated Aβ burden, the two highest PIB index subjects (Figure 1D-E) were removed from each regression model. In this subset analysis (n=18), the PIB index versus aHV relationship remained significant (ΔR^2= 0.28, t= -2.50, p=0.026), whereas significant relationships were no longer present in PIB index versus EM (ΔR^2=0.03, t= -0.74, p=0.47; Figure 4) and aHV versus EM (ΔR^2=0.11, t=1.42, p=0.18).

Within the BAC NC group, PIB index was not significantly correlated with caudate volume (ΔR^2=0.0005, t= 0.094, p= 0.93), whole brain volume (ΔR^2=0.008, t= 0.41, p= 0.69), working memory (ΔR^2= 0.15, t= -1.55, p= 0.15) or frontal function (ΔR^2= 0.06, t= -0.97, p=0.35).

Figure 3: PIB index versus HV and EM within BAC NCs

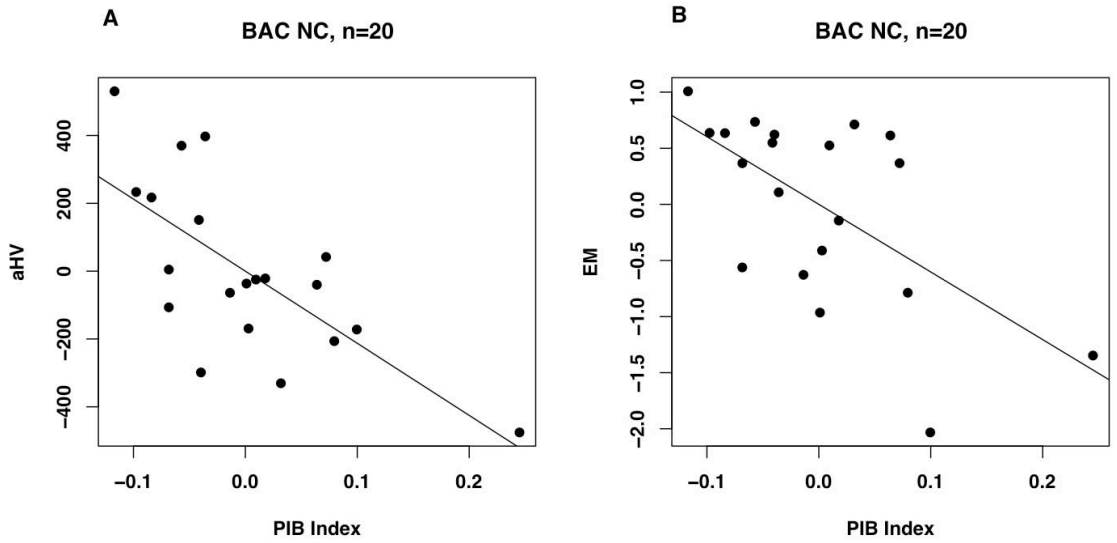

Figure 3: Partial regression plots showing the relationships between PIB index and aHV (A) and EM (B) within the BAC NC group. Residuals are plotted for each variable to adjust for the effects of age, gender and education. Both regression models are significant (A: ΔR^2=0.45, p=0.0016; B: ΔR^2=0.35, p=0.0086).

Figure 4: PIB index versus HV and EM within BAC NCs, outliers removed

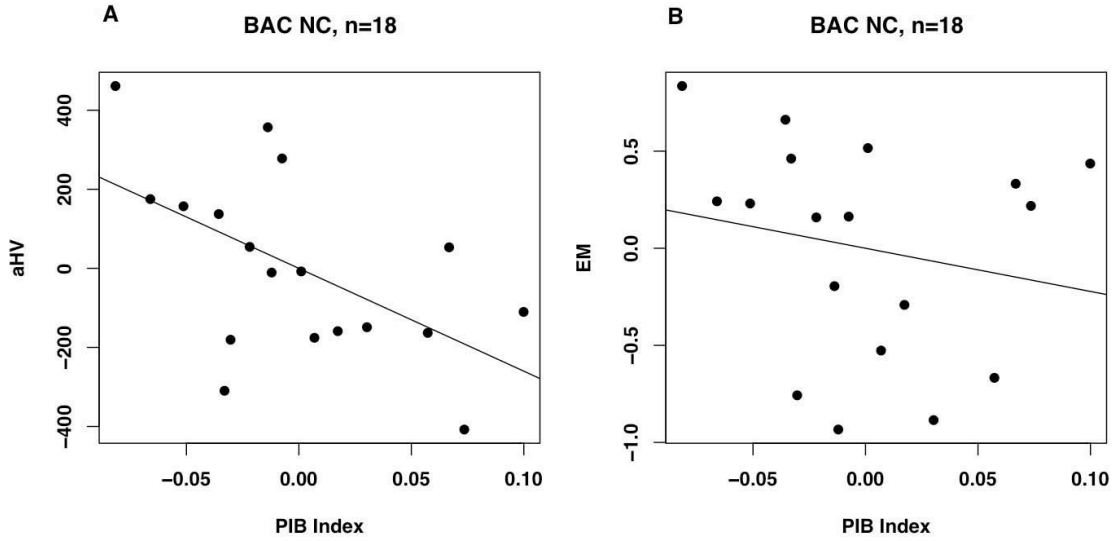

Figure 4: Partial regression plots showing the relationships between PIB index and aHV (A) and EM (B) after removing the two subjects with the highest PIB uptake from the BAC NC group. Residuals are plotted for each variable to adjust for the effects of age, gender and education. PIB index versus aHV remains significant (ΔR^2=0.28, p=0.026), whereas PIB index versus EM is no longer significant (ΔR^2=0.03, p=0.47).

<u>ADNI group characteristics</u>

Demographics and group PIB index values for ADNI groups are summarized in

Table 1. ADNI NC subjects did not significantly differ from AD or MCI subjects in education or gender. NC subjects were significantly older than MCI (t= 2.41, p= 0.021) and AD subjects (t= 2.26, p= 0.034). NC subjects scored significantly higher on the MMSE than MCI (t= 2.86, p = 0.0066) and AD subjects (t= 7.11, p = 6.81e-07). NC subjects had higher EM scores than MCI (t= 4.07, p = 0.00034) and AD (t = 7.41, p = 5.03e-07).

Figure 5 shows the distribution of SUVR PIB index values across the ADNI groups. Although the majority of AD cases (13/15) show highly elevated PIB index values, NC and MCI subjects show a continuous range of values. Quantitatively, PIB index was significantly lower in NC compared to MCI (t = -2.09, p = 0.046) and AD (t = -3.30, p = 0.0025). Additionally, there was a trend for MCI subjects to have lower PIB index than AD subjects (t = -1.8773, p = 0.072). It should be noted that the SUVR PIB index values in Figure 5 are not directly comparable to the partial volume corrected DVR PIB index values displayed in Figure 2. Direct comparison of SUVR and DVR PIB index values within the BAC NC group revealed an average difference of 5.5% between these two methods.

Interestingly, many demographic differences were present between BAC NC and ADNI NC groups. In comparison to ADNI NC, BAC NC were significantly younger (t= -3.29, p = 0.0023), more educated (t = 3.38, p = 0.0019), and scored higher on the MMSE (t = 2.52, p = 0.020). There was no significant difference in gender between BAC and ADNI NC groups.

Figure 5: Distribution of SUVR PIB index values in ADNI

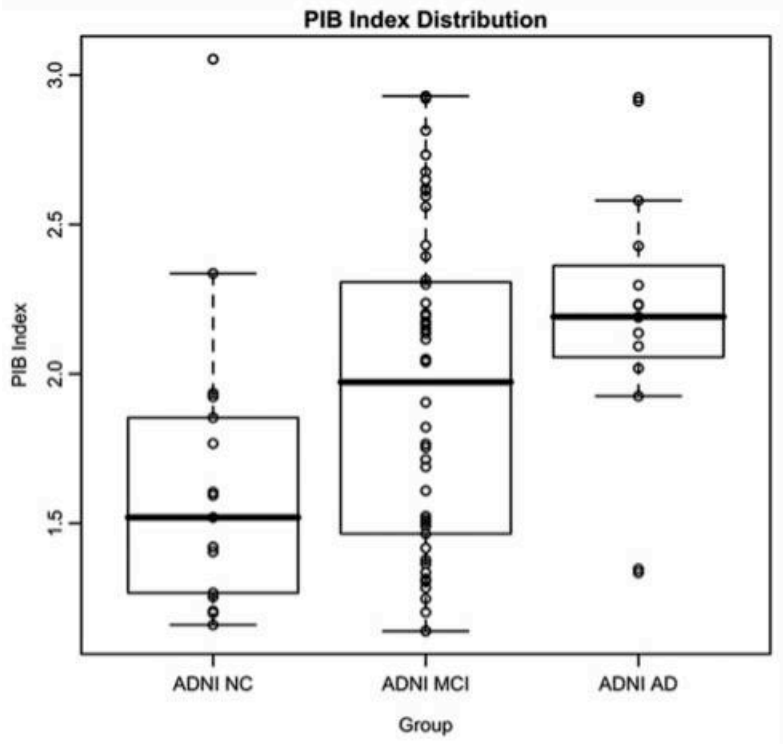

Figure 5: Box and whiskers plot showing the distribution of SUVR PIB index values in ADNI groups. ADNI SUVR PIB index values are not directly comparable to BAC NC and UCSF AD DVR PIB index values in Figure 2 due to differences image processing (see Methods).

Relationships between PIB index and preclinical AD markers in ADNI NC

Age, education and gender were not significantly associated with either aHV or EM within ADNI NC. PIB Index was significantly associated with aHV (ΔR^2= 0.22, t = -2.21, p=0.047), but was not significantly associated with EM (ΔR^2= 0.02, t= 0.53, p= 0.60; Figure 6). aHV was not significantly associated with EM in this group (ΔR^2= 0.01, t= -0.44, p=0.67).

Figure 6: PIB index versus HV and EM within ADNI NCs

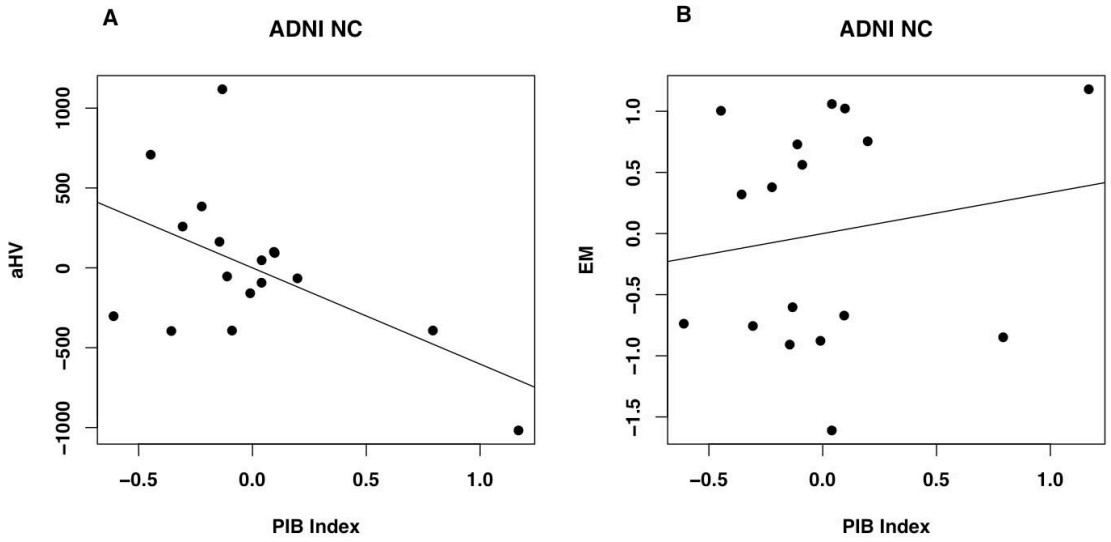

Figure 6: Partial regression plots showing the relationships between PIB index and aHV (A) and EM (B) within the ADNI NC group. Residuals are plotted for each variable to adjust for the effects of age, gender and education. Only PIB index versus aHV shows a significant association (A: ΔR^2=0.22, p=0.047; B: ΔR^2=0.02, p=0.60).

Relationships between PIB index and preclinical AD markers in ADNI PIB+ MCI

In order to assess whether similar relationships between these variables exist in subjects who are not demented but do have memory impairment, we utilized MCI subjects from the ADNI database as described above. For these subjects, we confined our analyses to cases that were defined as PIB+ (based on a threshold obtained via a receiver-operating characteristic (ROC) approach) in order to exclude MCI cases with hippocampus abnormalities that might be unrelated to AD pathology, such as hippocampal sclerosis (Jicha et al., 2006). SUVR PIB index values for BAC NC and UCSF AD were used in this ROC curve analysis, and the resulting cut off was applied to ADNI MCI subjects.

A cut off value of 1.465 optimized discrimination between BAC NC and UCSF AD subjects (sensitivity of 0.90 and specificity of 0.90 for the diagnosis of AD) and was selected as the threshold for PIB-positivity. Application of this cut off value to the ADNI MCI cohort stratified 39/52 (75%) MCI subjects as PIB+ and 13/52 (25%) as PIB-. PIB+ MCI subjects were not significantly different from PIB- MCI subjects in age, gender, education, MMSE, aHV, or EM (p>0.05). Comparisons between ADNI NC and dichotomized MCI groups are summarized in Table 1. PIB- MCI subjects were not significantly different than NC subjects

in gender, education or MMSE. PIB- MCI subjects were younger (t = -2.308, p = 0.032), had a lower PIB index values (t= -2.81, p = 0.012) and lower EM scores (t = -3.96, p = 0.00047) than NC subjects. PIB+ MCI subjects were not significantly different than NC in age, gender, or education. PIB+ MCI subjects scored lower on the MMSE (t= -2.64, p = 0.012), had higher PIB index values (t= 3.64, p= 0.0011) and lower EM scores (t= -3.65, p= 0.00086) than NC subjects.

Demographic variables were not significantly associated with either aHV or EM within the PIB+ MCI group. PIB index was significantly associated with aHV (ΔR^2= 0.27, t= -3.73, p=0.00070) and EM (ΔR^2= 0.11, t= -2.08, p= 0.046; Figure 7). Additionally, aHV was significantly associated with EM (ΔR^2= 0.28, t= 3.797, p=0.00058).

Figure 7: PIB index versus HV and EM within ADNI PIB+ MCI

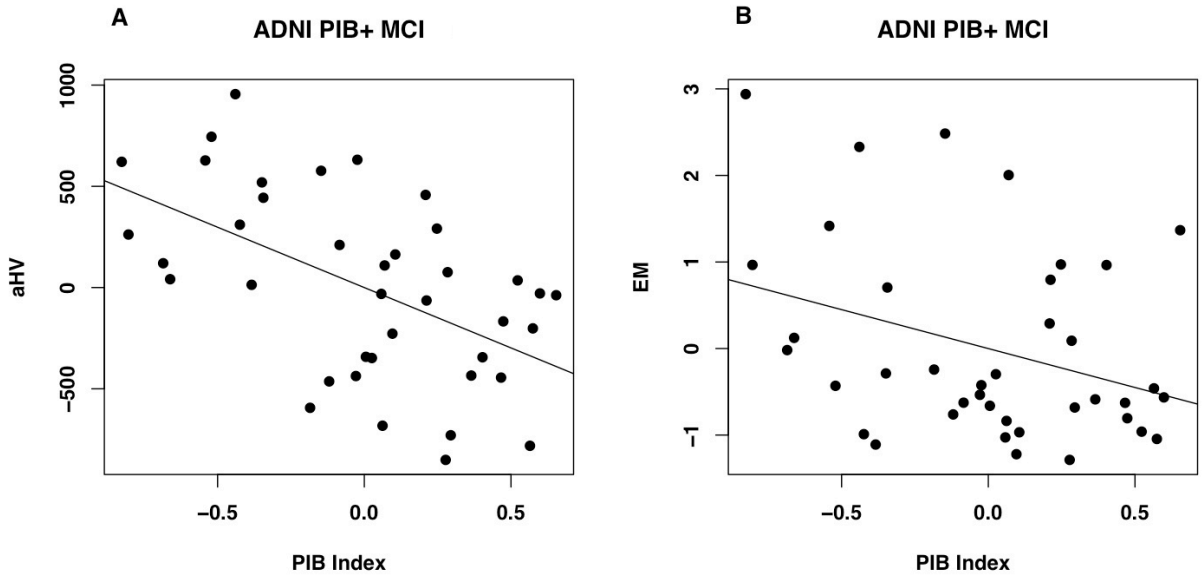

Figure 7: Partial regression plots showing the relationships between PIB index and aHV (A) and EM (B) within the ADNI PIB+ MCI group. Residuals are plotted for each variable to adjust for the effects of age, gender and education. PIB index is significantly associated with both aHV and EM (A: ΔR^2=0.27, p=0.00070; B: ΔR^2=0.11, p=0.046).

<u>Testing the sequential relationship between Aβ pathology, hippocampus atrophy, and episodic memory</u>

ADNI NC and ADNI PIB+ MCI subjects were combined to test the hypothesized sequential relationship between the three variables of interest (n=56). In the first step of this analysis, all three separate linear regression models were significant: PIB index predicting EM (overall model: R^2= 0.17, p= 0.049; PIB index: t= -2.983, p= 0.0044), PIB index predicting aHV (overall model: R^2= 0.38, p= 0.000061; PIB index: t= -5.18, p= 0.0000038), and aHV predicting EM (overall model: R^2= 0.32, p=0.00059; aHV: t= 4.662, p=0.000023). In the second step of this analysis, the model incorporating PIB index and aHV as simultaneous predictors of EM was also significant (R^2= 0.32, p=0.0013). When

examining the independent contributions of each predictor in this multivariate model, aHV remained significant (ΔR^2= 0.15, t= 3.36, p=0.0015) whereas PIB index was no longer significant (ΔR^2= 0.00, t= -0.676, p=0.50; Figure 8). These results are consistent with a model in which PIB index, aHV, and EM are sequentially related, with aHV mediating the relationship between PIB index and EM.

Figure 8: Sequential relationship between PIB, HV and EM

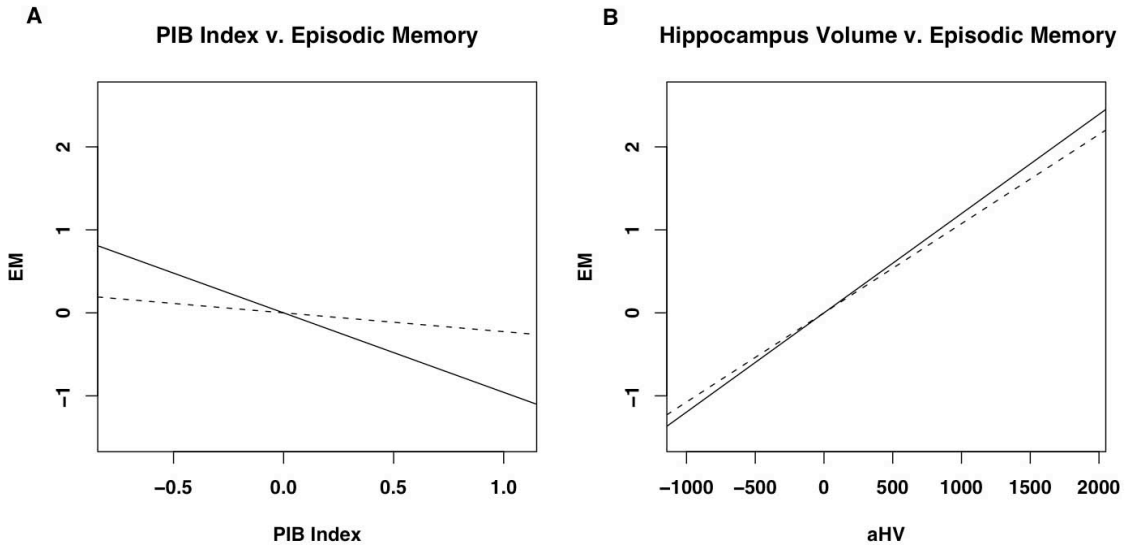

Figure 8: Partial regression plots showing results from a recursive regression procedure suggesting a sequential relationship between the 3 variables, with aHV mediating the relationship between PIB index and EM. Residuals are plotted for each variable to adjust for the effects of age, gender and education. A) The relationship between PIB index and EM before (solid line; ΔR^2=0.15, p=0.0044) and after controlling for aHV (dashed line; ΔR^2=0.01, p=0.50). B) The relationship between aHV and EM before (solid line; ΔR^2=0.29, p=0.000023) and after controlling for PIB index (dashed line; ΔR^2=0.15, p=0.0015).

2.4 Discussion

In this study, we examined the relationships between Aβ burden and putative preclinical AD markers in multiple groups of nondemented subjects. Despite numerous differences across the examined cohorts, we consistently observed that higher PIB uptake was associated with reduced HV. Although PIB was associated with EM in our primary BAC NC group and the ADNI PIB+ MCI group, this relationship in BAC NC was driven by the two subjects with the highest PIB uptake and was not replicated in the ADNI NC group (Table 2). Furthermore, results from a recursive regression procedure support the hypothesis that HV mediates the relationship between PIB and EM. Overall, these results suggest that Aβ and HV atrophy are directly related, whereas the relationship between Aβ and EM is indirect and may be mediated by HV atrophy.

Table 2: Regression model summary across different groups

Regression Model	BAC NC, n=20	BAC NC, n=18	ADNI NC	ADNI PIB+ MCI
aHV=PIB	**ΔR^2=0.45, p=0.0016**	**ΔR^2=0.28, p=0.026**	**ΔR^2=0.22, p=0.047**	**ΔR^2=0.27, p=0.00070**
EM=PIB	**ΔR^2=0.35 p=0.0086**	ΔR^2=0.03, p=0.47	ΔR^2=0.02, p=0.60	**ΔR^2=0.11, p=0.046**

Table 2: Regression models were conducted twice within the BAC NC group. The first analysis used the entire BAC NC sample (n=20) whereas the second analysis was conducted after removing the two subjects with the highest PIB index (n=18). Significant models are in bold. A consistent relationship between aHV and PIB index is observed in each group examined.

Aβ burden and Hippocampus Atrophy

The relationship between Aβ burden and HV in the primary group of normal controls persisted after removal of the two subjects with the greatest PIB uptake, and was replicated in independent samples of NC and MCI subjects. Furthermore, PIB uptake was not correlated with the other brain volumes examined (caudate and whole brain volume), suggesting that the relationship between PIB uptake and HV is regionally specific and not due to general brain atrophy. This finding in normal subjects with relatively low PIB values implies that even slightly elevated global Aβ levels may inflict damage or coincide with neurotoxic events in hippocampus. Although Aβ plaques are not common in the medial temporal lobe (Arnold et al., 1991), possible mechanisms exist that may explain the observed relationship between Aβ burden and HV atrophy.

One possibility is that cortical Aβ burden leads to HV atrophy by disrupting cortico-hippocampal connectivity. Cortical connections with the hippocampus are associated with successful memory formation (Ranganath et al., 2005) and are compromised in AD (Greicius et al., 2004; Wang et al., 2006). Thus, cortical plaques may disrupt cortico-hippocampal networks, resulting in HV atrophy as innervation to this structure is eliminated. Another explanation is that cortical deposition of Aβ coincides with accumulation of neurofibrillary tangles (NFTs) in the hippocampus during the early stages of AD development. Although postmortem studies have shown that hippocampus atrophy correlates with NFTs (Braak and Braak, 1997; Jack et al., 2002), hippocampus atrophy is an indirect measure of this pathology, and PET imaging agents that directly target this pathology would help illuminate the role of NFTs in nondemented populations. A further possibility is that global Aβ plaque quantities may be a marker of soluble Aβ levels, which are undetected with PIB-PET imaging (Lockhart et al., 2007). Soluble species are considered the most toxic form of Aβ, and have been shown to correlate with synapse loss and disease severity better than Aβ plaques (Walsh and Selkoe, 2007). Thus, soluble Aβ may directly inflict hippocampal damage as plaques are deposited in cortex. Although the data presented in this study do not clarify the mechanism by which cortical Aβ burden and HV atrophy are related, the reproducibility of this relationship across three samples gives convincing evidence that such a relationship exists.

Aβ burden and Episodic Memory

We found a significant negative relationship between Aβ burden and EM in our primary normal control group, albeit driven by two high PIB subjects. This correlation was

not replicated in the other cognitive domains examined (working memory and frontal function), suggesting that episodic memory shows heightened vulnerability to Aβ accumulation (at least when levels of this pathology are high). This finding is consistent with longitudinal data showing that in most subjects EM is the first cognitive domain compromised in the years leading to AD onset (Grober et al., 2008; Small et al., 2000). One study to date has found a relationship between EM and PIB uptake within a group of normal individuals (Pike et al., 2007), and it is possible that our study lacked the statistical power to replicate this finding after excluding the two highest PIB subjects.

Although modest PIB increases were associated with HV atrophy in our data, these increases were not accompanied by EM memory deficits after removal of the two subjects with highest PIB values. This dissociation between Aβ burden and EM in this study may reflect a window in which cognitive reserve processes are sufficient to mask underlying pathological processes and brain atrophy (Stern, 2006). Supporting this hypothesis, it was recently shown that despite equivalent cognitive status, AD subjects with high education show more PIB uptake than AD subjects with low education (Kemppainen et al., 2008). In addition, relationships between EM and PIB uptake were more pronounced in the MCI subjects in whom Aβ levels are higher and reserve or compensatory processes are more likely to be exhausted. The role of cognitive reserve in dampening the relationship between Aβ burden and cognitive deficits is speculative in this dataset, and future studies that examine whether cognitive reserve measures are a modifying factor are needed to address this possibility.

The lack of association between Aβ burden and EM within the normal control groups may also be explained by a sequential relationship between the three variables examined, with HV mediating the relationship between Aβ burden and EM. In this study, we found evidence for this sequential relationship using a recursive regression procedure. A similar sequence has been suggested based on postmortem findings demonstrating that NFTs mediate the relationship between Aβ plaques and cognitive function (Bennett et al., 2004). Our results mirror these findings, using imaging measures (PIB-PET and MRI-derived HV) as a surrogate for Aβ and NFT pathologies. An indirect relationship between Aβ burden and cognitive change would make an association between these measures difficult to detect (especially within small groups of nondemented subjects) and may explain discrepancies among the studies that have examined this relationship.

Quantifying and classifying PIB uptake

We choose to quantify Aβ burden by averaging values across multiple cortical areas, an approach that has been employed by many other groups (Fotenos et al., 2008; Jack et al., 2008; Mintun et al., 2006; Pike et al., 2007; Rowe et al., 2007). It has long been established that the pattern of Aβ deposition varies between subjects (Braak and Braak, 1991) and we believe that this method gauges total Aβ quantity without overemphasizing a single brain region. However, it is possible that regional deposition of Aβ is biologically meaningful (Meyer-Luehmann et al., 2008) and should be addressed in future PIB studies of aging.

The general trend amongst postmortem and PIB-PET studies is to divide normal subjects into low- and high-pathology groups (Bennett et al., 2006; Fotenos et al., 2008; Goldman et al., 2001; Hulette et al., 1998; Jack et al., 2002; Mintun et al., 2006; Rowe et al., 2007; Schmitt et al., 2000). This approach is especially intriguing from the clinical

perspective since it provides a possible diagnostic criterion for at-risk individuals. However, the cutoff point for determining low- and high-groups is somewhat arbitrary and ignores all accumulation below the determined threshold. Furthermore, our study agrees with previous PIB-PET studies in demonstrating that PIB uptake values are continuous rather than dichotomous in cognitively normal populations (Jack et al., 2008; Pike et al., 2007; Rowe et al., 2007). By treating PIB index as a continuous variable in our statistical models, we found that quantities below this 'high-level' cutoff are meaningful and coincide with hippocampal atrophy in normal elderly subjects. It is likely that the negative impact of Aβ pathology begins during initial stages of accumulation in nondemented individuals, far before AD-comparable levels are reached. This point is further explored using a larger cohort of NC subjects in Appendix B.

Classification of MCI subjects as PIB+ is motivated by research showing that MCI subjects with high PIB uptake are likely to convert to AD (Forsberg et al., 2007). Furthermore, a postmortem study revealed that although the majority of amnestic MCI subjects that later convert to dementia have AD pathology, 29% show pathology in the medial temporal lobe unrelated to AD (Jicha et al., 2006). Using an ROC-curve approach to dichotomize ADNI MCI subjects based on PIB index values, 75% were classified as PIB+ while 25% were classified as PIB-. These percentages are consistent with the aforementioned postmortem study, and it is possible that pathological processes unrelated to AD are present in the hippocampus of the PIB- MCI subjects. Since the focus of this study was to examine the relationships between Aβ burden and preclinical AD markers, we deemed regression analyses within the group of PIB+ MCI subjects to be the most appropriate. Follow-up to determine whether PIB+ MCI subjects convert to AD and PIB- MCI subjects convert to other forms of dementia (such as Vascular Dementia, Frontotemporal Dementia, etc) will provide further support for dichotomizing this group.

Limitations

A main limitation in the present study is the small sample size of our normal control group. We addressed this concern by removing outliers and using a replication group from ADNI. Furthermore, many differences exist between the primary and replication groups that may have confounded results (such as differences in demographics, imaging acquisition, and neuropsychological testing). As larger samples are collected it will be possible to employ the replication group approach within a single cohort, achieving similarity across measures while varying the subjects in the primary and replication groups. Nevertheless, the reproducibility of results despite these differences suggests that the relationship between Aβ burden and HV will generalize to other populations. However, subjects recruited through BAC and ADNI may not be representative of the general population (for example, both groups were highly educated). Additionally, the cross-sectional design of this study allows only speculation that elevated PIB index is a preclinical AD marker. Longitudinal studies will help determine whether the presence of Aβ plaques predicts AD conversion, and whether this pathology precedes hippocampal atrophy and episodic memory decline.

Conclusions

Despite many differences across cohorts, we found an inverse relationship between Aβ burden and HV in two independent samples of normal elderly subjects. This finding was also observed in a PIB+ MCI group, strengthening the implication that levels of PIB uptake in nondemented populations is biologically meaningful. The exact mechanisms underlying this relationship between cortical Aβ burden and HV atrophy are unclear, and may reflect disruption of cortico-hippocampal connectivity, co-occurrence of cortical Aβ plaques and hippocampus NFTs, or the local impact of soluble Aβ species in the hippocampus. Within our primary NC group, the relationship between Aβ burden and EM was highly influenced by two high PIB subjects and did not replicate across different cohorts, suggesting that this relationship is more complex and may be modified by other factors (such as cognitive reserve and the degree of HV atrophy). The observed lack of association between Aβ burden and EM may also reflect a sequential relationship between the examined variables, with HV atrophy mediating the relationship between Aβ pathology and EM decline. Overall, these results suggest that low levels of Aβ accumulation may reflect early AD development and contribute to the HV atrophy and EM decline observed in studies of aging.

Chapter 3

Relationships between beta amyloid and functional connectivity in different components of the default mode network in aging

Abstract

Although Aβ deposition is a characteristic feature of AD, this pathology is commonly found in elderly normal controls. Given the impact of Aβ on synaptic function, it is likely that this pathology has early effects on brain function. Furthermore, the pattern of Aβ deposition as detected with PIB-PET imaging shows substantial spatial overlap with the default mode network (DMN), a group of brain regions that typically deactivates during externally driven cognitive tasks. In this study, we show that DMN functional connectivity (FC) during rest is altered with increasing levels of PIB uptake in normal controls. Specifically, FC decreases were identified in regions implicated in episodic memory processing (posteromedial cortex, ventral medial prefrontal cortex and angular gyri) whereas connectivity increases were detected in dorsal and anterior medial prefrontal and lateral temporal cortices. This pattern of decreases is consistent with previous studies that suggest heightened vulnerability of episodic memory related brain regions in AD, whereas the observed increases in functional connectivity may reflect a compensatory response.

3.1 Introduction

Although fibrillar beta amyloid (Aβ) plaques are a hallmark of Alzheimer's disease (AD) (Walsh and Selkoe, 2007), this pathology is frequently found in cognitively intact older people (Bennett et al., 2006; Davis et al., 1999; Hulette et al., 1998; Knopman et al., 2003; Price and Morris, 1999; Savva et al., 2009; Tomlinson et al., 1968). The recent advent of Pittsburgh compound-B positron emission tomography (PIB-PET) imaging allows *in vivo* investigation of fibrillar Aβ plaques (Klunk et al., 2004), and has been used to study the relevance of Aβ deposition in normal controls (NC) (Bourgeat et al., 2010; Dickerson et al., 2009; Jack et al., 2008; Mormino et al., 2009; Pike et al., 2007; Rabinovici and Jagust, 2009; Sperling et al., 2009; Storandt et al., 2009). Many researchers speculate that Aβ accumulation may be an initiating event that leads to neuronal dysfunction and neurodegeneration, cognitive loss and eventually AD (Jack et al., 2010a; Morris et al., 2009; Walsh and Selkoe, 2007).

Interestingly, Aβ plaque deposition shows a high degree of spatial overlap with a network of brain regions that together constitute the default mode network (DMN) (Buckner et al., 2005). Comprised of medial prefrontal, posteromedial (precuneus, posterior cingulate and retrosplenial) and lateral parieto-temporal cortices, as well as the medial temporal lobe, the DMN is typically deactivated during externally driven cognitive tasks and activated during internally driven processes, such as mind wandering, future planning and autobiographical memory (Buckner et al., 2008).

The DMN network is commonly studied with task-free resting state functional magnetic resonance imaging (fMRI) (Fox et al., 2005; Greicius et al., 2003). Functional connectivity (FC) analyses of resting state fMRI data captures brain regions showing correlated, low frequency (<0.1Hz) spontaneous activity, and have been used to define multiple networks with known anatomical connectivity and co-activation during task-related fMRI (Fox and Raichle, 2007). Independent components analysis (ICA) has been employed in some FC studies, robustly defining the DMN, as well as motor, sensory, and frontal-executive networks (Beckmann and Smith, 2004; Damoiseaux et al., 2006). Although the biological mechanism underlying these low frequency fluctuations remains unclear, it is possible that resting state networks reflect spontaneous cognitive processes, an intrinsic property of the brain's "baseline" state, or a combination of both (Buckner and Vincent, 2007; Raichle and Snyder, 2007).

Two recent studies combining PIB-PET imaging with resting state fMRI in NC showed that elevated Aβ deposition measured globally in cerebral cortex was associated with decreases in DMN FC (Hedden et al., 2009; Sheline et al., 2009). A question left unaddressed in these studies is whether the specific pattern of Aβ deposition is related to dysfunction in specific nodes of the network. Interestingly, there are discrepancies between the location of Aβ deposition and patterns of neuronal dysfunction seen with both imaging and neuropathology (Arnold et al., 1991; Bourgeat et al., 2010; Jack et al., 2008). In particular, the medial temporal lobe shows pronounced atrophy in AD when it shows little Aβ deposition, whereas the prefrontal cortex is relatively preserved despite extensive early PIB uptake (Jack et al., 2008). An area of convergence is in the precuneus/posterior cingulate, which shows both early hypometabolism (Minoshima et al., 1997) and Aβ deposition (Mintun et al., 2006). Studying the DMN in this context is important since nodes

of this network reflect both congruence and incongruence in the relationship between Aβ deposition and neuronal integrity.

The goal of this study was therefore to investigate associations between amyloid deposition and connectivity within the DMN and to examine mechanisms that might underlie network alterations.

3.2 Methods

Subject recruitment

Older NC subjects were recruited from the community via newspaper advertisement. Eligibility requirements for recruitment in this study were no MRI contradictions, living independently in the community, MMSE≥26, absence of neurological or psychiatric illness, lack of major medical illnesses and medications that affect cognition, and normal performance on cognitive tests. Forty-four subjects underwent positron emission tomography (PET) imaging and functional magnetic resonance imaging (fMRI) for this study.

Additionally, resting state fMRI data were collected on 17 young subjects to define a template for the DMN (mean age=23.0(2.9), 9 females). Young subjects were recruited from the community through online postings. PIB-PET data from 22 Alzheimer's disease (AD) patients were used for comparison purposes (mean age=65.9(10.7), 10 females). AD patients were recruited from the University of California San Francisco (UCSF) Memory and Aging Center. The diagnosis of AD was based on a comprehensive multi-disciplinary evaluation that includes a clinical history and physical examination, a caregiver interview and a battery of neuropsychological tests (Kramer et al., 2003). All AD subjects met NINDS criteria for probable AD (McKhann et al., 1984) and had no significant co-morbid medical, neurologic or psychiatric illnesses.

Neuropsychological Testing

All NC subjects underwent detailed cognitive testing in multiple domains to ensure normality. Normal cognitive performance was defined by creating composite scores in episodic memory [long delay free recall portion of the California Verbal Learning Test (CVLT) (Delis et al., 2000) and Wechsler Memory Scale (WMS-R) visual reproduction (Wechsler, 1987b)], working memory [Wechsler Adult Intelligence Scale (WAIS-R) digit span backwards (Wechsler, 1987a) and listening span total recall (Salthouse et al., 1991)] and frontal function [Trails B minus A (Reitan, 1958) and Stroop total correct in 60 seconds (Zec, 1986)] across a larger cohort of subjects ≥ 60 years old who underwent neuropsychological testing [198 subjects aged ≥ 60 were enrolled at the time of this study, mean age=73.1(7.6) and MMSE=28.7(1.7)]. Subjects were considered ineligible if 1 composite score fell below 2 standard deviations from our cohort defined age/gender/education adjusted means. The individuals in this cohort were high-functioning, such that a 2SD cutoff yielded raw scores that were generally well within the range of age-adjusted normative data. These scores are thus more conservative than normative-derived cut offs used in diagnosing MCI.

For subjects that had undergone multiple testing sessions, scores closest to the PET

scan date were used [mean delay between PET and closest testing session was 3.93 (2.62) months, and the maximum delay was 10.2 months]. Given the minimal amount of cognitive decline that may be expected in high PIB subjects in this short time period (Storandt *et al.*, 2009), as well as the very slow rates of change in PIB uptake over time (Engler et al., 2006; Jack et al., 2009), this short delay is unlikely to have any effect on the results.

PET acquisition

PIB was synthesized at the Lawrence Berkeley National Laboratory's (LBNL) Biomedical Isotope Facility using a published protocol and described in detail previously (Mathis et al., 2003; Mormino *et al.*, 2009). PIB-PET imaging was performed using a Siemens ECAT EXACT HR PET scanner (Siemens Medical Systems, Erlangen Germany) in 3D acquisition mode. 10-15 mCi of PIB was injected into an antecubital vein. Dynamic acquisition frames were obtained as follows: 4 x 15 sec, 8 x 30 sec, 9 x 60 sec, 2 x 180 sec, 8 x 300 sec and 3 x 600 sec (90 minutes total). A ten minute transmission scan for attenuation correction were obtained for each PIB scan. Filtered backprojected reconstructions were performed on the transmission and emission data to judge transmission alignment with each frame of emission data. In the case of misalignment, the transmission image was coregistered to that individual emission frame, and then forward projected to create an attenuation correction file specific to that head position. PET data were reconstructed using an ordered subset expectation maximization algorithm with weighted attenuation. Images were smoothed with a 4mm Gaussian kernel with scatter correction.

MRI acquisition

Magnetic resonance imaging (MRI) data on old and young NC subjects were collected at LBNL on a 1.5T Magnetom Avanto System (Siemens Medical Systems, Erlangen Germany) with a 12 channel head coil run in triple mode. The MRI session includes the following sequences (in order of acquisition): a T2-weigted fluid attenuated inversion recovery scan (FLAIR, axially acquired, TR/TE=9730/100ms, flip angle = 150°, 0.80x0.80mm^2 in plane resolution, 3.00mm thickness with no gap), 3 T1-weighted volumetric magnetization prepared rapid gradient echo scans (MPRAGE, axially acquired, TR/TE/TI=2110/3.58/1100ms, flip angle = 15°, 1.00x1.00mm^2 in plane resolution, 1.00mm thickness with 50% gap), a T1 structural scan in plane to the resting state scan (axially acquired, TR/TE=500/10ms, flip angle = 150°, 0.80x0.80mm^2 in plane resolution, 3.5mm thickness with 15% gap), and a resting state functional MRI scan (acquired axially, TR/TE=1890/50ms, flip angle = 90°, 3.0x3.0mm^2 in plane resolution, 3.5mm^3 thickness with 15% gap, 250 TRs total). The FLAIR scan was used to screen for stroke, whereas the in plane T1 and MPRAGE scans were used in subsequent processing steps. There was a mean time delay of 2.7(6.3) months between PET and MRI scanning.

Resting state fMRI was not available for UCSF AD subjects. MPRAGE scans for these subjects were used in the analysis of PIB-PET data. For 13 UCSF AD subjects, MPRAGE scans were collected coronally on a 1.5T Vision System (Siemens Medical Systems, Erlangen Germany) with a quadrature head coil (TR/TE/T1=10/7/300ms, flip angle = 15°, 1.00x1.00mm^2 in plane resolution, 1.40mm slice thickness with no gap). For the remaining 9 UCSF AD subjects, MPRAGE scans were collected sagittally on a Bruker MedSpec 4T

system with an 8 channel head coil (TR/TE/T1=2300/3.37/950ms, flip angle = 7°, 1.00x1.00mm^2 in-plane resolution, 1.00mm slice thickness with no gap).

PET preprocessing

PIB data were preprocessed using the SPM2 software package (http://www.fil.ion.ucl.ac.uk/spm). Realigned PIB frames corresponding to the first 20 minutes of acquisition were averaged and used to guide coregistration to the subject's structural MRI scan. Distribution volume ratios (DVRs) for PIB images were created using Logan graphical analysis with frames corresponding to 35-90 min post-injection and a gray matter masked cerebellum reference region (Logan et al., 1996; Price et al., 2005).

When applicable, PET images were co-registered to the subject's high-resolution structural scan, and transformed to MNI space using parameters defined from non-linear alignment between the high-resolution structural scan and MNI template (see the fMRI preprocessing section). After normalization to template space, these PET images were smoothed an additional 8mm, resulting in a total of 8.9mm smoothing for these images.

Structural MRI processing

MPRAGE scans were processed as described previously using FreeSurfer version 4.3 (http://surfer.nmr.mgh.harvard.edu/) (Mormino *et al.*, 2009). In brief, MPRAGE scans were realigned and averaged to create a single high-contrast structural image. Anatomical masks relevant to PET processing were derived in each subject's native space using this analysis stream (Dale et al., 1999; Fischl et al., 2001; Fischl et al., 2002; Segonne et al., 2004). Specifically, a gray matter only cerebellum mask was used as a reference region for PIB and the mean PIB DVR value from a FreeSurfer derived cortical gray matter mask was extracted for each subject and used as a measure of global PIB uptake ("global PIB") and as a regressor in the voxelwise FC analysis. These global PIB values were highly correlated with the PIB index value used in our previous publication (R^2=0.98) (Mormino *et al.*, 2009).

fMRI preprocessing

fMRI data were processed using FSL version 4.1 (http://www.fmrib.ox.ac.uk/fsl). Images were motion corrected, lowpass (2.8s) and highpass filtered (100s) and smoothed with a 5mm Gaussian kernel. To define the spatial transformation from fMRI space to MNI template space, a multistep registration procedure was employed. First, the mean fMRI image was linearly registered to the subject's in plane T1 structural image using 7 degrees of freedom. The in plane T1 image was then registered to the high-resolution structural scan using 6 degrees of freedom. Finally, the high-resolution structural scan was nonlinearly aligned to the standard MNI 152 brain using FNIRT, and resulting parameters were used to transform fMRI data.

Functional connectivity analysis

Functional connectivity analyses were conducted with FSL version 4.1 and adapted from the goodness of fit procedure described by Greicius et al. (Greicius et al., 2004). Supplementary figure 1 in Appendix A provides a detailed schematic flow chart of the processing stream. A DMN template was defined using resting state fMRI data from the group of 17 young subjects. A seed in the posterior cingulate cortex (sphere of 8mm centered at MNI coordinates -12, -50, 32) was transformed from template space into native

fMRI space for each young subject. Additionally, nuisance regions were defined on the MNI template and transformed to native space (a white matter 8mm spherical seed centered at MNI coordinates -24, -16, 36, a lateral ventricle mask drawn on the template, and a whole brain mask derived from segmenting the template brain and combining gray and white matter). Time-series were extracted across all these regions and entered into a general linear model, and resulting contrast maps reflecting voxels correlated with the PCC time-series (covarying the signal associated with white matter, lateral ventricle and whole brain) were entered into a higher-level 1-sample t-test (height and extent joint threshold of $p<0.05$, corrected). Based on evidence that the DMN may be "split" into posterior and anterior components with ICA (Damoiseaux et al., 2008; Damoiseaux *et al.*, 2006), we excluded the anterior mPFC portion from this map and used the remaining posterior clusters as our template during the goodness of fit procedure (a "posterior" DMN template). This would ensure that posterior DMN components were selected for subjects with separable DMN components (27/44 subjects showed separable DMN components). A posterior rather than anterior template approach was employed because the posterior regions of the DMN have been implicated in episodic memory processes (Andrews-Hanna et al., 2010) and show early dysfunction in Alzheimer's disease (Killiany et al., 2002; Minoshima *et al.*, 1997; Sorg et al., 2007; Thompson et al., 2007). Resting state data for each older NC was decomposed at the individual subject level using independent components analysis (ICA) with FSL's MELODIC (Beckmann and Smith, 2004). MELODIC isolates a multitude of components for each subject, and for each component voxels are assigned a z-score that reflects the extent to which that voxel's timeseries is correlated with the time-series associated with the specific component. A goodness of fit procedure was applied to spatially normalized z-maps for each subject to determine which component most closely resembled the DMN template (average z-score of voxels within the template minus average z-score of voxels outside the template; z-values from the removed mPFC area were excluded from this calculation to ensure that high mPFC connectivity did not inflate the average value "outside" the template). The z-map for the best-fit component for each subject was used in subsequent higher-level analyses.

Statistical Analyses

Correlations between global PIB and demographic variables were completed using the statistical programming language R version 2.8 (http://www.r-project.org/). Partial correlation coefficients (r) were reported for relationships between global PIB and episodic memory/MMSE (controlling for demographic predictors). Caret version 5 was used to display voxelwise results (http://brainvis.wustl.edu/wiki/index.php/Caret:About).

Spatial overlap between the DMN and PIB uptake was qualitatively examined by overlaying statistical maps. The DMN FC map was derived from a 1-sample t-test of DMN best-fit components from the elderly NC group whereas the PIB uptake map was derived from contrasting low PIB NC with high PIB NC DVR images (defined with a median split of global PIB values). The FC map was thresholded at $p<0.001$ and $k=100$, uncorrected and the PIB map was thresholded at $p<0.0002$ and $k=100$, uncorrected, binarized and overlaid upon a 3D rendered brain.

Within the NC group, global PIB was treated as a continuous value and regressed against voxelwise DMN FC using permutation testing with FSL's Randomise (using 5000 permutations, http://www.fmrib.ox.ac.uk/fsl/randomise/). This analysis was restricted to

the voxels that were significant in the DMN 1-sample t-test of elderly NC subjects (thresholded at $p<0.001$ and $k=100$, uncorrected; this mask is displayed in figure 1). Age, gender and education were controlled for in this analysis, and results were considered significant at $p<0.05$ and $k=50$, uncorrected. Cluster size, maximum t-statistic/p-value, and peak MNI coordinates for significant regions are reported.

To explore focal PIB uptake within regions showing a relationship between FC and global PIB, ROI analyses were completed with R. Regions of interest (ROIs) were created from the primary FC voxelwise results by casting an 8mm sphere around the voxel with the highest t-value in a subset of significant clusters (voxels showing the strongest relationship between FC and global PIB). PIB values from these ROIs were extracted from spatially normalized PET images. A repeated measures ANOVA was conducted with PIB DVR values as the dependent variable, group (AD and NC) as a between-subjects factor and ROI as a within-subjects factor. Main effects of group and ROI were investigated further with post-hoc contrasts [(1) AD versus NC for each ROI, (2) each ROI versus global PIB controlling for diagnosis]. Within the NC group, mean FC was extracted from these ROIs and regressed against episodic memory. Age, gender and education were controlled for in each model. Results were considered significant at $p<0.05$.

3.3 Results

Demographics

Demographics for elderly NC subjects are listed in table 1. There was a significant relationship between global PIB and gender ($p=0.03$; higher PIB in females) and a trend between global PIB and age ($p=0.08$; higher PIB in older subjects).

Table 1: Subject characteristics

		Relationship with global PIB
N	44	--
Age	74.6 (6.3)	**r=0.27; t= 1.79, p=0.08**
Gender	29F, 15M	**r=-0.32, t=-2.20, p=0.03**
Education	17.1 (1.9)	r=-0.13, t= -0.82, p=0.42
MMSE	29.0 (1.1)	r=-0.08, t=-0.55, p=0.58
EM	0.22 (0.71)	r=-0.19, t= -1.31, p=0.20

Table 1: Cohort demographics and correlations with global PIB. Mean and standard deviations are listed for continuous variables. Demographic variables (age, gender and education) were controlled when examining relationships between global PIB and MMSE/EM. Significant relationships and trends are bolded. MMSE=Mini Mental State Examination. EM=Episodic memory.

Spatial Overlap of DMN and Aβ deposition

Results from the 1-sample t-test of best fit components of the DMN in elderly NC revealed significant clusters in medial and lateral prefrontal cortex, posteromedial cortex (precuneus/posterior cingulate and retrosplenial cortices), lateral parietal, middle temporal, and medial temporal cortices. Overlap between the DMN and Aβ deposition is displayed in figure 1. There is a large degree of convergence between DMN FC and PIB

uptake, most notably in the precuneus/posterior cingulate, angular gyri, and medial prefrontal cortex whereas limited overlap was present in the medial temporal lobe.

Figure 1: DMN functional connectivity and global PIB uptake overlap

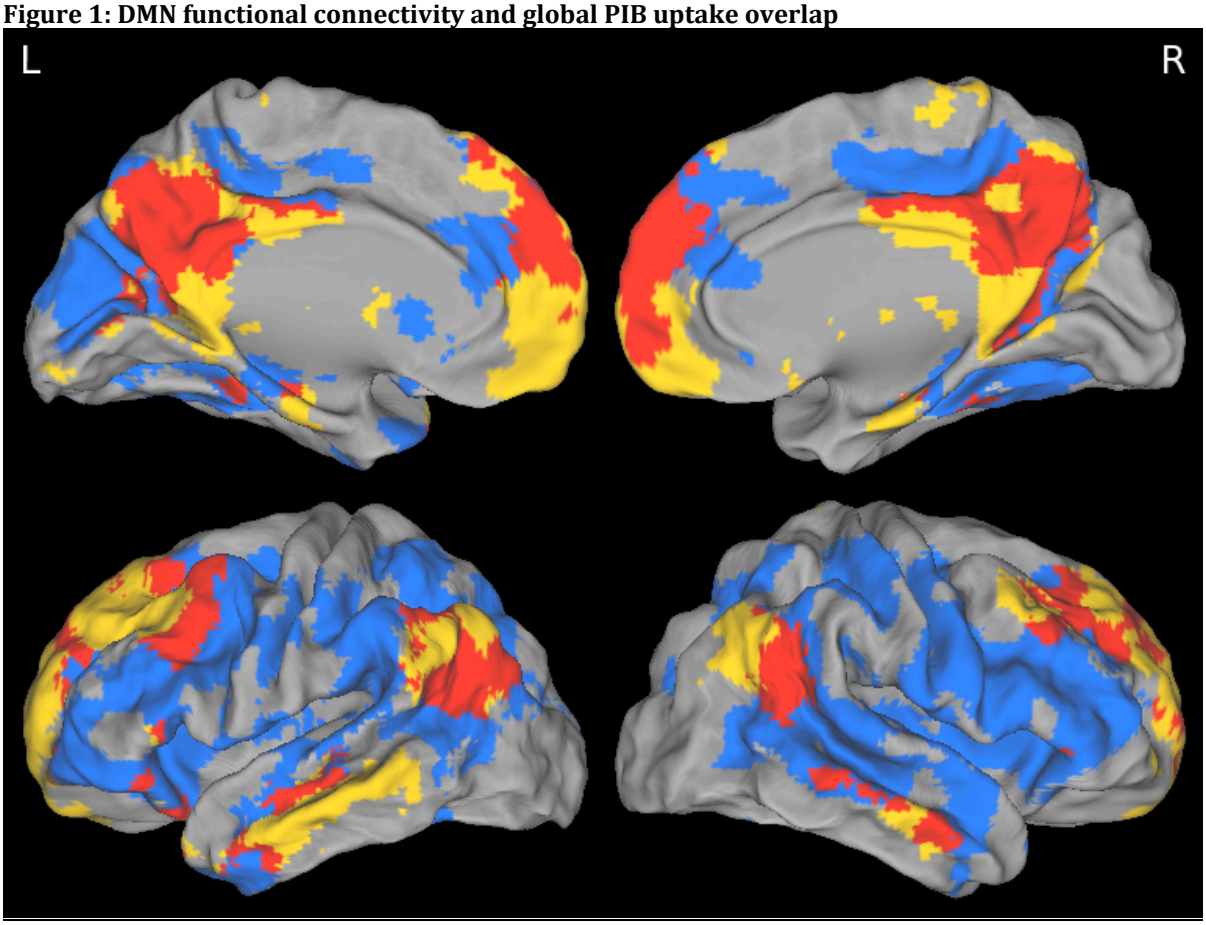

Figure 1: One sample t-test of DMN best-fit components (yellow), 2-sample t-test between high and low PIB subjects (blue) and overlap (red) are displayed. These maps highlight congruence and incongruence between the DMN and brain regions showing high levels of Aβ deposition. The greatest amount of overlap is in precuneus/posterior cingulate, medial prefrontal and angular gyri. Although PIB uptake is more diffuse than the DMN, there is minimal overlap in retrosplenial and medial temporal portions of the DMN.

Global PIB versus DMN FC

To examine the relationship between Aβ deposition and DMN FC, global PIB values were regressed against voxelwise DMN FC maps (figure 2 and table 2). Multiple regions in the posteromedial cortex showed reduced FC with increased levels of PIB (precuneus, posterior cingulate and retrosplenial cortex). Elevated PIB was also associated with decreased DMN FC in ventral medial prefrontal cortex, angular gyri, and the left middle and superior frontal gyri. Additionally, there were areas of the DMN that showed increased FC with higher levels of global PIB (right dorsal prefrontal, left anterior medial prefrontal and left middle temporal cortices). This analysis was repeated using PIB data that was corrected for partial volume effects as described in our previous publication (Mormino *et al.*, 2009), and results did not differ (see Appendix A: supplementary figure 2).

Given the novel finding of increased DMN FC with elevated PIB in NC, we conducted a series of seed based analyses similar to the methods employed in the two previously published papers examining DMN FC and PIB in NC (Hedden *et al.*, 2009; Sheline *et al.*, 2009). These analyses were consistent with the results obtained using ICA (see Appendix A: supplementary analysis 1, supplementary figures 3 and 4).

Figure 2: Global PIB versus DMN FC

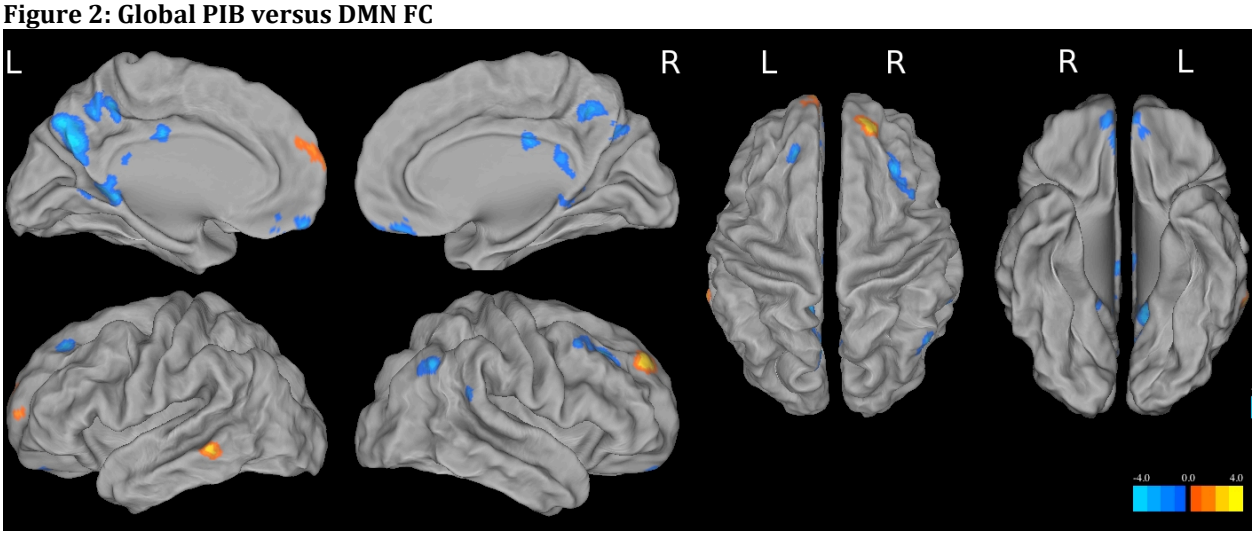

Figure 2: T-maps from voxelwise analysis correlating global PIB with DMN FC. Cool colors reflect a negative relationship whereas warm colors reflect a positive relationship between global PIB and DMN FC.

Table 2: Results from primary voxelwise analysis.

Location	Max T	Max P	Voxels	x	y	z
Negative Correlations						
L precuneus	3.68	0.0002	692	-4	-68	26
Bilateral ventral medial prefrontal cortex	3.55	0.001	113	2	36	-24
L retrosplenial cortex	3.27	0.001	133	-12	-48	-2
L posterior cingulate cortex	3.24	0.0002	69	0	-26	26
R middle frontal cortex	3.19	0.001	169	28	22	40
R angular gyrus	3.06	0.001	71	64	-46	16
R retrosplenial cortex	3	0.004	50	22	-50	4
Bilateral ventral medial prefrontal cortex	2.93	0.001	226	0	52	-20
R angular/occipital cortex	2.84	0.001	67	46	-62	36
L superior frontal gyrus	2.64	0.006	63	-18	30	44
R posterior cingulate	2.31	0.011	52	6	-44	16
R precuneus	2.11	0.017	54	10	-66	30
Positive Correlations						
R dorsal prefrontal cortex	3.91	0.001	162	14	42	34
L anterior medial prefrontal cortex	3.37	0.002	199	-8	66	14
L middle temporal gyrus	3.11	0.002	51	-66	-44	-8

Table 2: Regions showing negative and positive relationships between global PIB and DMN functional connectivity are listed. Values corresponding to the voxel within each cluster showing the strongest association between PIB and DMN FC are listed, as well as cluster size. Italics indicate regions selected for additional ROI analyses.

Co-localization of PIB uptake and Aβ-related DMN FC differences

To further explore Aβ-related DMN FC differences, the 6 ROIs showing the strongest negative and positive correlation with PIB (table 2 and Appendix A, supplementary figure 5) were selected from the ICA voxelwise analysis: ROIs in the left precuneus (L Precun), ventral medial prefrontal cortex (vmPFC) and left retrosplenial cortex (L RSC) that showed reduced FC with increased global PIB, as well as ROIs in right dorsal prefrontal (R dPFC), L anterior medial prefrontal (L amPFC) and left middle temporal gyrus (L MTG) that showed heightened FC with increased global PIB. Average PIB values were extracted from these ROIs and entered into a repeated measures ANOVA with diagnosis (AD, NC) as a between subjects factor and ROI as a within subjects factor (values across all ROIs are plotted in figure 3). To understand where PIB is elevated in NC and how this elevation differs from AD and across regions, this analysis was restricted to high PIB NC subjects (determined via a median split within the NC group). This analysis revealed significant main effects of both diagnosis ($F=33.132$, $p<0.001$) and ROI ($F=76.372$, $p<0.001$). Post-hoc contrasts between AD and NC revealed significant elevation in AD in all ROIs (Appendix A: supplemental table 1). To understand whether there was an appreciable pattern of uptake amongst these ROIs, each ROI was contrasted against global PIB (controlling for diagnosis). This analysis did not reveal concordance between PIB uptake and the direction of the ROI's relationship between global PIB and FC (ie 1 region showing decreased FC with elevated global PIB was significantly higher than global PIB (L Precun) where 1 region was significantly lower (L RSC); additionally, 1 region showing increased FC with more PIB was significantly higher than global PIB (R dPFC) whereas 2 regions were lower (L amPFC and LMTG); see Appendix A: supplemental table 1.)

To continue exploring a potential relevance of regional PIB uptake, we conducted an additional analysis to determine if focal PIB across any ROI shows heightened relevance to DMN FC (Appendix A: supplemental analysis 2). Specifically, it is possible that intra-regional PIB is strongly related with FC in specific DMN areas, or that PIB uptake in one region is a strong predictor of FC changes in distant DMN regions. To investigate this possibility, we conducted a series of regression analyses relating FC to PIB within each ROI and across ROIs. This analysis did not reveal evidence for a specific impact of regional PIB—areas that show relationships with increased PIB tend to do so across multiple PIB ROIs and to a similar extent to the correlation with global PIB (Appendix A: supplemental table 2). It is possible that the high covariance in PIB uptake across regions makes regional contributions difficult to disentangle (Appendix A: supplemental table 3).

Figure 3: Global and regional PIB values

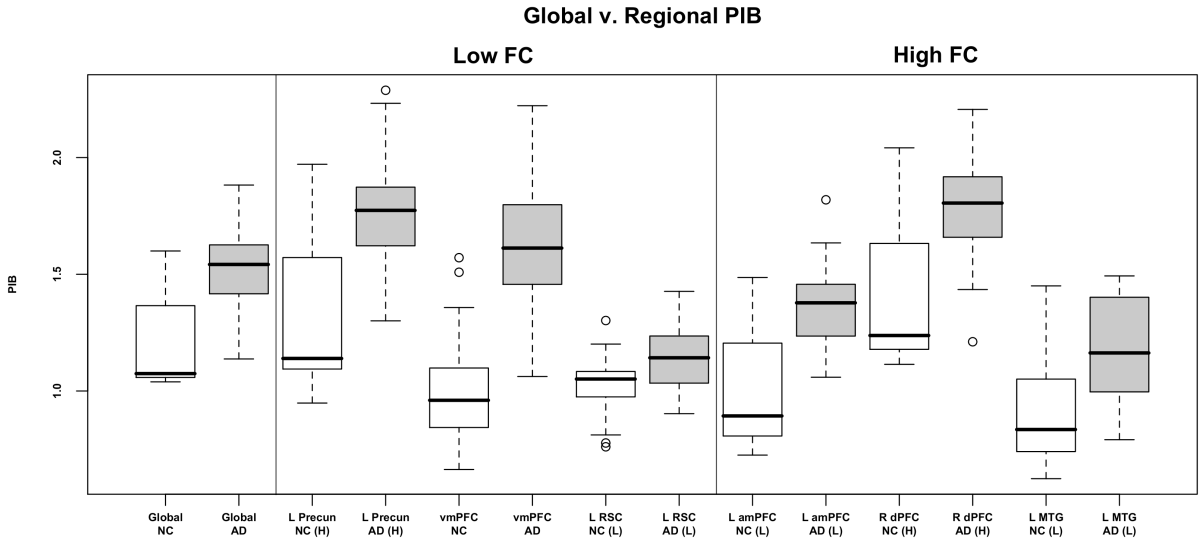

Figure 3: Boxplots of global and regional PIB values in high PIB NC (white boxes) and AD (gray boxes). Although AD subjects show heightened PIB, overlap between AD and NC suggests the early Aβ deposition in NC. Despite low PIB uptake in L RSC, L amPFC, and L MTG, these regions show FC changes with increased levels of global PIB. Precun=precuneus, vmPFC= ventral medial prefrontal cortex, RSC=retrospelinial cortex, amPFC=anterior medial prefrontal cortex, dPFC=dorsal prefrontal cortex, MTG=middle temporal gyrus.

Relationships between Aβ-related DMN FC differences and EM

Episodic memory (EM) was not correlated with global PIB (t=-1.31, p=0.20). There was a trend for a positive relationship between EM and DMN FC in RSC (t=1.82 p=0.08), and no other relationships were found with FC from any other ROI.

3.4 Discussion

In this study, we found relationships between global PIB uptake and DMN resting state FC in a group of elderly cognitively intact individuals. Specifically, increased Aβ deposition was associated with decreased DMN FC in multiple posteromedial regions (precuneus/posterior cingulate and retrosplenial cortices), as well as ventral medial prefrontal cortex, angular gyri, and the left middle and superior frontal gyri. These regions showing decreased DMN FC are consistent with previous studies combining resting state fMRI and PIB-PET imaging in NC (Hedden *et al.*, 2009; Sheline *et al.*, 2009) and have furthermore shown changes across multiple imaging modalities, demonstrating both glucose hypometabolism and atrophy in early AD (de Leon *et al.*, 2001; Greicius *et al.*, 2004; Killiany et al., 2002; Minoshima *et al.*, 1997; Sorg et al., 2007; Thompson et al., 2007). Interestingly, we also found that elevated PIB was associated with increased DMN FC in right dorsal prefrontal, left anterior medial prefrontal and left middle temporal cortices, which may reflect either compensatory processes or aberrant activity. Importantly, this dissociation was consistent across multiple analytic approaches, suggesting that these

results are not a methodological artifact. Furthermore, relationships between imaging measures and episodic memory were either absent or weak, suggesting that Aβ-related changes in DMN FC occur in the absence of overt cognitive deficits.

Differential relationships between DMN FC and Aβ may reflect region-specific properties

The results identified in this study suggest that regions within the DMN respond differently to high levels of Aβ deposition, and it is possible that the impact of this pathology is modified by region-specific properties. Interestingly, the reported pattern of Aβ-related FC differences aligns with proposed subsystems of the DMN (Andrews-Hanna et al., 2010; Greicius et al., 2009). Andrews-Hanna et al., 2010 recently described two distinct DMN subsystems that interact via the posterior cingulate cortex and the anterior mPFC (the "midline core"): a medial temporal lobe subsystem involved in episodic memory processes and a dorsal mPFC subsystem involved in self-relevant processes. Interestingly, the pattern of Aβ-related decreased FC identified in our study shows substantial overlap with the medial temporal lobe subsystem (retrosplenial cortices, ventral medial prefrontal cortex, angular gyri as well as regions in posteromedial cortex that may be considered part of the midline core). Furthermore, the pattern of Aβ-related increased FC overlaps with the dorsal mPFC subsystem (dorsal PFC and lateral temporal cortex, as well as a region in the anterior mPFC that may be considered part of the midline core).

This spatial dissociation of Aβ-related FC changes suggests differential effects on DMN subsystems. The pattern of decreased FC in the episodic memory/medial temporal subsystem suggests heightened vulnerability of this DMN subsystem to Aβ deposition, and is consistent with the trend we observed between decreased RSC FC and lower EM performance in our subjects. These results are consistent with two recently published resting state studies examining Aβ in aging (Hedden *et al.*, 2009; Sheline *et al.*, 2009) as well as numerous reports of brain changes to the medial temporal subsystem in AD; it is possible that disconnection in these regions eventually leads to more severe changes (such as neuronal atrophy) and underlies the episodic memory deficits observed in AD.

The pattern of increased FC observed in this study may be compensatory, excitatory, or a combination of both. Although the biological relevance of increased FC during rest is unclear, recent reports have suggested a compensatory role of elevated FC in subjects at risk for AD (Filippini et al., 2009; Qi et al., 2009). In the context of our study, it is possible that increased FC may compensate for failing medial temporal subsystem regions (Reuter-Lorenz, 2002), such that the DMN has a compensatory "shift" towards the dorsal mPFC subsystem as the medial temporal subsystem is negatively affected by Aβ. Consistent with potential compensatory capabilities, the PFC in particular appears less vulnerable to Aβ toxicity than posterior DMN regions, with PFC neuronal dysfunction associated with late stages of AD (Langbaum *et al.*, 2009) despite evidence of early PFC Aβ deposition (Mintun *et al.*, 2006). It has been proposed that brain regions show different time delays between initiating Aβ deposition and resulting regional abnormalities, with speculation that PFC has the longest delay (Jack et al., 2010a). Given these characteristics, the PFC is a potential source of compensation in response to Aβ accumulation, in particular the dorsal and anterior mPFC portion of the DMN. A compensatory shift towards the dorsal mPFC system may reflect neuronal plasticity or the potential to deploy new cognitive strategies in the face of Aβ deposition. Although not tested in this study, it is possible that high PIB subjects

have adopted new strategies that rely on cognitive processes subserved by the dorsal mPFC subsystem, such as self-referential processing during encoding (Andrews-Hanna 2010). Future studies that examine encoding strategies in aged individuals with high levels of Aβ deposition will offer insight into this potential source of neuronal compensation.

Conversely, FC increases may reflect an early aberrant excitatory response to Aβ. Interestingly, a recent task-related fMRI study reported a failure to deactivate medial prefrontal, precuneus/posterior cingulate and lateral temporal cortices during successful episodic memory encoding in elderly adults with elevated PIB uptake (Sperling *et al.*, 2009). The authors proposed that Aβ deposition may cause aberrant modulation in these DMN regions and it is possible that persistent activation in these areas reflects the aberrant spiking activity that has been seen with *in vitro* models and which may be excitotoxic (Palop et al., 2007). Although it is difficult to reconcile the results of task related fMRI and resting state FC studies, the fact that increases within DMN regions were observed in both contexts is intriguing. Inability to modulate DMN regions may additionally facilitate a cyclical process that promotes further Aβ production (Cirrito *et al.*, 2005) and eventually hypoactivation. This is consistent with observations that in AD patients regions in the dmPFC subsystem display the same pattern of DMN FC decreases that we identified in the medial temporal lobe subsystem in normal elderly (Greicius *et al.*, 2004). In this context compensatory and aberrant hyperactivation are not necessarily mutually exclusive; it is possible that compensatory responses may ultimately lead to downstream activity reductions as neurons undergo excitotoxicity.

Global versus regional Aβ deposition

The results presented in our primary analysis focused on relationships between global Aβ levels and FC in DMN regions. It is possible that differential deposition of Aβ in different subsystems or nodes of the DMN could be responsible for our reported regions of increased, as opposed to decreased FC. We explored these possibilities by examining the pattern of PIB uptake within regions showing strong relationships with global PIB and identified significant elevation in PIB uptake in AD compared to NC across all ROIs. Interestingly, we found that ROIs showing significant elevation compared to our global measure of PIB were present for ROIs showing both increased FC (R dPFC) and decreased FC (L Precun). The same pattern was observed for ROIs with significantly lower PIB than the global measure (increased FC: L amPFC and L MTG; decreased FC: L RSC). These findings were independent of diagnosis, suggesting that these low ROIs remain low even in the context of AD (when amyloid levels are much higher and more neuronal dysfunction has occurred).

To address the possibility of heightened relevance of amyloid in individual ROIs, we directly compared intra- and interregional relationships in DMN ROIs between PIB and FC. This analysis did not provide evidence for relationships that were specific to regional PIB uptake (areas that show relationships between FC and PIB tend to do so across multiple PIB ROIs). However, it is likely that high covariance amongst all regions made such a relationship difficult to detect.

It is possible that these null findings may be attributable to an inability to capture focal DMN changes before widespread Aβ deposition occurred. In particular, the precuneus and posterior cingulate cortex are likely candidates for focal effects of Aβ since

these regions have dense connections within and beyond the DMN (Buckner et al., 2009; Hagmann et al., 2008), and it is possible that disruption in either of these regions would affect other DMN regions. Studies that focus on earlier stages (ie. involving younger samples) may be able to capture initial Aβ deposition before widespread highly correlated uptake is observed, and will help clarify whether regional PIB has an impact. A further possibility is that fibrillar Aβ is not a primary pathological cause of disrupted DMN FC. It is possible that regional levels of soluble Aβ or neurofibrillary tangles may cause connectivity decreases within DMN nodes. Since PIB-PET binds predominately to fibrillar forms of Aβ (Ikonomovic et al., 2008), our data are unable address these potential relationships.

Overall, although the mechanism by which heightened Aβ levels affect the DMN in a widespread fashion remains unclear, our data suggests that Aβ-related DMN changes are not exclusively related to focal Aβ deposition, but rather reflect the interaction of a global pathological process with properties of the distinct DMN components (ie. nodes in the episodic memory subsystem of the DMN may show heightened vulnerability to amyloid deposition, whereas nodes in the dmPFC subsystem may show compensatory capabilities).

Relationships with episodic memory

Studies using PIB-PET imaging in NC have failed to find a consistent relationship between elevated PIB and concurrent EM (Jack et al., 2008; Mormino et al., 2009; Pike et al., 2007). However, recent studies have shown that elevated PIB is associated with subsequent cognitive decline in NC (Morris *et al.*, 2009; Storandt *et al.*, 2009). According to the timeline posited by Jack et al 2010, the relationship between EM and Aβ deposition within NC may be influenced by mediating factors (Jack et al., 2010a), which likely obscures potential correlations between EM and Aβ. Potential mediating factors include downstream changes caused by Aβ toxicity, such as neurofibrillary tangle deposition and neuronal loss (Bennett et al., 2004; Mormino *et al.*, 2009).

Relationships with EM investigated in this study were either null or weak. The correlation between global PIB and EM was insignificant, whereas there was a trend with DMN FC in left RSC. This pattern is consistent with FC changes representing downstream effects of Aβ toxicity, but the weak associations do not allow us to draw conclusions about the potential mediation of PIB effects on EM by DMN FC. Overall, our results emphasize that Aβ deposition and corresponding brain changes occur in subjects without overt cognitive deficits.

Limitations

This study has several limitations. PIB does not bind to diffuse plaques or soluble Aβ (Ikonomovic *et al.*, 2008), which may show more relevance than fibrillar Aβ in evaluating the regional impact of this pathology on DMN FC. The statistical thresholds used in our voxelwise analyses were liberal. However the pattern of DMN FC decreases is consistent with a large body of literature that suggests selective vulnerability of posterior episodic memory related regions in early AD development. Furthermore, the ability to detect regional effects of amyloid may be limited by the high covariance of PIB values across brain regions—studies with more subjects will be necessary to untangle potential relationships with regional deposition. Another limitation is reliance on cross sectional cognitive testing scores. Longitudinal cognitive data may be a superior indictor of

preclinical AD and show higher correlations with PIB and resting state DMN FC measures. Lastly, our analysis was limited to cognitively normal elderly individuals; a group in which small effect sizes are expected and studies with larger numbers are warranted.

Chapter 4

Beta amyloid deposition in aging is associated with beneficial increases in brain activation during successful memory encoding

Abstract

Although Aβ has been proposed to play a role in the etiology of AD, relationships between this pathology and neural function is unclear, especially during beginning stages of Aβ deposition. Furthermore, it is possible that compensatory neural processes exist that allow elderly normal controls (NCs) to remain cognitively intact despite pathological burden. To investigate these early effects of Aβ on neuronal function, elderly NCs were scanned with fMRI while performing an episodic memory encoding task of natural scenes, and relationships between brain activation and Aβ burden were assessed across task-positive (regions showing greater activation for subsequently remembered versus forgotten scenes) and task-negative regions (regions showing greater deactivation for subsequently remembered versus forgotten scenes). At the group level, significant activation in task-positive regions was present in a distributed network spanning ventrolateral prefrontal, lateral occipital, lateral parietal, posterior inferior temporal and the right parahippocampal/hippocampus, whereas deactivation was present in many default mode network regions (DMN; posteromedial, medial prefrontal, and lateral temporoparietal cortices) as well as in areas outside the DMN (bilateral medial occipital cortex, superior/dorsolateral prefrontal and left central/postcentral gyri). Task-positive activation was higher in PIB+ compared to PIB- elderly subjects, and this activation was positively correlated with memory performance within the PIB+ group. Although we didn't identify a relationship between impaired deactivation in PIB+ compared to PIB- subjects, a multiple regression approach revealed dissociable effects of activation and deactivation on performance within PIB+ subjects, suggesting that these networks have independent contributions to performance in this group (greater activation was associated with better performance whereas impaired deactivation was associated with worse performance). Overall, these results suggest that beneficial heightened activation during episodic memory encoding is present in NC elderly subjects with high Aβ.

4.1 Introduction

Modifying effects of cognitive reserve processes

The majority of work investigating early stages of Aβ deposition has focused on detrimental effects associated with this pathology (Becker et al.; Chetelat et al.; Dickerson et al., 2009; Mormino et al., 2009; Sperling et al., 2009; Storandt et al., 2009). Although converging evidence supports a negative impact of Aβ (Rabinovici and Jagust, 2009; Walsh and Selkoe, 2007), factors may exist that enable individuals to cope with this pathology, or at least extend the delay period between Aβ deposition and subsequent cognitive decline (Jack et al., 2010a). These protective factors are often described as cognitive reserve processes—it has been speculated that for a given level of pathological burden, an individual with high cognitive reserve will cope more optimally than an individual with low cognitive reserve (Stern, 2006). Traditionally, cognitive reserve has been quantified using gross measures such education, IQ, and socioeconomic status (SES), all of which have been shown to have protective effects against Alzheimer's disease (AD).

Initial PIB-PET studies have begun to uncover relationships between Aβ burden, cognitive reserve, and cognition, helping to elucidate mechanisms by which cognitive reserve is protective against cognitive decline. For instance, AD patients with high education show more PIB uptake than AD patients with low education, despite equivalent cognitive impairment across groups (Kemppainen et al., 2008). Fotenos et al reported that cognitively intact older normal controls (NCs) with high socioeconomic status (SES) had more brain atrophy than NCs with low SES for a given level of cognitive function, and that brain atrophy was in turn related to PIB uptake (ie. although Aβ burden is associated with brain atrophy, the relationship between neural damage and cognition was dampened in individuals with high reserve) (Fotenos et al., 2008). Consistent with this pattern, Rentz et al showed a lack of relationship between PIB uptake and cognition amongst high IQ NC subjects, whereas relationships were identified in low IQ subjects (Rentz et al., 2010). These results are consistent with the cognitive reserve theory, and extend our understanding of underlying mechanisms by drawing direct links with Aβ deposition.

Although the aforementioned studies have focused on measures of education, SES and IQ to assess cognitive reserve levels, neural evidence for cognitive reserve has been suggested in neuroimaging studies of aging (Park and Reuter-Lorenz, 2009; Reuter-Lorenz, 2002; Stern, 2006). It has been proposed that neural compensation may manifest as a higher magnitude of activation in regions typically engaged, as well as the recruitment of additional regions during a specific cognitive task. Consistent with this theory, researchers examining episodic memory change in aging have shown that recruitment of additional PFC regions may be beneficial to cognitive performance in older adults (Cabeza et al., 2002; Morcom et al., 2003; Rosen et al., 2002). Additionally, neural compensation during episodic memory processing has been demonstrated in AD (Grady et al., 2003; Weis et al., 2011) and in groups at risk for AD (Bookheimer et al., 2000; Dickerson et al., 2005; Trivedi et al., 2008). Specifically, AD subjects have shown recruitment of additional PFC and posterior regions, and this recruitment correlates positively with performance (Grady *et al.*, 2003). Furthermore, a higher magnitude of MTL activity was associated with preserved memory performance in ApoE4 carriers (Bookheimer *et al.*, 2000) and subjects with mild cognitive impairment (Dickerson *et al.*, 2005; Trivedi *et al.*, 2008). Interestingly, a recent

longitudinal fMRI study revealed an inverted-U pattern of activation in the hippocampus that tracked with longitudinal cognitive performance (a period of hippocampal hyperactivation preceded cognitive decline in NCs) (O'Brien et al., 2010). Thus, it is possible that hyperactivity reflects a compensatory response to underlying pathological burden, and that this activity helps preserve normal cognitive performance (and once it subsides, cognitive decline ensues).

Event-related subsequent memory paradigm

To investigate evidence for neural compensation in NCs with high Aβ burden, we implemented an incidental memory encoding paradigm of natural outdoor scenes while subjects underwent event-related functional MRI (fMRI). This task design is ideal for studying neural correlates of successful memory since trials can be sorted by performance (brain activation during successfully encoded events can be directly compared to unsuccessfully encoded events, ie. "subsequent memory effects"). Since the initial fMRI studies employed this design were published (Brewer et al., 1998; Wagner et al., 1998), numerous investigators have executed subsequent memory paradigms using different stimuli and encoding manipulations. Results across studies have revealed persistent involvement of ventolateral prefrontal and medial temporal cortices during successful encoding, as well as posterior visual processing regions during scene encoding, such as lateral occipital and superior parietal cortices (Blumenfeld and Ranganath, 2007; Gutchess et al., 2005; Spreng et al., 2010; Wagner et al., 1999).

Task deactivations during subsequent memory paradigm

In addition to investigating areas that show increased activation during successful memory encoding, attention has also been placed on "beneficial" deactivations that occur during successful memory encoding (Daselaar et al., 2004). These regions deactivate below baseline levels during successfully remembered events, and fail to do so for events that are later forgotten (also referred to as "negative subsequent memory effects"). These deactivations are modulated by task difficulty (Gould et al., 2006) and memory performance (de Chastelaine et al., 2011; Miller et al., 2008), suggesting that these deactivations reflect beneficial reallocation of resources essential for successful memory encoding. Many of the regions that show this behavior during successful encoding are apart of the so-called "default mode network" (DMN), a network of brain regions that consistently deactivates across a variety of externally driven cognitive tasks (Buckner et al., 2008). However, deactivations during successful memory encoding have also been reported in regions outside the DMN, which may reflect resource allocation specific to the demands of the current encoding task (Blumenfeld and Ranganath, 2007).

Given the large spatial overlap between Aβ deposition and the DMN (Buckner et al., 2005), many researchers have investigated this network in relation to AD development (Buckner et al., 2009; Greicius et al., 2004; Hedden et al., 2009; Mormino et al., 2011; Sheline et al., 2009). With respect to successful episodic memory encoding, recent work has suggested a deficit in DMN deactivations in NCs with high Aβ burden (Sperling et al., 2009; Vannini et al., 2011) that are similar to deficits in AD (Lustig et al., 2003) and mild cognitive impairment patients that later convert to AD (Petrella et al., 2007). Whereas observed increases in task positive regions have shown mixed relationships with

performance in studies of aging, there have been no studies linking a *lack of deactivation* to *better* performance during episodic memory encoding (*more deactivation* typically corresponds to *better performance*). Therefore, it is likely that reduced deactivation reflects a detrimental process rather than attempted compensation.

Overall, the aim of this study was to explore evidence for neuronal compensation in task-positive regions during successful memory encoding, as well as evidence for DMN deactivation impairment in cognitively normal controls with high Aβ burden.

4.2 Methods

Subjects

Recruitment

Subjects were recruited as described in chapters 1 and 2 of the dissertation. Subjects involved in this subset of analyses underwent a functional magnetic resonance imaging (fMRI) scanning session. fMRI data was obtained for 50 older normal control (NC) subjects and 17 young NC (yNC) subjects. Five elderly subjects and 2 young were excluded due to insufficient trials of high confidence hits (<20, N=3), problems with data acquisition (N=1), excessive motion (N=2), and memory performance at chance levels (N=1), resulting in a total number of 45 old and 15 young NC subjects for data analysis.

Neuropsychological Testing

Thirty-nine old NC subjects in this study underwent a detailed cognitive testing battery. To reduce this data, a maximum-likelihood factor analysis with varimax rotation was completed using data from a larger cohort of 349 cognitively normal subjects (age range=20-96, mean age=58.2 (22.8), mean MMSE=29.0 (1.5), mean education=16.8 (2.1), 133 males). The following measures were entered into the factor analysis: mental control, verbal paired associates, logical memory, and visual reproductions I and II from the Wechsler Memory Scale-Revised (WMS-R) (Wechsler, 1987b), digits forward/backward and digit symbol tests from the Wechsler Adult Intelligence Scale-Revised, recall sum across learning trials in the California verbal learning test (CVLT) (Delis et al., 2000), Boston Naming Test (Kaplan et al., 1983), Trails B minus A (Reitan, 1958), FAS phonemic fluency (Lezak, 1995), and total correct in 60 seconds from the Stroop Interference test (Zec, 1986). This factor analysis revealed 5 factors fulfilling Kaiser's criterion (eigenvalues>1), and were labeled according to the neuropsychological tests with the highest factor loadings [episodic memory, executive function, working memory, visual memory and semantic memory; table 1]. Thompson factor scores were estimated for each subject and used compare cognition to PIB uptake and fMRI activation within old subjects (Burt and Thomson, 1947). For subjects that had undergone multiple testing sessions, cognitive test scores closest to the PET scan date were used in the factor analysis [mean delay between PET and closest testing session was 4.4(3.0) months]. The remaining 6 old subjects underwent a different neuropsychological battery and were excluded from the factor analysis due to inter-session incompatibilities (however, neuropsychological testing for these subjects were used to ensure normality in these subjects).

Table 1: Factor analysis factor loadings

	Factor1/EM	Factor2/Exe	Factor3/WM	Factor4/VisMem	Factor5/SM
WMS-R mental control	0.14	**0.65**	0.20	0.15	0.30
WMS-R verbal paired associates	**0.77**	0.16	NA	0.17	0.17
WMS-R logical memory	**0.60**	0.24	NA	0.12	0.28
WMS-R visual reproduction I	**0.42**	0.31	0.12	**0.83**	0.11
WMS-R visual reproduction II	**0.57**	0.33	NA	**0.54**	NA
WAIS-R digit span forward	0.10	0.16	**0.97**	NA	0.11
WAIS-R digit span backward	NA	0.35	**0.43**	NA	0.33
WAIS-R digit symbol	**0.47**	**0.71**	NA	0.25	-0.13
CVLT 1-5 free recall	**0.67**	0.28	0.13	0.21	NA
Boston naming test	NA	NA	NA	NA	**0.40**
Trails B minus A	-0.21	**-0.44**	-0.13	-0.19	-0.18
FAS phonemic fluency	0.14	0.39	0.15	NA	**0.43**
Stroop	**0.39**	**0.62**	0.13	0.19	NA

Table 1: Factor loadings above 0.40 are bolded. NAs are indicated for loadings between -0.1 and +0.1. Based on these loadings, factors were label as episodic memory (EM), executive function (Exe), working memory (WM), visuospatial memory (VisMem) and semantic memory(SM).

Data acquisition

PIB-PET

See chapters 1 and 2 of the dissertation.

MRI

All subjects underwent MRI scanning at LBNL on a 1.5T Magnetom Avanto System (Siemens Medical Systems, Erlangen Germany) with a 12 channel head coil run in triple mode. A high resolution structural t1-weighted volumetric magnetization prepared rapid gradient echo scan (MPRAGE, axially acquired, TR/TE/TI=2110/3.58/1100ms, flip angle = 15°, 1.00x1.00mm^2 in plane resolution, 1.00mm thickness with 50% gap) and a low resolution structural t1-weighted in plane to the functional MRI scans were collected (axially acquired, TR/TE=591/10ms, flip angle = 150°, 0.90x0.90mm^2 in plane resolution, 3.40mm thickness with 15% gap). For fMRI scanning, 4 T2*-weighted gradient-echo echo planar imaging were collected (EPI, 28 axially acquired slices, TR/TE/TI=2200/50ms, flip angle = 90°, 3.40x3.40mm^2 in plane resolution, 3.40mm thickness with 15% gap).

Episodic Memory Paradigm

Two hundred outdoor images of natural scenes were presented for 4.4s each and subjects were instructed to indicate whether water was present at any point during the image's presentation (collected over 4 EPI scans, with 50 scenes and 185 TRs per EPI, see figure). Zero to 5 TRs of fixation (green cross-hair on black background) were randomly intermixed between scenes to allow separation of individual trials (average interstimulus interval=3.46s (3.01); (Dale, 1999)). A post-scan surprise recognition task with all stimuli presented during encoding, as well as 100 foils was used to assess performance and sort fMRI data (there was a 15 minute delay between the last stimuli encoded and the start of the post-scan memory test). For each target and foil, subjects were asked "Have you seen this image," and allowed to respond with 1 of 4 responses: high confidence yes, low confidence yes, high confidence no and low confidence no (figure 1). This recognition task was self-paced, and subjects were encouraged to be as accurate as possible. Memory

performance was assessed with the discriminability index d-prime, which uses signal detection theory to compare accuracy and false positive rates. All low confidence responses were discarded to calculate d-prime values.

Figure 1: Example stimuli from incidental memory paradigm

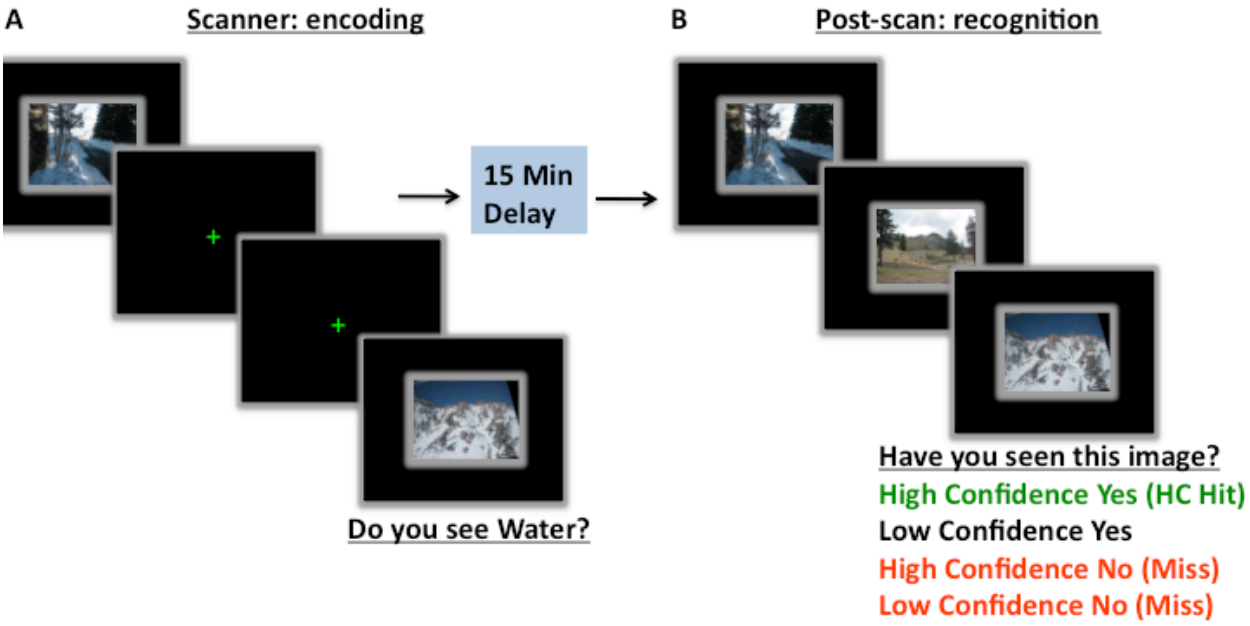

Figure 1: A) Natural scenes are presented in scanner, with randomly intermixed fixation trials. Subjects decide whether water is present in each image. B) After a delay, subjects are exposed to all the scenes presented in the scanner, along with novel scenes and asked to indicate whether they recognize the image (with a confidence judgment). In this specific example, a "high confidence yes" would be coded in the fMRI GLM as a high confidence hit, whereas a "no" response would be coded as a miss. "Low confidence yes" responses are entered in a separate covariate, but excluded from the subsequent memory contrast (HC hits>misses).

Data processing

PIB-PET

See chapters 1 and 2 for details on processing PIB-PET data and creation of distribution volume ratios (DVRs). PIB-PET data were not atrophy corrected in this study.

Structural MRI

See chapters 1 and 2 for details on processing of structural MPRAGE scans with FreeSurfer software. Resulting native space regions of interest (ROIs) from this processing stream were used to create a PIB index values for each subject (average PIB DVR values from prefrontal, cingulate, lateral temporal and parietal ROIs).

Dichotomization into PIB+ and PIB- groups

Older NC subjects were divided into PIB+ and PIB- groups based on cut off values defined in a group of presumable amyloid-free young normal control subjects (see

Appendix). This analysis revealed a cut off value of 1.08, and all subjects above this value were considered PIB+.

Functional MRI processing

fMRI data were processed using FSL version 4.1.6 (http://www.fmrib.ox.ac.uk/fsl). Images were motion corrected, highpass filtered (100s) and smoothed with a 5mm Gaussian kernel. To define the spatial transformation from fMRI space to MNI template space, a multistep registration procedure was employed. First, the mean fMRI image from each encoding run was linearly registered to the subject's in plane T1 structural image using 7 degrees of freedom. The in plane T1 image was then registered to the high-resolution structural scan using 6 degrees of freedom. Finally, the high-resolution structural scan was nonlinearly aligned to the standard MNI 152 brain using FNIRT, and resulting parameters were used to transform fMRI data.

fMRI modeling and higher-level analyses

fMRI trials were classified into 4 types (high confidence hits, low confidence hits, high/low confidence misses, and non-water response trials), modeled by a box function with duration of 4.4s, and convolved with a standard gamma hemodynamic response function (HDR). These covariates, as well as corresponding temporal derivatives and the 6 rigid-body realignment motion parameters, were entered in a general linear model predicting fMRI signal intensity. This lower level analysis was completed separately for each encoding run (N=4) for each subject, then combined across runs using a fixed effects analysis within each subject. Resulting contrast and variance maps (corresponding to high confidence hits versus misses) for all young and old subjects were carried forward into a 1-sample t-test random effects model to determine areas showing significant differences between conditions, covarying for memory performance (task-positive=higher activation in hits versus misses; task negative=lower activation in hits versus misses; cluster thresholded at $z>1.64$ and a cluster significance threshold of $p=0.05$, corrected for multiple comparisons).

Peak activations and deactivations were selected from this 1-sample t-test, and used to create spherical ROIs (6mm centered around selected peak coordinates). Contrast values were extracted from these spherical ROIs .pand used to test effects of age (young versus old) and PIB group (within old groups, controlling for age). In addition to the ROI analysis, an exploratory voxelwise analysis was conducted within old subjects to examine differences between PIB groups controlling for age in a manner unbiased by ROI selection. This analysis was completed using permutation testing with FSL's Randomise (using 5000 permutations, http://www.fmrib.ox.ac.uk/fsl/randomise/), and was restricted to the voxels that were significant in the 1-sample t-test mentioned above (results were considered significant at $p<0.05$, $k=50$, uncorrected).

Statistical analyses

All statistical analyses and plots were completed using R version 2.11 (http://www.r-project.org/). Group differences in demographic variables were determined with t-tests for continuous variables and chi-squared tests for dichotomous variables. Within the old NC group, multiple regression was used for relationships between PIB group and cognitive measures as well as fMRI activation (controlling for age). Within

group correlations between cognitive measures and fMRI contrast values were computed with Spearman rank correlations (all old, PIB- old, and PIB+ old group separately). $P<0.05$ was considered a significant difference.

4.3 Results

Group Characteristics

Group characteristics are listed in table 2. Old subjects were significantly more educated than young subjects ($t= 2.78$, $df= 58$, $p= 0.007$), and there was no difference in gender between old and young groups. Young subjects were more accurate than old subjects on the water/nowater judgment (91 versus 85%; $t = -4.18$, $df = 58$, $p<0.0001$), and there was a trend for better memory performance in young versus old subjects ($t= 1.68$, $df= 58$, $p= 0.10$). Furthermore, young subjects had faster reaction times than old subjects for the water/nowater judgment (1388 versus 1863ms; $t = -5.56$, $df = 58$, $p<0.0001$), as well as during the post-scan recognition judgment (1878 versus 3174ms; $t = -5.88$, $df = 58$, $p<0.0001$).

Based on the PIB index cut off value of 1.08 (see Appendix B), 15 NCs were classified as PIB+ and 30 NCs were PIB-. There were no significant differences between age, education or gender between PIB+ and PIB- groups. Controlling for age, there were no significant relationships between PIB status and MMSE or any factor score other than semantic memory (PIB- were higher than PIB+; $t=-2.58$, $p=0.014$). There were no differences in water/no water accuracy, memory performance or reaction time measures between PIB+ and PIB- subjects.

Table 2: Subject characteristics

	yNC	PIB- oNC	PIB+ oNC
N	15	30	15
Age	23.2 (3.6)	74.9 (6.6)	76.3 (7.9)
Gender	9M	11M	6M
Education	15.6 (1.7)	17.3 (2.0)	17.0 (2.0)
D'prime	1.24 (0.79)	0.98 (0.51)	0.81 (0.66)
PIB Index	NA	1.03 (0.04)	1.27 (0.18)
MMSE	NA	29.2 (1.1)	29.1 (1.1)
Factor Score 1 (EM)	NA	-0.02 (0.78)	-0.04 (0.63)
Factor Score 2 (Exe)	NA	-0.25 (0.79)	-0.29 (0.48)
Factor Score 3 (WM)	NA	-0.14 (0.62)	-0.24 (0.74)
Factor Score 4 (VisMem)	NA	-0.13 (1.08)	-0.17 (1.16)
Factor Score 5 (Sem)	NA	0.01 (0.57)	0.46 (0.49)

Table 2: Means and standard deviations are reported for continuous variables. Neuropsych factor scores were unavaible for 6 oNC (2 PIB+ and 4 PIB-). yNC=young normal controls, oNC=old normal controls. D-prime values were calculated after discarding low confidence responses.

Task activation and deactivation patterns in young and old subjects

A 1-sample t-test of young and old subjects combined identified regions activated during successful memory (hits>misses) and regions deactivated during successful memory (hits<misses, figure 2). Task activations are found bilaterally in ventrolateral prefrontal (bordering dorsolateral prefrontal), lateral occipital/parietal, posterior inferior

temporal, and right parahippocampal/hippocampus. Deactivations were present in bilateral medial occipital, precuneus, angular gyri, medial prefrontal, superior/dorsolateral prefrontal and left central/postcentral gyrus. To create task-positive ROIs, the highest peak coordinate for each cluster was selected (table 3). To create task-negative ROIs, the highest peak for clusters 3 and 4 were selected (table 4). For clusters 5 and 6, local maximum were selected in addition to or rather than the highest peak since the peak coordinate for these clusters did not coincide with regions typically considered part of the DMN (we choose to focus on DMN-typical regions due to previous publications stressing the concordance between this network and Aβ deposition (see Introduction). However, follow up voxelwise analyses enabled examination of all regions irrespective of criterion used to select ROIs). Specifically, for cluster 5, a local maximum in medial PFC was selected (an area typically associated with the DMN) rather than the highest peak for that cluster, which was in the frontal pole. For cluster 6, the peak coordinate was in medial occipital cortex, whereas a local maximum was in precuneus (consequently, 2 ROIs were created for this cluster, "LOcc" and "Precun"). Furthermore, ROIs from clusters 1 and 2 were not selected since these regions are outside the DMN. Overall, this resulted in 4 task-positive and 5 task-negative 6mm spherical ROIs.

Figure 2: Activation and deactivation statistical maps

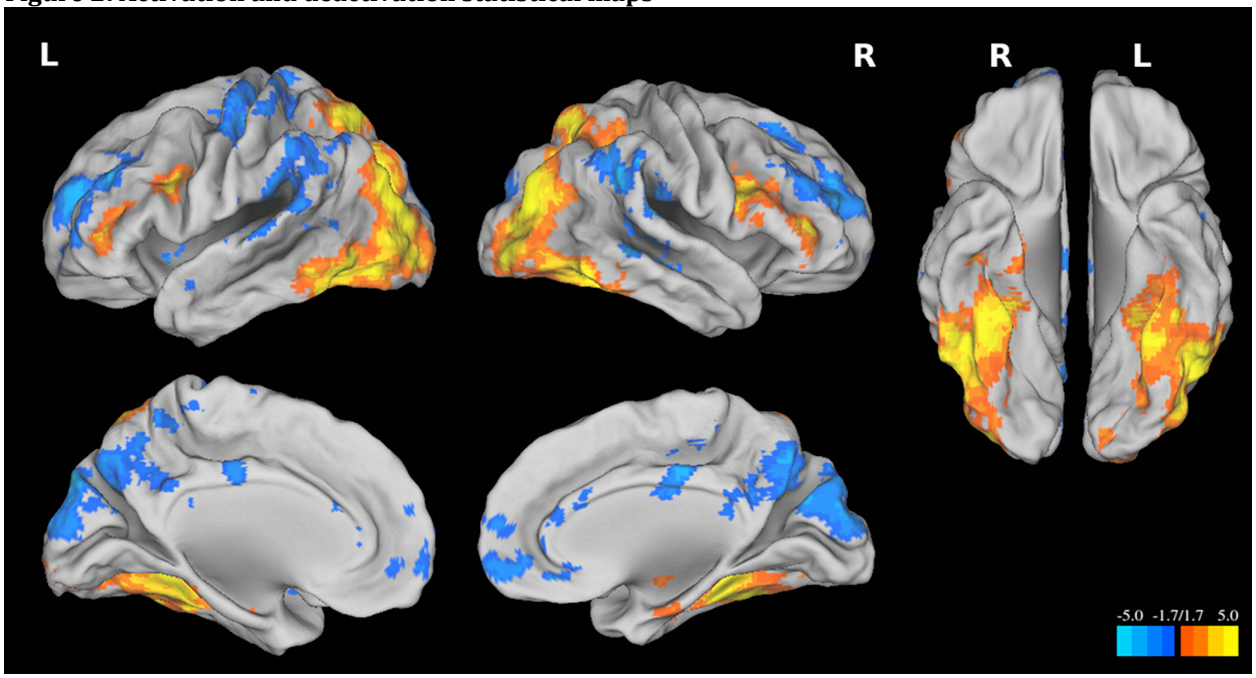

Figure 2: Statistical maps are defined by 1 sample t-tests across young and old subjects, covarying for memory performance. Warm colors are activations (hits>misses) while cool colors are deactivations (hits<misses), cluster thresholded at z>1.64 and a cluster significance threshold of p=0.05 (corrected for multiple comparisons).

Table 3: Activation clusters and peak coordinates

Cluster Index	Cluster Size	Z	x	y	z	Location
4	9724	**6.14**	**-30**	**-78**	**26**	**L Lat Occ**
4		6.06	-28	-90	26	L Lat Occ
4		5.83	-24	-68	50	L Lat Occ
4		5.57	-48	-56	-16	L IT
4		5.41	-24	-78	40	L Lat Occ
4		5.39	-34	-92	12	L Lat Occ
3	9494	**5.92**	**36**	**-86**	**20**	**R Lat Occ**
3		5.86	24	-38	-18	R Fusiform/Ant PHG and Hip
3		5.81	42	-80	18	R Lat Occ
3		5.75	28	-68	54	R Lat Occ
3		5.64	26	-68	46	R Lat Occ
3		5.62	38	-82	26	R Lat Occ
2	2046	**4.92**	**50**	**36**	**12**	**R Frontal Pole/IFG**
2		4.66	44	36	10	R Frontal Pole/IFG
2		4.61	44	6	28	R Precentral/IFG
2		4.4	40	14	24	R IFG
2		4.33	36	16	26	R IFG
2		4.29	40	6	32	R Precentral/IFG
1	2026	**3.99**	**-52**	**14**	**38**	**L MFG**
1		3.75	-44	38	8	L Frontal Pole/IFG
1		3.41	-38	28	16	L IFG
1		3.18	-46	44	2	L Frontal Pole
1		3.08	-56	32	18	L MFG

Table 3: Significant task positive clusters and corresponding local maxima from the 1-sample t-test of young and old subjects are listed. The highest peak within each cluster was selected for subsequent ROI analyses (bolded).

Table 4: Deactivation clusters and peak coordinates

Cluster Index	Cluster Size	Z	x	y	z	Location
6	6841	**5.64**	**-2**	**-90**	**24**	**L medial Occ**
6		4.69	2	-72	26	R cun/precun
6		4.49	-12	-90	28	L Occ
6		**4.42**	**0**	**-80**	**42**	**Precun**
6		4.24	-2	-64	42	L precun
6		4.08	0	-58	36	L precun
5	5894	4.41	-18	50	26	L frontal pole
5		4.11	-26	54	20	L frontal pole
5		**4.09**	**2**	**52**	**10**	**R mPFC**
5		3.97	26	46	32	R frontal pole
5		3.94	-24	46	22	L frontal pole
5		3.78	-22	42	22	L frontal pole
4	4104	**4.57**	**60**	**-46**	**32**	**R ang**
4		4.2	66	-46	32	R SMG
4		4.19	50	-26	-12	R MTG
4		3.85	58	-30	26	R Par
4		3.71	56	-48	44	R ang
4		3.62	60	-30	16	R temp
3	2547	**3.54**	**-62**	**-40**	**38**	**L SMG**
3		3.46	-66	-36	28	L SMG
3		3.41	-62	-26	8	L Temp
3		3.4	-62	-46	14	L SMG
3		3.27	-60	-36	24	L temp
3		3.25	-60	-32	18	L temp
2	1794	3.86	-42	-22	50	L postcentral
2		3.49	-32	-28	62	L postcentral
2		3.25	-42	-38	62	L postcentral
2		3.19	-34	-36	68	L postcentral
2		3.14	-24	-42	70	L postcentral
2		3.13	-46	-32	56	L postcentral
1	966	4	48	10	-8	R temp pole
1		3.2	54	12	-2	R temp pole
1		3.08	58	12	-4	R temp pole
1		3.06	54	18	-6	R temp pole
1		3.05	56	6	-18	R temp pole
1		2.97	52	22	-2	R IFG

Table 4: Significant task-negative clusters from the 1-sample t-test of young and old subjects are listed. Peaks selected for subsequent ROI analyses are bolded.

<u>Relationships between subsequent memory effects and amyloid in old subjects</u>

Older subjects showed reduced activation compared to young subjects across all 4 ROIs ($p<0.01$). Controlling for age, PIB+ NCs showed significantly increased activation compared to PIB- NCs in LOcc ($p=0.019$) and LMFG ($p= 0.025$), while a trend was present in ROcc ($p= 0.082$, figure 3A). An average activation value was computed across regions since a pattern for increased activation in PIB+ old compared to PIB- old was apparent

across ROIs, and was significantly different between PIB+ and PIB- groups (p=0.020, figure 3B).

A follow up exploratory voxelwise analysis was executed to compare fMRI activation to PIB group across each voxel limited to the areas showing significant activation within the 1 sample t-test. The results from this analysis were consistent with the ROI analysis, revealing multiple areas with greater activation in PIB+ versus PIB- subjects (figure 4, table 5). Interestingly, this voxelwise approach revealed increased activation in the right parahippocampus/hippocampus. There were no clusters showing reduced activation in PIB+ compared to PIB- old subjects.

Figure 3: Task activation across groups

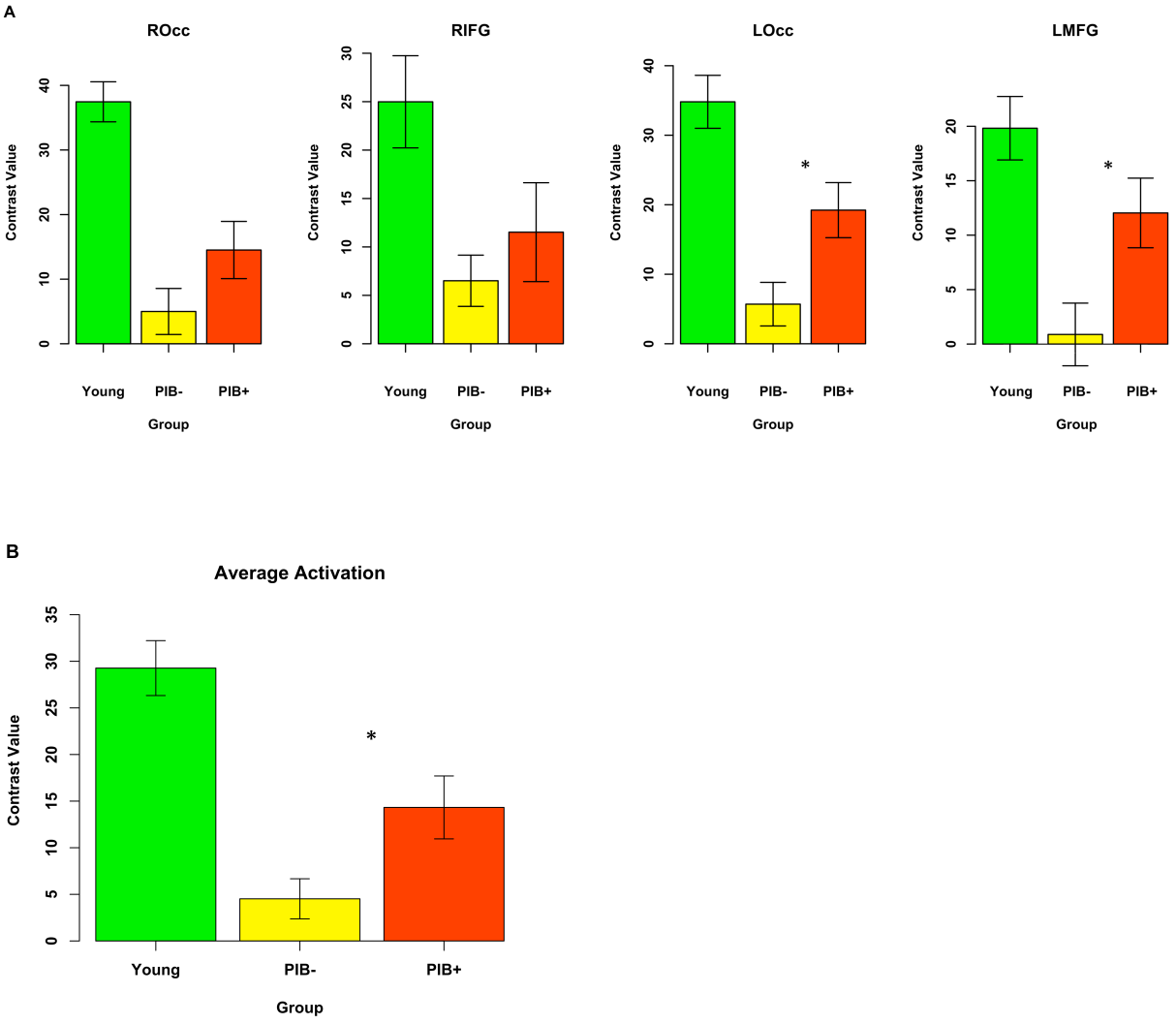

Figure 3: (A) Activation pattern across group is shown separately for each ROI. (B) Given the consistent pattern, average activation across regions was also examined. *Indicates significant difference between PIB+ and PIB- groups. ROcc=right occipital; RIFG=right inferior frontal gyrus; LOcc=left occipital; LMFG=left middle frontal gyrus.

Figure 4: Exploratory voxelwise analysis

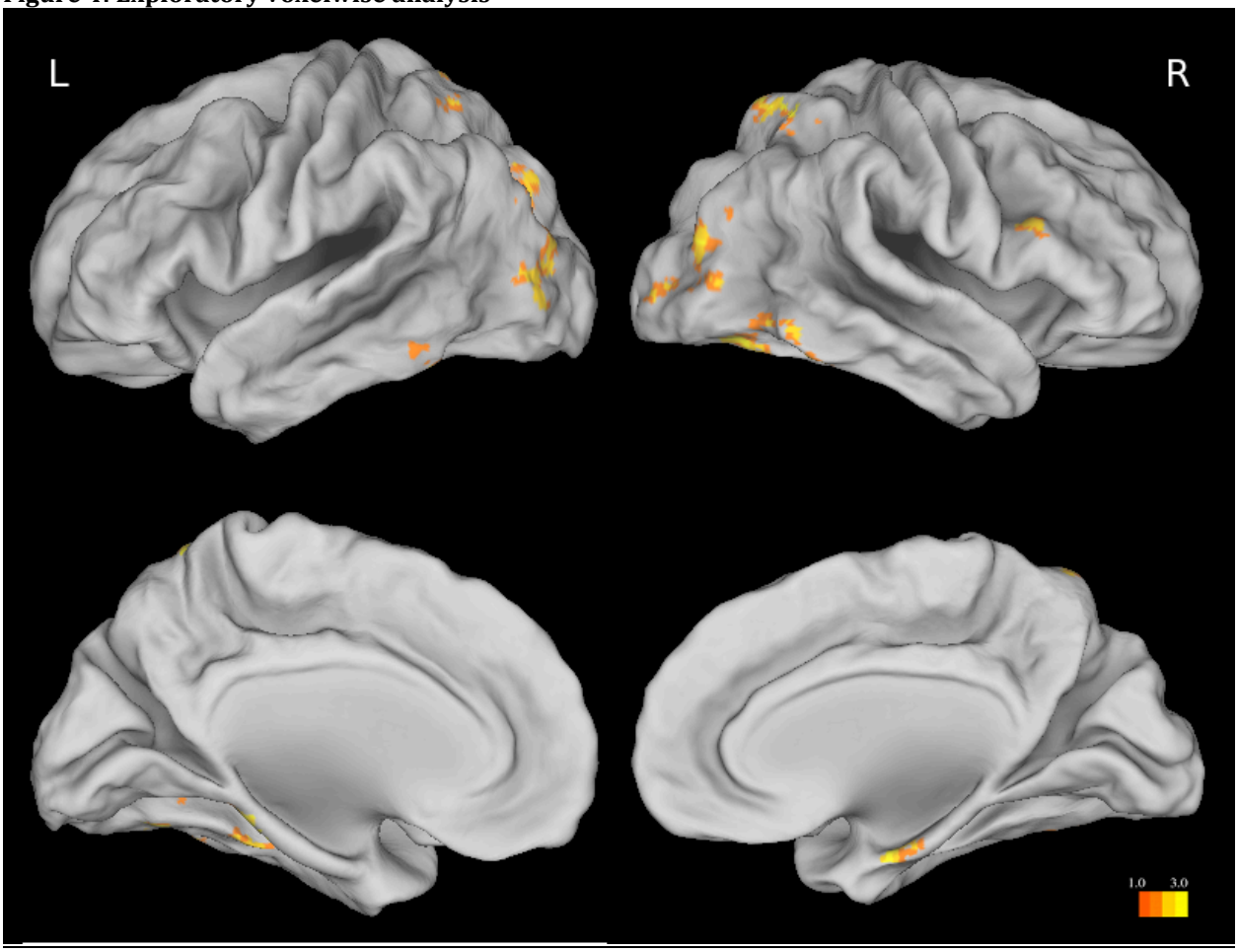

Figure 4: Statistical maps showing a positive relationship between activation during successful memory encoding and PIB status (thresholded at p<0.05, k=50)**.** Multiple regions show increased activation in PIB+ versus PIB- subjects.

Table 5: Significant clusters and peak coordinates from exploratory analysis in task-positive regions

Cluster Size	Max p-value	x	y	z	Location
673	0.0002	-34	-70	26	L Occ
356	0.0002	34	-76	16	R Occ
172	0.0002	-22	-36	-20	L Fus
147	0.001	24	-54	56	R Superior Par
128	0.001	54	16	40	R MFG
126	0.001	38	-72	-14	R Fus
123	0.001	-56	16	34	L MFG
104	0.001	52	-48	-22	R Inferior temporal gyrus
83	0.004	-18	-54	56	L Superior Parietal
68	0.003	-60	-48	-18	L Inferior temporal gyrus
63	0.003	-28	-64	-20	L Fusiform
52	0.001	22	-10	-26	R PHG/hippocampus

Table 5: Results from exploration analysis. Clusters showing heightened activation in PIB+ compared to PIB- are listed. These results are consistent with the ROI analysis, revealing increased activation throughout task-positive regions in PIB+ NCs.

Relationships between task activation and cognition

To explore whether heightened activation may reflect a compensatory response, average task activation (across the 4 task-positive ROIs, figure 3B) was related to memory performance, as well as 5 factor scores derived from neuropsychological data (episodic memory, executive function, working memory, visual memory and semantic memory). Across the entire old group, there were no relationships between task activation and performance or any factor score. Within PIB+ subjects, there was a trend between task activation and performance (rho= 0.39, p=0.16), and a significant relationship between task activation and the visual memory factor score (rho= 0.56, p= 0.046, figure 5A). Relationships between activation and the remaining factor scores were not significant within PIB+. Relationships were not significant in the PIB- group (figure 5B). There was no relationship between memory performance and activation within young subjects.

Figure 5: Relationships between activation and cognition within PIB- and PIB+ groups

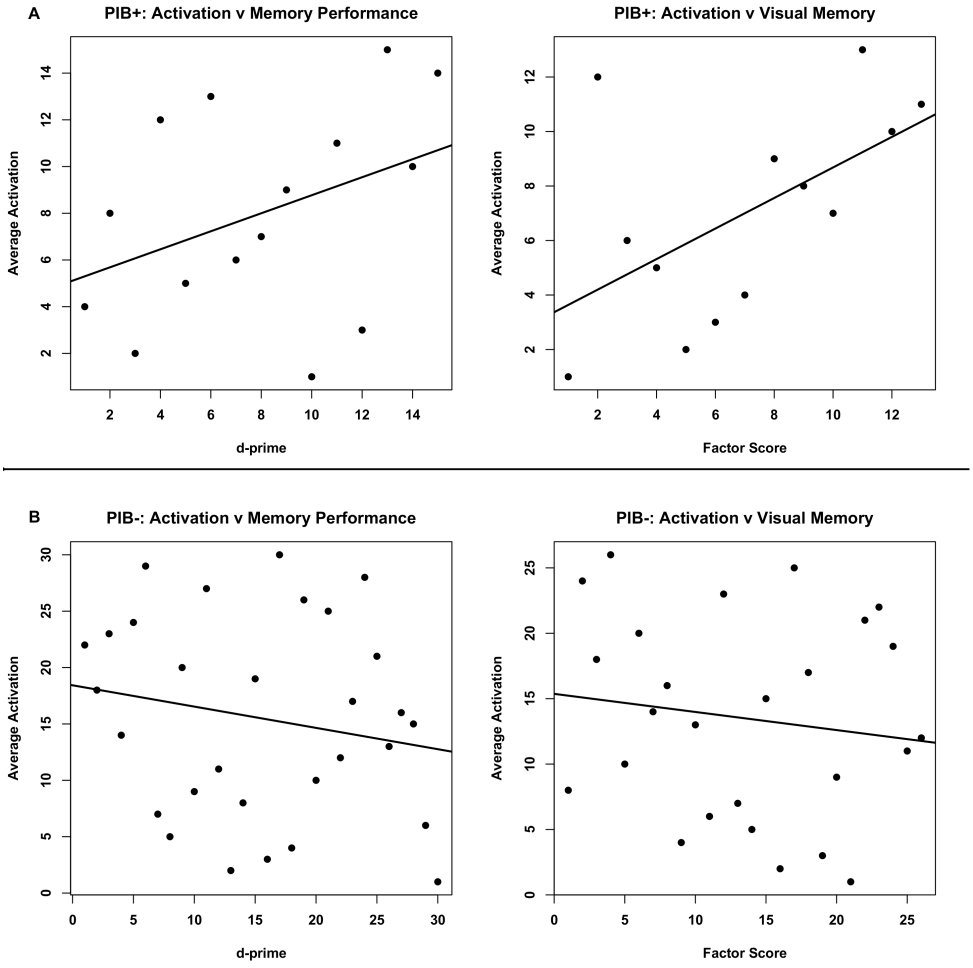

Figure 5: PIB+ subjects show a positive relationship between task activation and behavioral measures (memory performance and visual memory, A), whereas no relationship is seen in the PIB- group (B). Plotted values are ranked data. Two PIB+ and 4 PIB- subjects did not have visual memory scores.

Relationships with task deactivation

Examination of the parameters estimates across trial types for areas showing significantly lower activation for hits than misses revealed that selected task-negative regions show greater deactivation during hits than misses relative to fixation (rather than the equally plausible scenario of increased activation for misses relative to fixation versus hits relative to fixation, figure 6). This pattern is robust in young subjects, while diminished deactivation during hits is seen in old subjects, resulting in decreased contrast values in old compared to young subjects in 3/5 examined ROIs (LOcc: $p<0.001$; mPFC: $p=0.022$, Lpar: $p<0.001$, figure 7). There was no effect of PIB status on the contrast between hits versus misses in any task-negative ROI examined.

To ensure the null result between PIB status and task deactivations was not a consequence of ROI selection, an exploratory voxelwise analysis was conducted and failed to reveal strong evidence for an effect of amyloid on deactivations in this cohort. There were 2 clusters (left supramarginal gyrus and right medial occipital) showing reduced deactivation in PIB+ compared to PIB- subjects, and a single cluster in the medial occipital cortex showing reduced deactivation in PIB- compared to PIB+ subjects (table 6).

Figure 6: Trial parameter estimates for task-negative regions

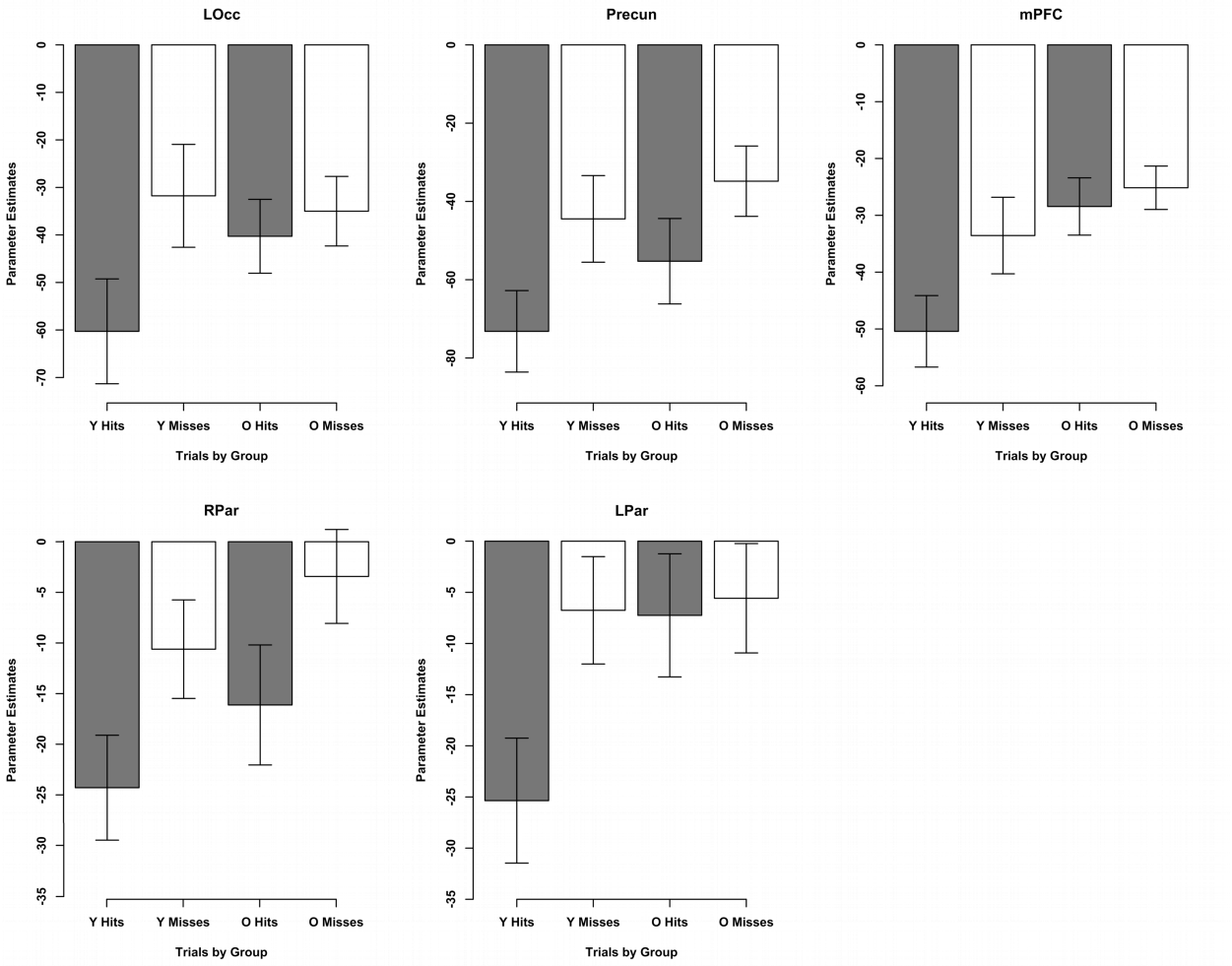

Figure 6: Trial parameters estimates in task-negative regions revealed greater deactivation during hits than during misses relative to fixation for young subjects, consistent with previous studies examining these regions during successful encoding. Old subjects show equivocal deactivation during both hits and misses in LOcc, mPFC and LPar ROIs. O=old, Y=young.

Figure 7: Task deactivation across groups

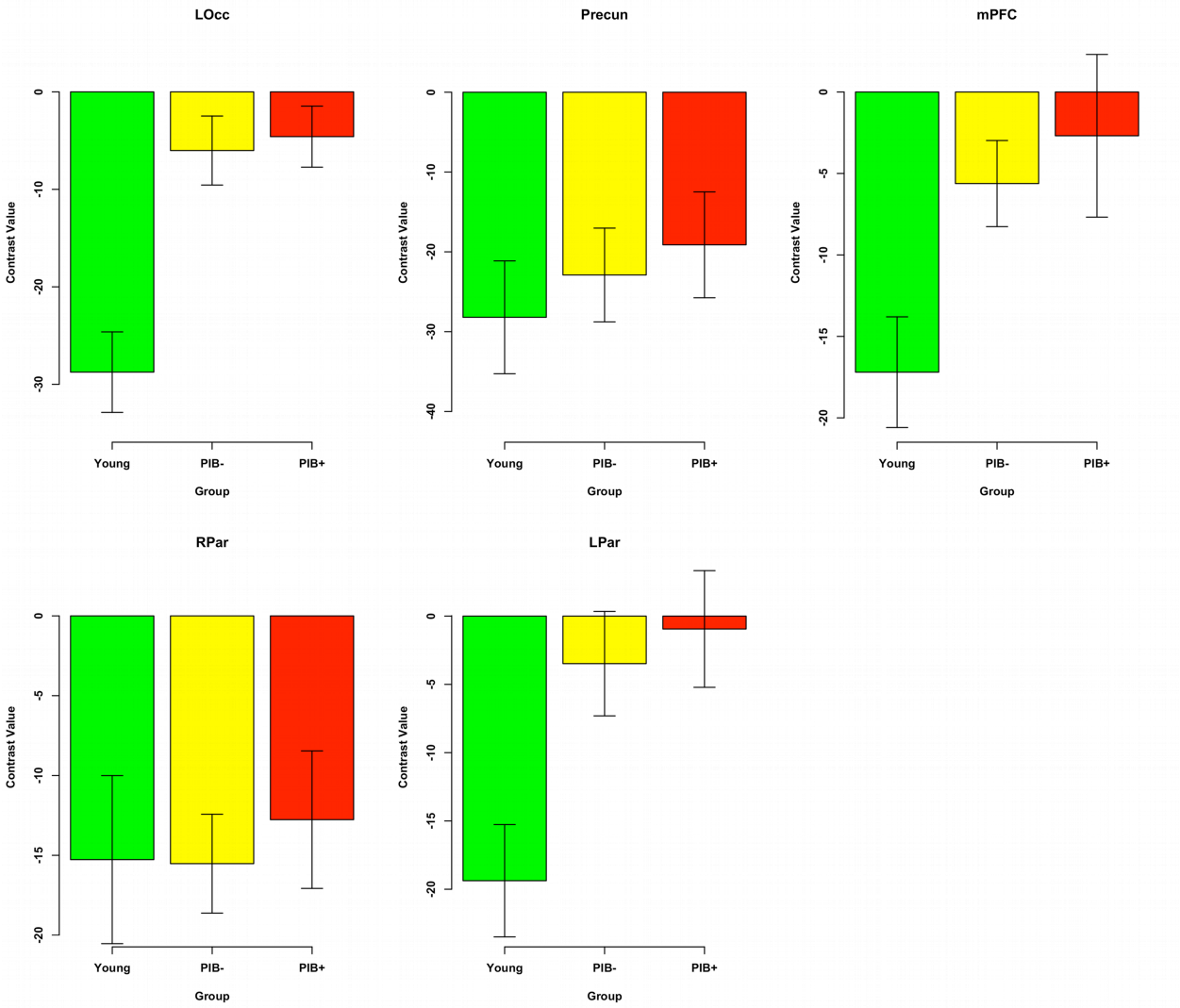

Figure 7: Contrast values for hits versus misses are depicted. Old subjects showed reduced deactivation compared to young across multiple ROIs, but an effect of amyloid was not identified.

Table 6: Significant clusters and peak coordinates from exploratory analysis in task-negative regions

Cluster Size	Max p-value	x	y	z	Location
Less Deactivation in PIB+ versus PIB-					
95	0.0002	-56	-50	26	L Supramarginal gyrus
78	0.001	6	-92	28	R Medial occipital
Less Deactivation in PIB- versus PIB+					
140	0.001	2	-92	8	Medial occipital

Table 6: Exploratory analysis within task-negative regions failed to reveal strong evidence for an effect of amyloid within old subjects.

Relationship between task deactivation, cognition and task activation

Although an effect of amyloid was not found in task-negative regions, we nevertheless sought to determine whether deactivations relate to memory performance in our cohort, as previously reported (de Chastelaine *et al.*; Miller *et al.*, 2008). An average task deactivation measure was calculated by averaging across the 5 selected ROIs and was related to task performance, as well as the 5 neuropsychological factor scores. Across all old subjects, there was a negative relationship with memory performance (ie. more deactivation, better performance; rho = -0.46, p=0.001), as well as within PIB+ (rho=-0.54, p=0.037) and PIB- groups (rho=-0.46, p= 0.011, figure 8). There was no relationship with any factor score. There was no relationship between memory performance and deactivation within young subjects.

To assess independent contributions to memory performance (de Chastelaine et al., 2011), multiple regression models were conducted with task-negative and positive contrast values as simultaneous predictors of memory performance (conducted in all old subjects, as well as within PIB+ and PIB- groups separately). These models revealed an independent effect of deactivation on performance across all old subjects, as well as a trend for dissociable effects of activation and deactivation on performance within PIB+ subjects (such that reduced deactivation in task-negative regions was independently associated with worse performance, while increased task-positive activation was independently associated with better performance, table 7 and figure 9).

Figure 8: Relationship between task deactivation and memory performance

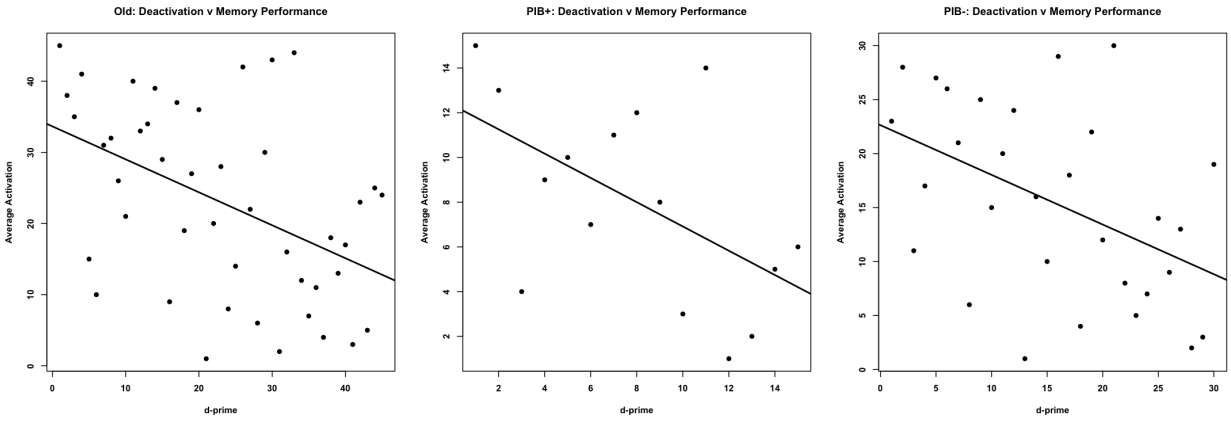

Figure 8: Relationships are plotted separately for all old, PIB+ and PIB- subjects. Plotted data are ranked. A negative relationship is consistent across groups. Average activation for the contrast hits>misses is plotted on the y-axis—therefore, low ranked values reflect deactivation (these negative activation values are apparent in figure 6 and 7). Therefore, more deactivation (ie less activation) is associated with better performance.

Table 7: Multiple regression model predicting memory performance

Model: Memory performance~Average Activation+Average deactivation			
	parameter estimate	**standard error**	**p-value**
All old, N=45			
Average Dectivation	-0.014	0.005	**0.011**
Average Aactivation	0.007	0.006	0.237
PIB+, N=15			
Average Dectivation	-0.016	0.008	**0.065**
Average Activation	0.019	0.008	**0.041**
PIB-, N=30			
Average Dectivation	-0.009	0.007	0.212
Average Activation	-0.004	0.009	0.649

Table 7: Multiple regression models predicting memory performance reveal an independent effect of task deactivation on performance, as well as a trend for dissociable effects of deactivation and activation on performance within PIB+ subjects (reduced deactivation in task-negative regions was associated with worse performance, while increased task-positive activation was associated with better performance). Significant relationships and trends are bolded.

Figure 9: Dissociable effects within PIB+ group

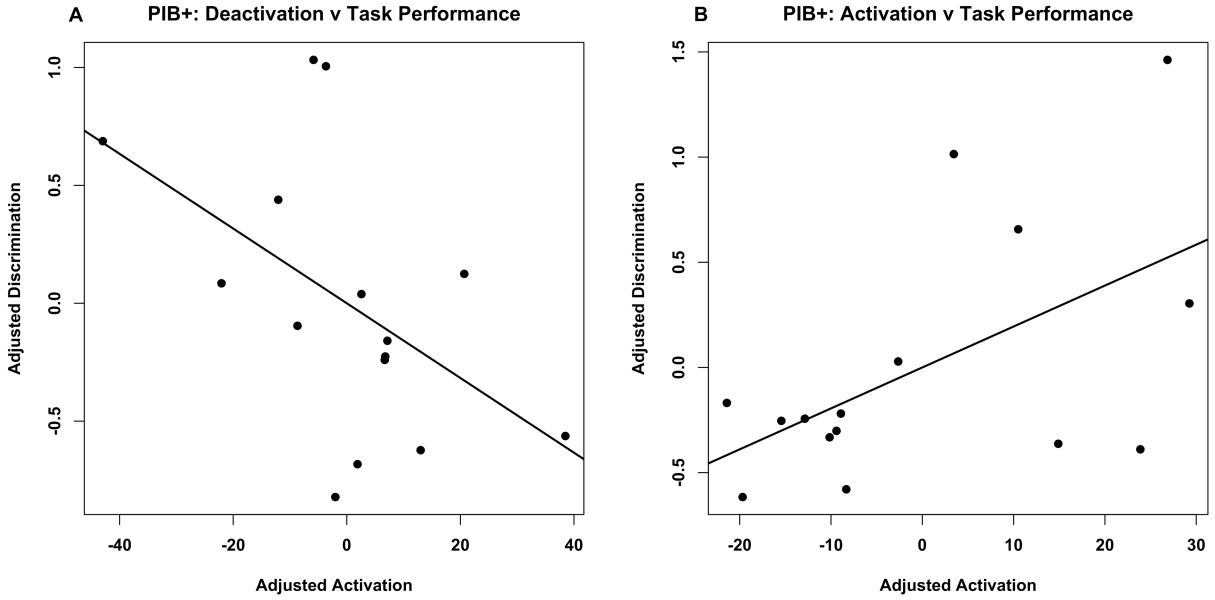

Figure 9: Visual depiction of independent contributions of deactivation and activation effects on memory performance within PIB+ subjects (residuals are plotted on each axis). A) The relationship between task deactivation and performance with both variables adjusted for task activation. B) The relationship between task activation and performance with both variables adjusted for task deactivation.

<u>Further interrogation of task deactivation and amyloid levels</u>

The lack of relationship between PIB status and DMN deactivations prompted further investigation. Differences between the current analysis and the analysis presented

by Sperling et al., 2009 (which identified a relationship between DMN deactivation and PIB status in a group of nondemented elderly individuals) were considered. There are at least 2 data analysis differences: (1) Sperling et al. used precuneus PIB as a measure of amyloid burden while the current analysis used global PIB index and (2) Sperling et al. compared hits to fixation while the current analysis compared hits to misses to define deactivations. To this end, we re-analyzed our data to take into account the 2 aforementioned data analysis inconsistencies.

Firstly, old subjects were re-catagorized into PIB+ and PIB- groups based on precuneus PIB values. Resulting PIB classification was the same for all but 2 subjects. We did not identify any significant relationships using this classification approach, albeit there was a trend in the LPar ROI (p= 0.196, figure 10). Secondly, relationships between PIB status and deactivation were investigated by comparing hits to fixation. No significant relationships were detected (figure 11), and these results were unaltered when classification was based on precuneus rather than global PIB.

Figure 10: Task deactivation across groups, old subjects classification with precuneus PIB

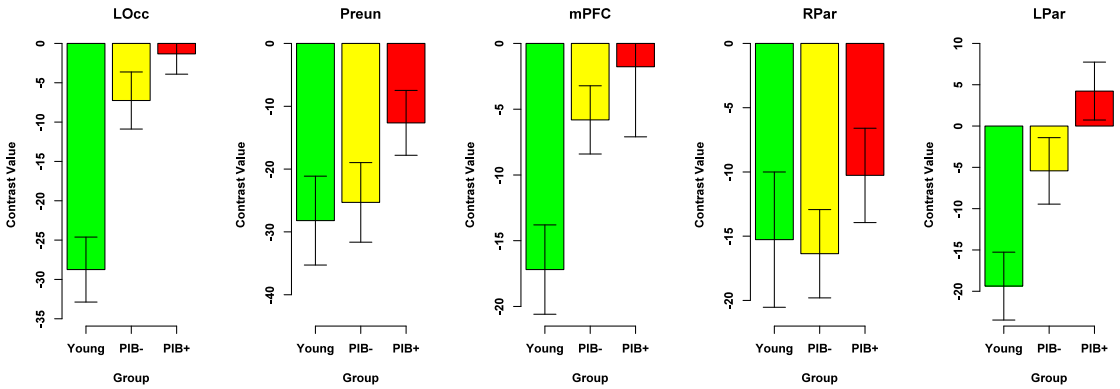

Figure 10: Reclassification of old subjects based on precuneus PIB did not reveal a significant effect of amyloid on task deactivations.

Figure 11: **Task deactivation across groups, with hits compared to fixation**

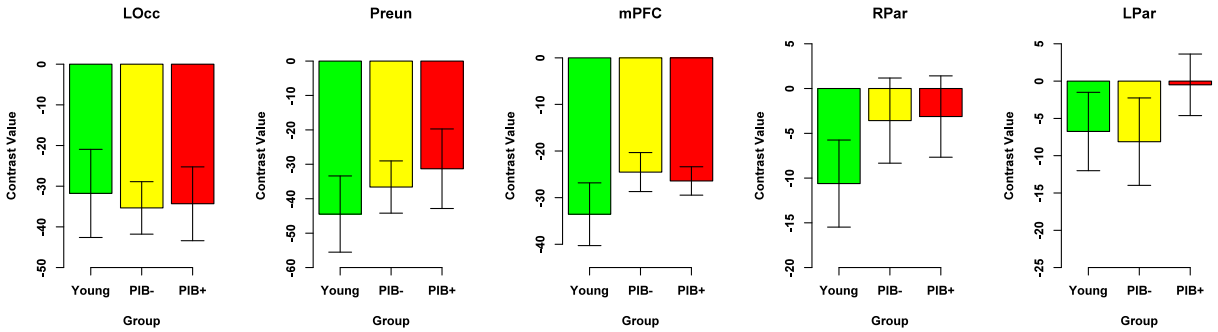

Figure 11: Contrasting hits to fixation did not reveal a significant relationship between deactivation and PIB status.

4.4 Discussion

In this study, we scanned young and old subjects with fMRI while performing incidental scene encoding, allowing isolation of brain regions associated with successful memory formation. Consistent with previous studies, we identified regions showing greater activation for successfully remembered versus subsequently forgotten scenes bilaterally in ventrolateral prefrontal, lateral occipital, lateral parietal, posterior inferior temporal and the right parahippocampal/hippocampus (task-positive regions). Furthermore, significant deactivations (hits<misses) were present in default mode network (DMN) regions (precuneus, angular, medial prefrontal and lateral superior temporal gyri) as well as in areas outside the DMN (bilateral medial occipital cortex, superior/dorsolateral prefrontal and left central/postcentral gyri). Young subjects showed more activation in task-positive regions and greater deactivation in task-negative regions compared to old subjects. Within the old group, PIB+ subjects showed increased activation in task-positive regions compared to PIB- old subjects. Furthermore, there was a trend between higher activation in task-positive regions and better memory performance within PIB+, and a significant relationship with task-positive activation and a measure of visual memory. Although we didn't identify impaired deactivation in PIB+ subjects, a multiple regression approach revealed dissociable effects of activation and deactivation on performance within this group, suggesting that these networks have independent contributions to performance amongst PIB+ subjects (greater activation was associated with better performance; impaired deactivation was associated with worse performance). Overall, our data suggests that heightened task-positive activation in PIB+ old subjects reflects a compensatory response to underlying pathological burden, and that the ability to initiate these compensatory responses is unrelated to deficits in deactivation.

Age differences in task-positive and task-negative regions

We identified a consistent reduction of activation in old subjects compared to young subjects in task positive regions, as well as reduced deactivations in task-negative regions. This pattern of results is consistent with previous studies of aging, although some studies have reported increased activation in old compared to young subjects (Duverne *et al.*, 2009; Gutchess *et al.*, 2005). We did not perform follow up analyses to thoroughly inspect whether regions of greater activation exist in older subjects since differences between young and old subjects was not a primary focus of this experiment. Furthermore, although we selected ROIs in a manner unbiased by group status (young and old subjects were combined to identify peak voxels for the ROI analysis), interpretation of age differences is complicated by impaired neuronal–vascular coupling in elderly subjects (D'Esposito et al., 1999; Riecker et al., 2003). Importantly to the focus of this study, it is unlikely that changes in neuronal-vascular coupling underlies the pattern of increased activation identified between PIB+ and PIB- elderly subjects.

Heightened task activation in PIB+ NCs may reflect compensatory processes

The pattern of elevated activation in PIB+ NC subjects is consistent with previous work showing elevated activation in elderly NCs destined for episodic memory decline (Persson et al., 2006; O'Brien et al., 2010), as well as in subjects at risk for AD (Bookheimer et al., 2000; Dickerson et al., 2005; Trivedi et al., 2008). Our results provide direct support

for previous hypotheses that this hyperactivation may be a compensatory response to underlying AD pathology.

The design of this experiment allowed isolation of activation specific to successful memory. Therefore, the task-positive increases we identified in PIB+ NCs specifically occur during successful encoding. Additionally, we identified positive relationships between memory ability and heightened task activation within PIB+ subjects. Taken together, this pattern implies that heightened activation within PIB+ subjects during encoding promotes better overall memory performance that extends beyond the specific scanning session since relationships were identified with an independent measure of visual memory performed on a separate day.

Although the mechanism underlying this effect is unclear, a number of potential explanations exist. One possibility is that hyperactivity may reflect increased neuronal demand that counteracts detrimental effects of Aβ that occur at the level of synaptic function (Selkoe, 2002). Another possibility is that PIB+ NC implement alternative processing strategies in the context of Aβ-related functional decline. It has been shown that heightened activation within task-positive regions is related to deep encoding (Fletcher et al., 2003) as well as encoding effort (Reber et al., 2002), which may represent mechanisms implemented by PIB+ subjects during this task. While the incidental encoding nature of our design makes it unlikely that different encoding strategies were implemented by PIB+ subjects, it is possible that heightened activation reflects these mechanisms at work during online task demands. The online demand of the current experiment was a basic visual search task, where subjects indicated whether or not water was present. A possibility is that PIB+ subjects engaged in deeper processing during visual search of presented scenes, and that this deeper processing was beneficial for successful memory, whereas a similar level of processing was unnecessary for successful memory in PIB- subjects. Interestingly, the areas showing increased activation in PIB+ NCs (lateral occipital cortex and the medial temporal lobe) remain relatively free of Aβ deposition throughout AD development (Braak and Braak, 1991; Thal et al., 2002), suggesting that these regions may compensate for amyloid-induced dysfunction in multimodal association areas that are highly vulnerable to Aβ deposition.

<u>Heightened task activation may precede Aβ deposition</u>

It is also possible that increased activation within this network predates Aβ deposition. This direction of causality is supported by the observation that Aβ release is activity dependent (Cirrito et al., 2005), and that Aβ deposition occurs in the most metabolically active areas of the brain (Buckner et al., 2005; Vlassenko et al., 2011). Furthermore, recent evidence from a mouse model of AD suggests that early neuronal activity is predictive of what brain areas are subsequently vulnerable to Aβ deposition (Bero et al., 2011). The positive relationships we identified between heightened activation and behavioral measures suggest that this hyperactivation is nevertheless beneficial for these individuals who perhaps have pre-existing limitations that require higher brain activity for normal cognitive function. Thus, it is possible that this activation pattern may confer early life advantages, although detrimental in the long term by promoting Aβ deposition. This is consistent with the observation that carriers of the APOE4 allelle show increased hippocampal activation during EM processing in their late twenties (Filippini et al., 2009), which is likely before Aβ deposition has begun (Kok et al., 2009). Although we

did not identify a relationship between APOE status and activation, the high age of our subjects makes the current study suboptimal for examining effects preceding Aβ deposition. Studies that have implicated a temporal sequence of events by investigating young APOE carriers [presumably before Aβ deposition, (Mondadori et al., 2007; Filippini et al., 2009)] or longitudinal brain activation preceding cognitive decline [presumably concomitant with Aβ deposition; (Persson et al., 2006; O'Brien et al., 2010)] have not converged to reveal a consistent mechanism underlying activation increases. The combination of amyloid imaging with fMRI will help disentangle the temporal order of these events by directly measuring underlying pathology rather than relying on proxy markers of AD risk.

Deactivations are impaired in aging and relate to memory performance

In addition to isolating task-positive regions that show elevated activity for successfully remembered scenes, we also investigated task-negative regions (specifically, these areas show more deactivation during hits than misses). Many of the regions showing this behavior belong to the default mode network (DMN; bilateral medial prefrontal, precuneus/posterior cingulate, angular, and superior temporal gyri), a network that consistently deactivates across a variety of different externally driven cognitive tasks (Buckner *et al.*, 2008). Task-negative regions were also identified outside the DMN, namely bilateral medial occipital, dorsolateral PFC and left central gyrus. These non-DMN deactivations may be a specific response to the employed cognitive task. For instance, previous studies employing a subsequent memory paradigm have identified deactivations in dorsolateral prefrontal cortex (Daselaar *et al.*, 2004), which may reflect reallocation of resources from this area when organization and manipulation are not involved in online task demands (Blumenfeld and Ranganath, 2007). Consistent with previous studies, we found reduced deactivation in old compared to young subjects, as well as a relationship between cognitive performance and deactivation within old subjects (such that more deactivation was associated with better performance) (de Chastelaine et al., 2011; Duverne et al., 2009; Gutchess et al., 2005; Kukolja et al., 2009; Morcom et al., 2003).

Deactivations were not exclusively related to Aβ

Although we identified an effect of aging on deactivations during successful encoding, we did not find a relationship between deactivation failure and PIB status amongst our NC cohort. This result is inconsistent with a recent study investigating Aβ in aging (Sperling *et al.*, 2009). There are many discrepancies between our study and Sperling et al. which may contribute to this inconsistency. One possibility is that additional factors associated with aging contribute to deactivations, obscuring relationships between Aβ and deactivations in older subjects. For instance, precuneus deactivation has been shown to relate to levels of dopamine synthesis in elderly subjects (Braskie et al., 2010), and it is likely that age-related changes in the dopamine system are unrelated to levels of Aβ. Future studies that simultaneously measure multiple age-related brain changes may reveal distinct contributors of impaired deactivation in aging. Differences in study design may also contribute to the null finding reported in our study. For instance, Sperling et al. combined CDR 0 and CDR 0.5 subjects (however, a significant effect was still identified within the CDR 0 subjects). Furthermore, Sperling et al. used face-name pairs as stimuli, and subjects were specifically told to encode task stimuli (intentional encoding). It is

unclear how stimuli differences and encoding intent affects relationships between deactivations and Aβ burden in aging.

Despite the lack of relationship between PIB status and deactivation in our elderly group, a multiple regression approach revealed dissociable effects of these networks on performance within PIB+ subjects (greater activation was associated with better performance; impaired deactivation was associated with worse performance). These relationships suggest that task-negative and positive networks have independent contributions to performance amongst PIB+ subjects, suggesting a biological relevance of these activation patterns during the early stages of Aβ deposition.

Conclusions

In this study we show that increased activation amongst task-positive regions is related to Aβ burden in cognitively normal elderly controls. Although the mechanisms underlying these increased activations remains unclear, occurrence during successful memory encoding and positive relationships with overall measures of memory ability suggest they are beneficial to individuals with high Aβ burden. The ability to elicit compensatory neuronal activation may allow cognitively normal elderly individuals to cope with underlying pathology and delay the onset of cognitive decline. It is also possible that heightened activation has a direct causal role in Aβ deposition in aged individuals.

Chapter 5

Concluding remarks

5.1 Summary

The work presented in this dissertation provides a number of findings concerning the biological relevance of Aβ in aging. Our findings indicate both a negative impact of this pathology [hippocampal atrophy and disconnection in the episodic memory (EM) sub-component of the default mode network (DMN)] as well as evidence for compensatory responses (heightened connectivity in non-EM components of the DMN and increased activation during successful EM encoding). These results are consistent with a cascade model of Alzheimer's disease (AD)—Aβ is an early event that triggers a multitude of downstream processes before cognitive impairment is apparent. These processes are most likely prevalent in brain regions subserving EM, a cognitive domain compromised early in AD. Furthermore, these results offer insight into protective factors that may prevent cognitive decline despite pathological burden. Specifically, increased functional connectivity and/or increased activation during EM processes may enable NCs to remain cognitively intact despite high levels of Aβ deposition. Overall, our data suggests that Aβ deposition in NC is indicative of early AD development, and that the relationship between this pathology and cognition is influenced by downstream changes to brain structure and function. It is likely that this cascade of events occurs over many years. These findings are relevant to understanding AD development, as well as the neural changes reported in studies of "normal" aging.

I was fortunate to begin research with PIB-PET imaging immediately after the first human study was published in 2004 (Klunk et al., 2004). Thus, I began my research at the forefront of in vivo amyloid imaging. Although postmortem work provided speculation as to what researchers would uncover in NCs, the last few years have provided many advancements to our understanding of Aβ deposition in NCs. The results presented in my dissertation are consistent with a number of studies published by other labs. For instance, the mediation effect of brain structure between PIB uptake and cognition was implicated by Storandt et al. (Storandt et al., 2009). Results with hippocampus volume have been mixed, with some groups finding a negative relationship in NC (Jack et al., 2008; Rowe et al., 2010), others not finding this relationship (Becker et al., 2011; Driscoll et al., 2010), and 1 study reporting *increased* hippocampus volume in PIB+ NCs (Chetelat et al., 2010b). However, the relationship between hippocampus atrophy and PIB status is more consistent in mild cognitive impairment (Jack et al., 2010b; Rowe et al., 2010; Wolk et al., 2009), a group that has progressed closer to AD than NCs and are therefore more likely to have undergone downstream brain atrophy. Functional disconnection in EM-related DMN regions has also been reported by 2 research groups (Hedden et al., 2009; Sheline et al., 2009). Although these studies did not identify evidence for increased connectivity, increased prefrontal connectivity has been identified in AD subjects (Zhou et al., 2010).

Finally, evidence for increased task-positive activation during EM encoding was reported by Sperling et al., although comparisons between increased activation and memory performance were not investigated (Sperling et al., 2009). Overall, convergence of findings across research groups strengthens the much of the work presented in this dissertation. A major limitation across all our studies is the small samples, which will be resolved in ongoing studies with larger NC cohorts.

5.2 Personal opinion

Although not tested explicitly by myself or other researchers, I believe that results from initial PIB-PET studies of aging are suggestive of heterogeneity within PIB+ NC individuals. Specifically, I argue that PIB+ NCs may be categorized into 2 types—preclinical-PIB+ and resilient-PIB+. Preclinical-PIB+ individuals are on the trajectory towards AD, and are concurrently cognitively normal because they are at the beginning stage of Aβ deposition. Longitudinal follow-up of these subjects will reveal conversion to AD. Conversely, resilient-PIB+ individuals have somehow "cheated" Aβ. They may have as much or more pathology than an individual with clinical impairment, but have escaped a similar fate—perhaps through neural compensatory processes, enhanced neuronal development, optimal genetics, etc. Longitudinal follow-up of these NCs will reveal that they have remained normal. It is likely that these scenarios are extreme ends of a spectrum, but for the sake of argument I consider them 2 distinct outcomes within the population of PIB+ NCs. Of relevance when interpreting studies of aging employing PIB-PET imaging is that an appreciation of these 2 PIB+ subtypes will be averaged out when examining group differences. Thus, it is possible that inconsistencies across labs reside in the proportion of these 2 categories in each cohort. This also may explain why the effects we tend to identify with NCs are so subtle. In a cross-sectional design, it is impossible to differentiate between preclinical-PIB+ and resilient-PIB+ NCs—researchers are forced to examine PIB positivity as a homogenous condition. Longitudinal studies will offer insight into this potential distinction. For example, a retrospective study examining differences in PIB+ NCs converters versus PIB+ NCs nonconverters will be able to unveil neural and genetic differences between these subtypes. Furthermore, longitudinal studies will confirm whether or not truly resilient-PIB+ individuals exists: eg. are there PIB+ NCs that will not convert to AD after 5, 10, 15….25 years? These questions are relevant to our understanding of AD development, and also for consideration of whether theoretical anti-Aβ treatments will be necessary and/or effective amongst cognitively normal elderly individuals.

5.3 Future directions

The results I have presented in this dissertation are purely correlational and can only offer support for theoretical models of the impact of early Aβ deposition. To establish a causal relationship between Aβ and AD in humans, evidence from longitudinal studies, as well as intervention studies, are needed. Longitudinal studies will confirm the validity of

proposed cascades (ie. Aβ deposition→brain changes in structure/function→cognitive impairment). Whereas longitudinal studies may offer support for this temporal sequence of events, intervention trials will be the true test to the Aβ hypothesis of AD: is AD prevented if you remove or prevent Aβ deposition? It is likely that such an intervention would fail when applied to individuals with AD—at this point, neuronal damage and dysfunction may be too profound (a treatment geared towards neurotrophic processes may be more appropriate at this stage). However, within elderly NCs, where neuronal dysfunction is subtle and compensatory processes are active, intervention approaches may be successful and if so, would prove a causal link between Aβ and AD.

From the cognitive aging perspective, incorporating Aβ imaging in studies of aging may provide a biological mechanism for a proportion of the neural change observed in cohorts of "normal" elderly individuals. As mentioned in the personal opinion section, an understanding of heterogeneity within PIB+ NCs is of utmost importance to uncover early mechanisms and consequences of Aβ, and variability amongst NCs in response to Aβ burden. Furthermore, an understanding of NCs that are resilient to Aβ may offer insight into compensatory neural mechanisms, as well as neuronal plasticity in aging. It is also important to consider that sources of heterogeneity in "normal" aging exist beyond Aβ deposition—it is known that multiple types of pathological change occur in seemingly normal elderly individuals, such as vascular disease, dopamine depletion, etc. Traditionally, studies of aging examine changes that occur in old compared to young subjects, or changes within old subjects that relate to cognitive processes. However, it is possible that pathological processes have different neural effects in aging. The ability to measure these age-related pathologies enables researchers to directly address these sources of heterogeneity within aged populations, and understand whether distinct factors track with age-related impairment (it is also possible that different pathologies have additive effects on brain function and cognitive impairment). Thus, further research should simultaneously investigate distinct contributions of these pathologies to age-related changes in brain function.

Appendix A

Supplemental materials for chapter 3 of the dissertation

The following analyses are supplemental materials for the work reported in Chapter 3 of this dissertation. Overall, these additional figures and analyses provide clarification for data processing steps, as well as evidence that results are not an artifact of employed ICA functional connectivity methods.

Supplementary Figure 1: Schematic representation of functional connectivity method. [Part 1] A DMN template is established in a group of young subjects. [Part 1a] The PCC seed is defined on the MNI template and then registered to native subject space using the transformation matrixes defined between the subject's high-resolution structural scan and MNI template. Masks in the white matter, lateral ventricle, and whole brain are also transformed into subject space (all are shown except the whole brain mask). [Part 1b] The timeseries were extracted for all these masks and entered into a GLM, resulting in a FC map that reflects the amount each voxel correlates with the PCC, covarying signal from white matter/lateral ventricles/whole brain. [Part 1c] The PCC FC map was transformed to MNI space for each subject. [Part 1d] A 1-sample t-test was conducted using all FC maps and was thresholded at $p<0.001$, $k=100$. [Part 1e] A mask of all posterior clusters from the thresholded 1-sample t-test is used as the "posterior "DMN template during part 2 (the medial PFC cluster is removed from the template). [Part 2] Selection of best fit component for each old subject. [Part 2a] Each subject's preprocessed data is decomposed using ICA. [Part 2b] A number of components are isolated for each subject. [Part 2c] Each component is transformed to MNI space. [Part 2d] Transformed images are overlaid on the posterior DMN template and a goodness of fit index is calculated. In this example, component 8 is selected (denoted with a star). [Part 3] Higher level analysis examining relationship between PIB and DMN FC. [Part 3a] Best fit components from old subjects are used in a group level analysis regressing global PIB against voxelwise FC. Negative and positive relationships are examined. [Part 3b] Peaks from significant clusters are used to define spherical ROIs and subsequently used to contrast PIB values between old and AD subjects, and to explore relationships between FC and regional PIB.

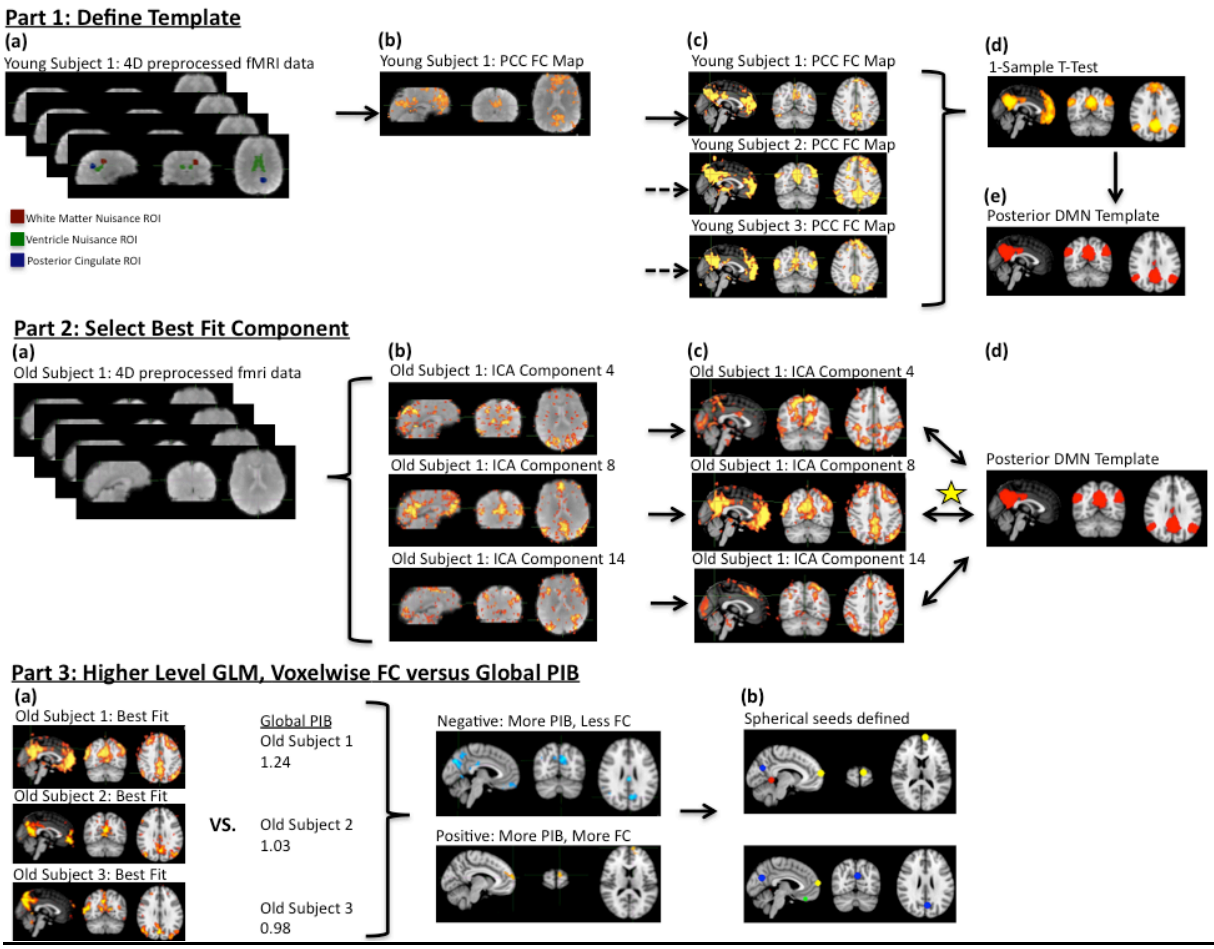
Part 1: Define Template
(a)
Young Subject 1: 4D preprocessed fMRI data
White Matter Nuisance ROI
Ventricle Nuisance ROI
Posterior Cingulate ROI
(b)
Young Subject 1: PCC FC Map
(c)
Young Subject 1: PCC FC Map
Young Subject 2: PCC FC Map
Young Subject 3: PCC FC Map
(d)
1-Sample T-Test
(e)
Posterior DMN Template
Part 2: Select Best Fit Component
(a)
Old Subject 1: 4D preprocessed fmri data
(b)
Old Subject 1: ICA Component 4
Old Subject 1: ICA Component 8
Old Subject 1: ICA Component 14
(c)
Old Subject 1: ICA Component 4
Old Subject 1: ICA Component 8
Old Subject 1: ICA Component 14
(d)
Posterior DMN Template
Part 3: Higher Level GLM, Voxelwise FC versus Global PIB
(a)
Old Subject 1: Best Fit
Old Subject 2: Best Fit
Old Subject 3: Best Fit
VS.
Global PIB
Old Subject 1
1.24
Old Subject 2
1.03
Old Subject 3
0.98
Negative: More PIB, Less FC
Positive: More PIB, More FC
(b)
Spherical seeds defined

Supplementary Figure 2: Comparison of results using (A) non-partial volume corrected PIB data and (B) partial volume corrected PIB data. Results are highly similar between these 2 approaches. Cool colors reflect a negative relationship whereas warm colors reflect a positive relationship between global PIB and DMN FC.

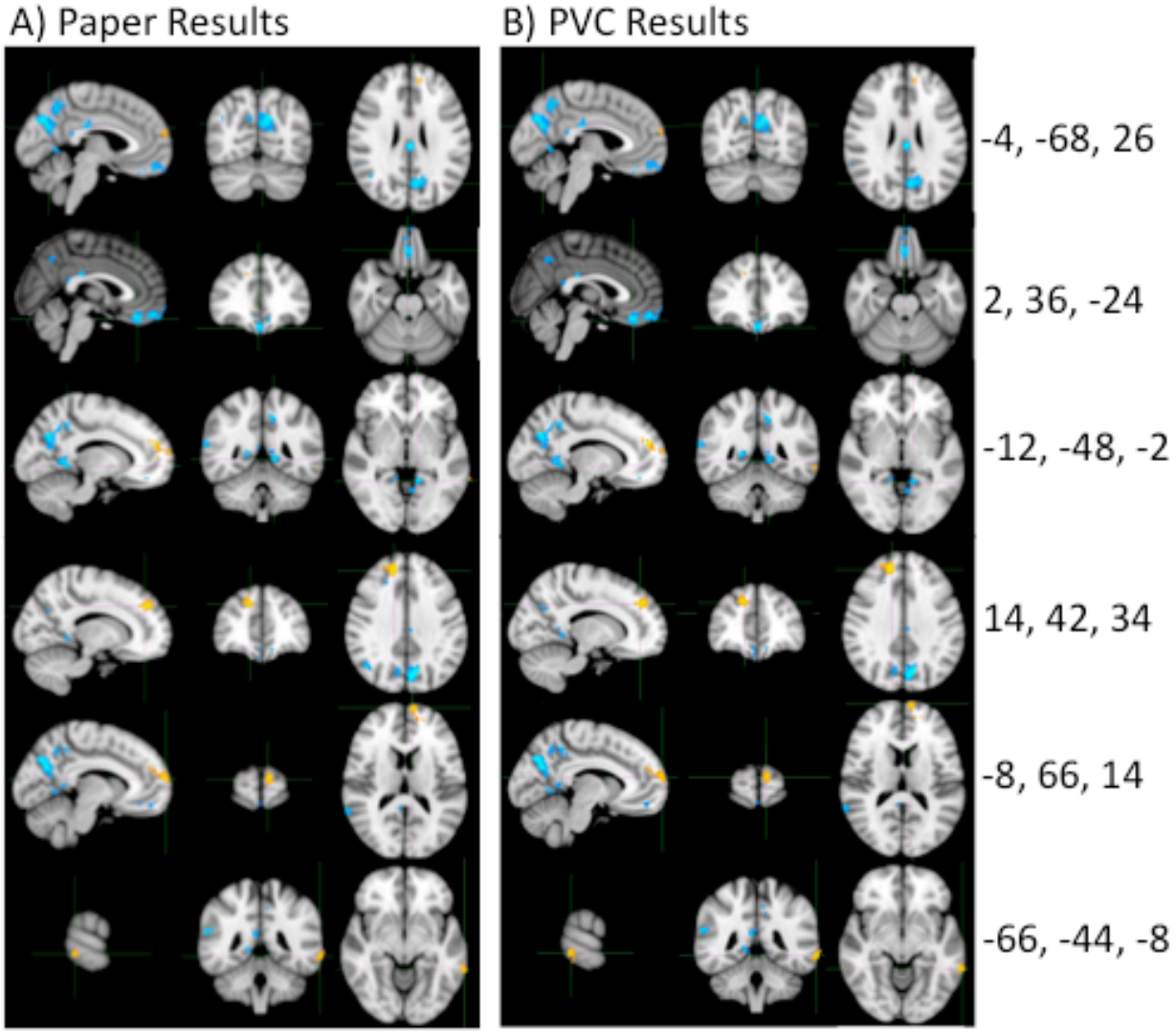

Supplemental Analysis 1: Comparison of seed analyses with ICA results. Given the novel finding of increased FC in the PFC and MTG, we conducted 3 additional analyses to determine whether these findings were dependent upon the employed ICA approach. To this end, we conducted seed analyses similar to those reported in the 2 previously published studies examining PIB and FC in normal controls (Hedden et al., 2009; Sheline et al., 2009). Three voxelwise seed analyses were conducted consistent with approaches used in these published manuscripts: (1) Hedden PCC seed (4mm sphere centered at 0, -53, 26), (2) Hedden mPFC seed (4mm sphere centered at 0, 52, -6) and (3) Sheline precuneus seed (12mm bilateral seed region centered at ±7, -60, 21). For this supplemental analysis,

preprocessing was unchanged from our manuscript (filtering, smoothing, motion correction) and additional steps were taken to remove the signal associated with motion and non-neuronal confounds (preprocessed data were first regressed against motion parameters, and the time-series extracted from nuisance ROIs [white matter, ventricles, and whole brain]). Using the resulting residual images, time series were extracted for each seed and regressed against the timeseries in every voxel. Thus, resulting connectivity maps reflect the extent to which that voxel is correlated with each seed region (r values converted to z values). Voxelwise analyses were conducted to relate resulting z values with global PIB using FSL's randomize (age/gender/education were covaried).

The result of each seed analysis is displayed in supplemental figures 3 and 4. For consistency, all analyses were masked with the 1 sample t-test used to mask the ICA analysis presented in the paper, and resulting significance maps were thresholded at $p<0.05$ and $k=50$ (identical to the results presented in the paper). In each case, cool colors reflect areas of decreased FC with increased PIB, and warm colors reflect increased FC with increased PIB. A consistent pattern of results across methods was identified—decreased FC in PMC and vmPFC, and increased FC in the amPFC and MTG. The left dPFC cluster is the only area to show increased FC only in the ICA method.

Supplementary Figure 3: Comparison of ICA and seed analyses at the level of the 6 peak coordinates identified in the ICA analysis.

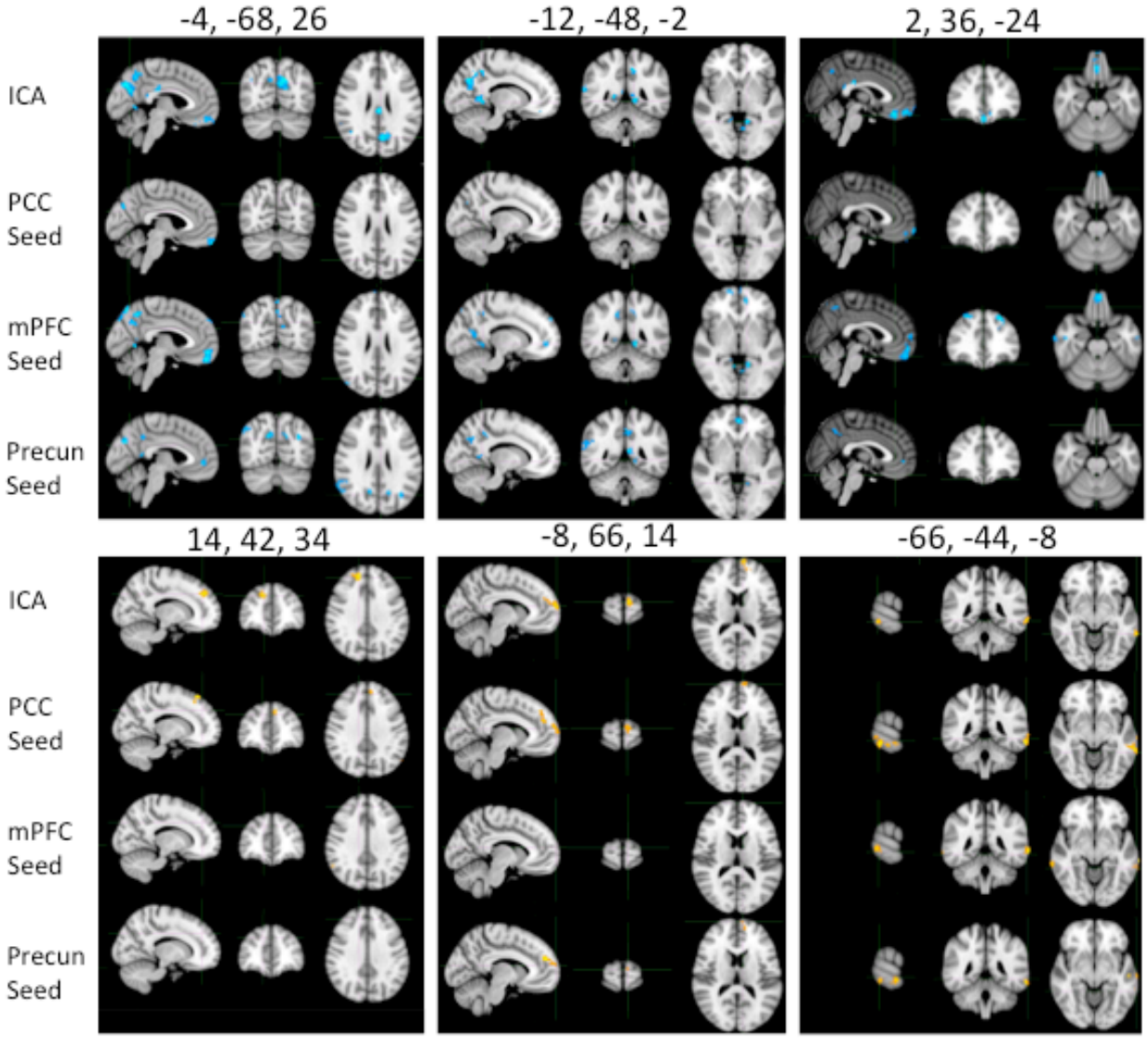

Supplementary Figure 4: Overlap between results from ICA and seed analyses. Voxels are red if they were significant in 3/4 analyses, blue if significant in 2/4 analyses and green if significant in 1 analysis.

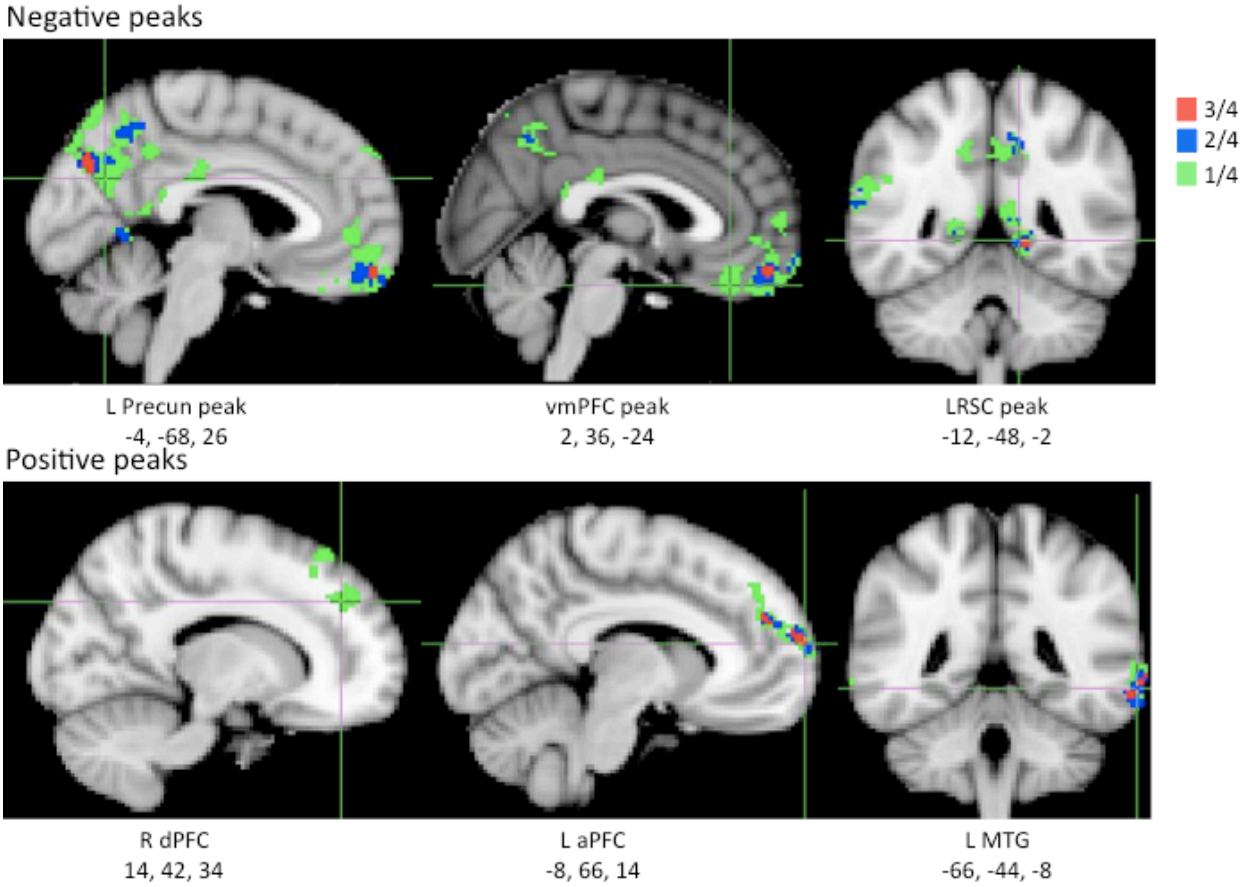

Supplementary Figure 5: Scatter plots showing relationships between DMN FC and global PIB in the 6 selected spherical ROIs. FC and PIB values were residualized by age/gender/education and plotted on each axis.

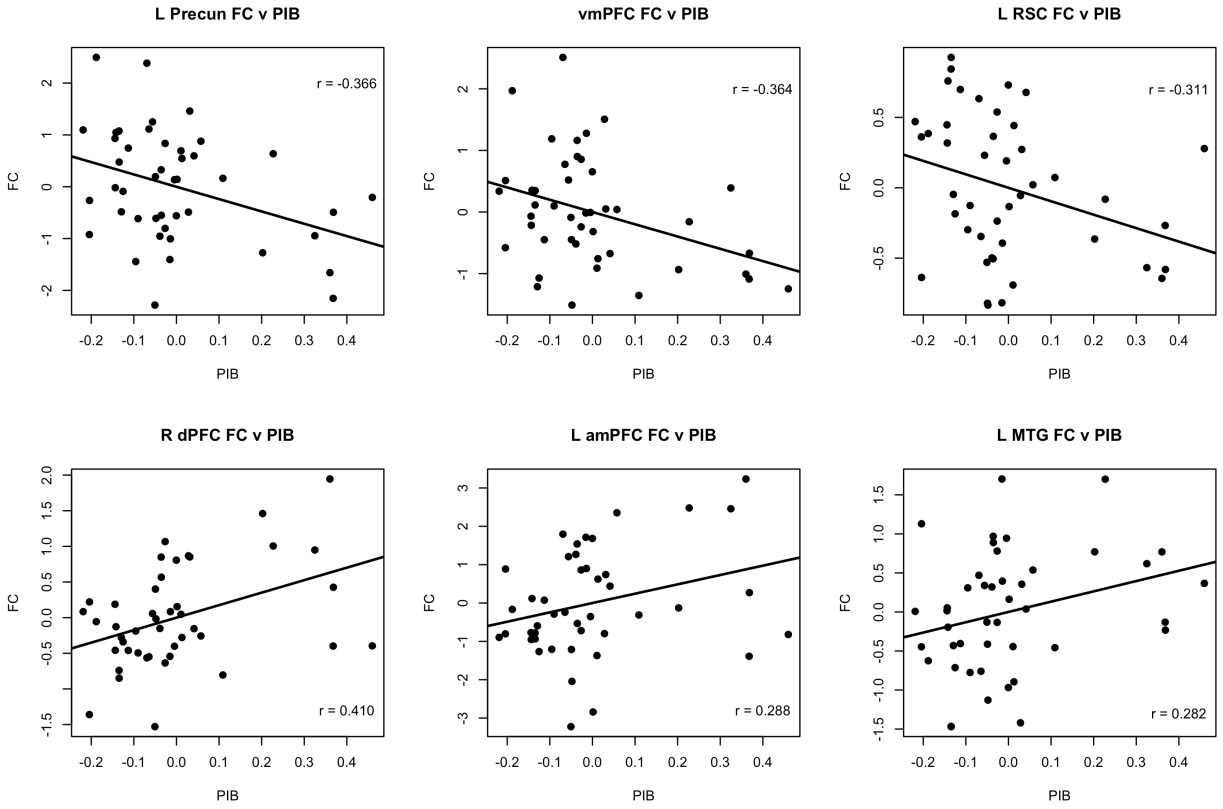

Supplemental Table 1: Comparison of regional PIB values between high PIB old and AD subjects. All ROIs showed significant elevation in AD compared to NC ($p<0.001$). L Precun and R dPFC were significantly higher than global PIB, whereas L RSC, L amPFC and L MTG were significantly lower.

	NC Mean	NC SD	AD Mean	AD SD	AD versus NC	ROI versus Global PIB
PIB Global	1.204	0.213	1.526	0.169	T=5.55, p<0.001	NA
PIB L Precun	1.311	0.338	1.762	0.274	T= 4.86, p<0.001	F=34.813 p<0.001
PIB L RSC	1.030	0.137	1.140	0.138	T= 2.652, p=0.011	F=121.21 p<0.001
PIB vmPFC	1.015	0.244	1.616	0.273	T= 7.695, p<0.001	F=2.2012 p=0.1452
PIB R dPFC	1.407	0.315	1.775	0.244	T=4.327, p<0.001	F=140.22 p<0.001
PIB L amPFC	1.014	0.255	1.363	0.180	T=5.242 p<0.001	F=170.09 < p<0.001
PIB L MTG	0.939	0.253	1.195	0.217	T=3.603 p<0.001	F=158.17 p<0.001

Supplementary Analysis 2: PIB versus FC ROI analysis. To investigate potential regional effects of Aβ, mean PIB and FC were extracted from the 6 ROIs defined in the main analysis. Although these ROIs are biased towards a relationship with global PIB since they were defined based on the relationship between global PIB and FC, we sought to determine

whether relationships were additionally present with local PIB values. Average PIB and FC values were residualized by age/gender/education, and Spearman rank correlations were conducted between all ROI PIB values versus ROI FC values (to determine whether there are focal and/or distal relationships between Aβ and DMN FC). Relationships with global PIB were also listed for comparison. The pattern of results in this analysis failed to reveal evidence for a specific relationship with regional PIB on DMN FC (supplemental table 2). Rather, areas that show relationships with increased PIB tend to do so across multiple PIB ROIs and to a similar extent to the correlation with global PIB.

It is possible that high covariance in PIB amongst brain regions makes identifying a specific effect of focal uptake difficult to dissociate from global PIB. Examination of interregional covariance between all ROIs confirmed a high level of correlation between ROI PIB and global PIB [average r=0.702 (0.138); as well as between all pairwise ROI comparisons (average r=0.625 (0.137); supplemental table 3)].

Supplemental Table 2: ROI analysis of PIB versus FC values. Pearson correlation coefficients are listed, significant relationships are bolded ($p<0.05$), and intraregional relationships are italicized (ie PIB versus FC within the same ROI). Average r absolute values are listed in the final column for each PIB ROI.

	FC L Precun	FC L RSC	FC vmPFC	FC R dPFC	FC L amPFC	FC L MTG	Average r
PIB Global	**-0.332**	**-0.317**	**-0.271**	**0.357**	**0.257**	0.182	0.286
PIB L Precun	***-0.347***	**-0.415**	**-0.347**	**0.275**	0.216	0.204	0.300
PIB L RSC	**-0.275**	***-0.294***	**-0.337**	**0.296**	0.199	0.086	0.248
PIB vmPFC	-0.101	-0.031	***-0.255***	0.252	0.101	0.022	0.127
PIB R dPFC	**-0.415**	**-0.327**	**-0.299**	*0.244*	0.246	0.228	0.293
PIB L amPFC	**-0.323**	**-0.367**	-0.116	**0.333**	***0.361***	**0.273**	0.296
PIB LMTG	**-0.294**	**-0.323**	**-0.290**	0.082	**0.267**	***0.375***	0.272

Supplemental Table 3: Pearson correlation coefficients amongst PIB ROI values.

	PIB Global	PIB L Precun	PIB L RSC	PIB vmPFC	PIB R dPFC	PIB L amPFC	PIB L MTG
PIB Global	1.000						
PIB L Precun	0.816	1.000					
PIB L RSC	0.693	0.741	1.000				
PIB vmPFC	0.532	0.554	0.485	1.000			
PIB R dPFC	0.881	0.805	0.657	0.479	1.000		
PIB L amPFC	0.732	0.793	0.596	0.547	0.767	1.000	
PIB L MTG	0.559	0.738	0.507	0.347	0.735	0.620	1.000

Appendix B

PIB+ classification based on young data

The following are analyses that have been prepared regarding classification of PIB scans. This work was motivated by the difficulty inherent in determining an appropriate cut off value for PIB positivity amongst our cohort of elderly NCs. This technical issue was avoided in early studies (chapters 1 and 2) by treating PIB as a continuous variable. However, our opinion regarding this approach evolved as more data was collected, and is directly addressed below.

Not quite PIB-positive, not quite PIB-negative: slight PIB elevations in elderly normal control subjects are biologically relevant

Abstract

Researchers employing Pittsburgh Compound B positron emission tomography (PIB-PET) imaging have consistently indentified old normal control (oNC) subjects with elevated tracer uptake, suggesting the presence of beta-amyloid deposition in these individuals. However, a consensus regarding the level at which PIB reveals a biologically meaningful signal does not exist (ie. an appropriate cutoff value for PIB positivity remains unclear). In this exploratory study, we sought to investigate the range of PIB distribution volume ratio (DVR) values present in our oNC cohort (N=75, age range=58-97). oNC subjects were classified based on global PIB index values (average DVR across prefrontal, parietal, lateral temporal and cingulate cortices) by employing two approaches: (1) an iterative outlier approach that revealed a cutoff value of 1.16 (IO-cutoff) and (2) an approach using data from a sample of young normal control subjects (N=11, age range=20-30) that yielded a cutoff value of 1.08 (yNC-cutoff). oNC subjects falling above the IO-cutoff had values similar to AD subjects ("PIB+", 15%). Subjects falling between the 2 cutoffs were considered to have ambiguous PIB status ("Ambig", 20%) and the remaining oNC were considered "PIB-" (65%). Additional measures capturing focal DVR magnitude and extent of elevated DVR values were consistent with the classification scheme using PIB index values, and revealed evidence for elevated DVR values in a subset of PIB- oNC subjects. Furthermore, there were a greater proportion of ambiguously elevated values compared to low values, and these elevated values were present in regions known to show amyloid deposition. The analyses presented in this study, in conjunction with recently published pathological data, suggest a biological relevance of slight PIB elevations in aging.

Introduction

Following the landmark human Pittsburgh Compound B positron emission tomography (PIB-PET) study in 2004 (Klunk et al., 2004), many researchers have applied amyloid imaging to investigate the relevance of beta-amyloid (Aβ) deposition in cognitively normal elderly "controls" (NC) (Rabinovici and Jagust, 2009). Consistent with data from post-mortem examination, these studies have re-affirmed that many NCs have extensive Aβ deposition. Furthermore, elevated PIB in NCs has been associated with differences in brain structure (Bourgeat et al., 2010; Dickerson et al., 2009; Fotenos et al., 2008; Jack et al., 2008; Mormino et al., 2009; Oh et al., 2010; Storandt et al., 2009) and brain function (Hedden et al., 2009; Mormino et al., 2011; Sheline et al., 2009; Sperling et al., 2009; Vannini et al., 2011), as well as subsequent decline in memory and conversion to AD (Morris et al., 2009; Storandt et al., 2009; Villemagne et al., 2011), suggesting that Aβ in NCs is not benign and may reflect an early stage of AD development.

Although PIB scans from some NC subjects display uptake indistinguishable from a typical AD scan, less-obvious cases exist that show sub-AD levels of tracer uptake. A major difficulty in assessing the relevance of these slightly elevated PIB values is that the conversion between actual plaque burden and tracer uptake is unclear. Comparison of PIB values to Aβ detected in brain tissue (via postmortem examination and brain biopsy) have shown that elevated PIB uptake is present in cases with high quantities of neuritic Aβ plaques, however the concordance between these measurements is inconclusive in subjects with evidence of low Aβ burden (Bacskai et al., 2007; Cairns et al., 2009; Ikonomovic et al., 2008; Leinonen et al., 2008). The ideal approach would involve comparison of postmortem measurements of Aβ with PIB in NCs, but these data are extremely difficult to obtain, and nearly impossible to obtain with a short delay between scanning and autopsy in NC individuals. To our knowledge, one study directly comparing PIB uptake with postmortem levels of Aβ in cognitively normal controls has been published (Sojkova et al., 2011). In this study, 3 of the 6 NC subjects showed slightly elevated pre-mortem PIB values and had a moderate CERAD rating in at least 1 of 3 regions examined at autopsy. Although limited by sample size, this data suggests that low levels of PIB uptake in NCs may reflect the presence of low quantities of Aβ deposition before AD-comparable levels are reached.

Given the limited data in older NCs, it is not surprising that a consensus regarding "PIB+" categorization is not established. For example, some groups have treated PIB as a continuous variable (Mormino et al., 2009; Pike et al., 2007) whereas other groups have dichotomized into PIB- and PIB+ groups (Aizenstein et al., 2008; Dickerson et al., 2009; Fotenos et al., 2008; Jack et al., 2008; Rowe et al., 2010). A cutoff value for group dichotomization is avoided by treating PIB as a continuous variable, however, the skewed distribution of this variable violates the assumptions of least-square regression and it is likely that there are low PIB values that merely reflect noise. Furthermore, there is variability in categorization approaches amongst studies that dichotomize into PIB+ and PIB- groups [hierarchical clustering (Rowe et al., 2010), iterative outlier removal (Aizenstein et al., 2008), etc]. Moreover, classification into PIB+ and PIB- is often dependent on the distribution of PIB values present in the NC group under investigation rather than on a group of subjects lacking Aβ deposition. Therefore, we cannot be confident that resulting PIB- subjects are definitively negative for Aβ.

To this end, we acquired PIB-PET data from a group of subjects 20 to 30 years of age under the assumption that these individuals have no Aβ deposition and therefore the

corresponding PET signal should only reflect noise. Although the age at which Aβ deposition begins is unknown, it has been shown that deposition is minimally present before age 50. For example, Kok and colleagues reported 7 of 114 subjects under age 50 had sparse CERAD ratings; no subjects under age 50 had moderate or frequent plaques (Kok et al., 2009). It is therefore highly unlikely that 20-30 year olds will have appreciable Aβ deposition and are an appropriate representation of true PIB- scans. Thus, the goal of this study was to investigate the presence of slightly elevated PIB values by employing different techniques to define positive scans and evaluate the likelihood that slight elevations in PIB uptake represent biologically significant Aβ deposition.

Methods

Subject Recruitment

All subjects underwent PIB-PET imaging and magnetic resonance imaging (MRI) for this study (table 1). Seventy-five older normal control (oNC) subjects were recruited via advertisements and word of mouth, and 11 young NC (yNC) subjects were recruited via online postings. Eligibility requirements for all NC subjects were no MRI contradictions, living independently in the community, MMSE≥26, normal performance on cognitive tests, absence of neurological or psychiatric illness and lack of major medical illnesses and medications that affect cognition.

Ten age-matched Alzheimer's disease (AD) patients were selected from a larger pool of subjects recruited from the University of California San Francisco (UCSF) Memory and Aging Center that have been scanned with PIB-PET and MRI. AD diagnosis was based on a comprehensive multi-disciplinary evaluation that includes a clinical history and physical examination, a caregiver interview and a battery of neuropsychological tests (Kramer et al., 2003). All AD subjects met NINDS criteria for probable AD (McKhann et al., 1984) and had no significant co-morbid medical, neurologic or psychiatric illnesses.

APOE Genotyping

DNA from blood samples for oNC and AD subjects were analyzed for apolipoprotein E (APOE) polymorphisms using a standard protocol. For statistical comparison between groups, subjects were dichotomized into carriers and non-carriers of the E4 allele. Genotyping was unavailable for 4 oNC subjects and 1 AD patient.

PIB-PET Acquisition

PIB was synthesized at the Lawrence Berkeley National Laboratory's (LBNL) Biomedical Isotope Facility using a published protocol and described in detail previously (Mathis et al., 2003; Mormino et al., 2009). PIB-PET imaging was performed at LBNL using an ECAT EXACT HR PET scanner (Siemens Medical Systems, Erlangen Germany) in 3D acquisition mode. 10-15 mCi of PIB was injected into an antecubital vein. Dynamic acquisition frames were obtained as follows: 4 x 15 sec, 8 x 30 sec, 9 x 60 sec, 2 x 180 sec, 8 x 300 sec and 3 x 600 sec (90 minutes total). Ten minute transmission scans for attenuation correction were obtained for each PIB scan. Filtered backprojected reconstructions were performed on the transmission and emission data to judge transmission alignment with each frame of emission data. In the case of misalignment, the transmission image was coregistered to that individual emission frame, and then forward

projected to create an attenuation correction file specific to that head position. PET data were reconstructed using an ordered subset expectation maximization algorithm with weighted attenuation. Images were smoothed with a 4mm Gaussian kernel with scatter correction.

Structural MRI Acquisition

For oNC and yNC subjects, T1-weighted volumetric magnetization prepared rapid gradient echo scans (MPRAGE, axially acquired, TR/TE/TI=2110/3.58/1100ms, flip angle = 15°, 1.00x1.00mm^2 in plane resolution, 1.00mm thickness with 50% gap) were collected at LBNL on a 1.5T Magnetom Avanto System (Siemens Medical Systems, Erlangen Germany) with a 12 channel head coil run in triple mode. For AD patients, MPRAGE scans were collected on a 1.5T Vision System (Siemens Medical Systems, Erlangen Germany) with a quadrature head coil (coronally acquired, TR/TE/T1=10/7/300ms, flip angle = 15°, 1.00x1.00mm^2 in plane resolution, 1.40mm slice thickness with no gap).

PIB-PET Processing

PIB-PET data were preprocessed using the SPM8 software package (http://www.fil.ion.ucl.ac.uk/spm). Realigned PIB frames corresponding to the first 20 minutes of acquisition were averaged and used to guide coregistration to the subject's structural MRI scan. Distribution volume ratios (DVRs) for PIB images were created using Logan graphical analysis with frames corresponding to 35-90 min post-injection and a gray matter masked cerebellum reference region defined using FreeSurfer software (Logan et al., 1996; Price et al., 2005).

Structural MRI Processing

MPRAGE scans were processed as described previously (Mormino et al., 2009) using FreeSurfer version 4.5.0 (http://surfer.nmr.mgh.harvard.edu/) to derive regions of interest (ROIs) in each subject's native space (Dale et al., 1999; Fischl et al., 2001; Fischl et al., 2002; Segonne et al., 2004). PIB index values were derived by averaging PIB DVR values from prefrontal, cingulate, lateral temporal and parietal ROIs. Additionally, mean PIB DVR values were extracted from the 68 cortical ROIs defined automatically by FreeSurfer (Desikan et al., 2006).

Classification approaches

Primary approach

Two methods to define cutoffs using PIB index values were employed: an iterative outlier approach (Aizenstein et al., 2008) and an approach using PIB index values from the yNC group. The iterative outlier approach removes oNC cases from the oNC group until all outliers are excluded (defined as values greater than the upper quartile value plus 1.5 times the interquartile range). Once all outliers are removed from the data set, 2.5% is added to the PIB index of the highest remaining case (corresponding to the upper inner fence of the box-and-whisker plot) and the resulting value is used as the cutoff. A global PIB index value was used in this procedure rather than multiple ROIs (Aizenstein et al.,

2008). The yNC derived cutoff was 2 standard deviations above the mean yNC PIB index value.

Subjects were classified into 3 categories based on these 2 cutoffs—subjects classified as high in both methods were labeled "PIB+" and subjects classified as low in both methods were classified as "PIB-." Cases with incongruent labeling (high in 1 approach and low in the other) were labeled "Ambiguous" (Ambig).

Secondary Approaches

To investigate PIB uptake in a manner unbiased by the pattern of regional deposition (as is the case with the PIB index approach), additional approaches were taken to explore focal DVR magnitude, as well as measures investigating the extent of PIB elevation in each subject. Focal DVR magnitude was investigated by examining the maximum ROI value for each participant (mean DVR values from all 68 FreeSurfer cortical ROIs were investigated). To restrict this analysis to ROIs outside the range shown by PIB-yNCs, ROI-specific cutoff values were determined for each ROI using 2 standard deviations above the young group's mean for that particular ROI. ROIs below the corresponding ROI-specific cutoff were excluded from this analysis for each subject. To explore uptake extent, the distribution of ROI values for each subject was compared against the distribution of ROI values from the yNC group using a Kolmogorov–Smirnov test. Resulting d-statistics from this test provides a measure of the overall shift in the distribution of ROI values for each subject relative to the young population, thus reflecting the degree to which PIB extent is elevated irrespective of specific spatial location (both rightward and leftward shifts were tested). A final measure simultaneously combined focal magnitude and extent. For this approach, the number of "high" ROIs (2 standard deviations above the yNC mean for that ROI) was counted for each subject.

Comparison between ambiguous elevations and analogous decreases

Instances of ambiguously elevated PIB values were directly compared to analogous reductions in oNC subjects using chi-squared and paired t-tests. This analysis was performed using the 3 aforementioned measures of PIB uptake: (1) PIB Index (the number of subjects falling above and below 2 standard deviations from the mean of yNC PIB index values), (2) d-statistics from the KS-tests (the number of subjects showing significant deviation from the young distribution [$p<0.01$] in either direction [ie. a rightward shift indicates a greater extent of increased PIB values whereas a leftward shift indicates a greater extent of reduced PIB values]) and (3) high versus low ROIs (the number of ROIs above and below 2 standard deviations from the yNC mean for each specific ROI). PIB+ oNC were excluded from this analysis, enabling direct investigation of values falling in the ambiguous range.

Spatial distribution of elevated brain regions

To explore the spatial pattern of heightened PIB uptake in a data driven manner, the percentage of oNCs showing elevated uptake for each ROI was computed and overlaid on a brain schematic. Percentages were re-computed within each oNC group separately to determine whether a pattern of deposition was apparent across different levels of PIB uptake.

Statistical analyses and graphics

All statistical analyses and plots were completed using R version 2.11 (http://www.r-project.org/). Group differences in demographic variables were determined with Wilcoxon signed rank tests for continuous variables and chi-squared tests for dichotomous variables. Within oNC subjects, multiple regression with planned contrasts (PIB+ oNC versus PIB- oNC; PIB+ oNC versus Ambig oNC; Ambig oNC versus PIB- NC) were used to assess relationships between MMSE and PIB (controlling for age, sex and education). $P<0.05$ was considered a significant difference, and trends corresponding to $p<0.15$ were noted. Brain schematics were designed in GIMP version 2.6 (http://www.gimp.org/).

Results

Group Characteristics

Group characteristics are listed in table 1. There were no significant differences in gender or education across yNC, oNC and AD groups, although there was a trend for a higher frequency of males than females in AD compared to oNCs ($\chi^2 = 2.38$, df = 1, p= 0.123) and a trend for higher education in oNCs than yNCs (W = 291, p= 0.106). yNCs showed significantly lower PIB index values than oNCs (W = 576, p= 0.035) and AD (W = 103, p= 0.0003), and oNC subjects had lower PIB index values than AD (W = 667, p= 7.008e-05). AD patients had lower MMSE scores than yNCs (W = 5, p= 0.0004) and oNCs (W = 19, p= 3.09e-07). MMSE was not different between yNC and oNC subjects.

Table 1: Subject characteristics

	yNC	PIB- oNC	Ambig oNC	PIB+ oNC	AD
N	11	49	15	11	10
Age	23 (20, 30)	74 (58, 91)	74 (62, 87)	76 (71, 97)	76 (63, 90)
Gender	5M	20M	6M	3M	7M
Education	16 (14, 20)	17 (12, 20)	18 (13, 18)	16 (14, 20)	16 (13, 22)
APOE (ε4+/-)	NA	11/34	5/10	6/5	6/3
MMSE	29 (26, 30)	29 (26, 30)	30 (28, 30)	29 (26, 30)	21 (1, 28)
PIB Index	1.03 (1.00, 1.08)	1.04 (0.88, 1.08)	1.10 (1.09, 1.15)	1.40 (1.20, 1.69)	1.61 (1.03, 1.80)

Table 1: yNC=young normal controls, oNC=old normal controls, AD=Alzheimer's disease patients. Medians and ranges are reported for continuous variables. APOE status was unavailable for 4 oNC subjects and 1 AD patient.

Group Classification

The iterative outlier approach revealed a cutoff value of 1.16 (IO-cutoff), whereas the young-derived cutoff was 1.08 (yNC-cutoff; yNC mean=1.04, sd=0.02; figure 1). Fifteen percent (11/75) of oNC subjects were above the IO-cutoff (PIB+), 20% (15/75) were below the IO-cutoff but above the yNC-cutoff (Ambig) and 65% (49/75) were below the yNC-cutoff (PIB-). Nine AD patients were PIB+ while 1 AD patient was PIB-.

AD subjects had greater PIB index values than PIB- oNC (W = 35, p= 1.613e-06) and Ambig oNC groups (W = 15, p= 0.0004). There was a trend for AD subjects to have higher PIB index values than PIB+ oNC (W = 33, p= 0.132), and this relationship became significant after removal of the single PIB- AD subject (W = 22, p= 0.038).

PIB+ oNC subjects were significantly older than Ambig subjects (W = 44, p= 0.047) and there was a trend for PIB+ oNCs to be older than PIB- oNCs (W = 192, p= 0.143). There were no pair wise differences in education and gender across the 3 oNC groups. Controlling for age/gender/education, there was a trend for worse MMSE in PIB+ oNC than Ambig oNC (t=-1.548, p=0.126).

The APOE4 allelle was present in 24% PIB- oNC, 33% Ambig oNC, 55% PIB+ oNC and 67% of AD subjects. There was a significant pairwise difference in APOE4 allelle frequency between AD and PIB- oNCs (χ^2 = 4.396, df = 1, p= 0.036) and a trend for more e4 carriers in PIB+ oNCs than PIB- oNCs (χ^2 = 2.498, df = 1, p= 0.114). No other pairwise comparison was significant.

Figure 1: Distribution of PIB index values

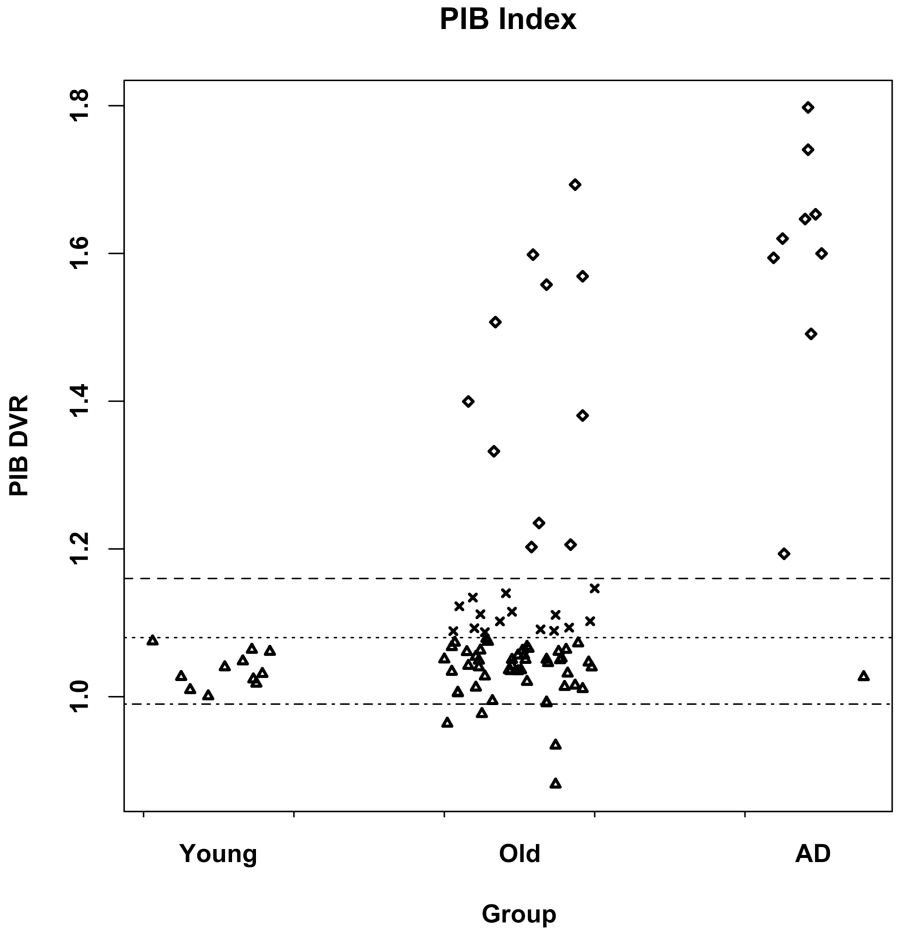

Figure 1: Values are randomly scattered on the x-axis to allow visualization of individual subjects. The iterative outlier cut off is shown with a dashed line ("IO-cutoff", 1.16) while the yNC derived cut off is shown with a dotted line ("yNC-cutoff", 1.08). Additionally, an analogous yNC derived low cut off is shown with a dash-dotted line ("yNC-cutoff-low", 0.99). Based on the IO- and yNC-cutoffs, subjects were classified into 3 groups: PIB+ (above IO-cutoff; diamonds), Ambig (below IO-cutoff and above yNC-cutoff; 'x's) and PIB- (below yNC-cutoff; triangles).

<u>Secondary Measures of PIB Uptake</u>

Three additional measures were derived to investigate PIB uptake in a manner unbiased by the spatial pattern of PIB uptake. The first approach examined the highest ROI value for each subject, restricting the analysis to only those ROIs exceeding an ROI specific cutoff value (cutoffs are listed in table 2). In this analysis, 12 of 49 PIB- oNCs and 7 of 11 yNCs did not have an ROI that exceeded the young-defined ROI cutoffs, whereas all Ambig oNC, PIB+ oNC and AD subjects had at least 1 high ROI. The ROI with the highest DVR value for each subject is plotted against group status in figure 2A, and reveals an upward trend between maximum ROI value and group status. Of note is 1 yNC subject with a maximum ROI value of 1.44 located in the left caudal anterior cingulate.

To investigate the extent of elevated ROIs irrespective of spatial location, Kolmogorov–Smirnov (K-S) tests were performed to compare the distribution of the 68 ROI values for each individual subject to the distribution across all young NC subjects. Resulting d-statistics from this test are plotted in figure 2B (a d-statistic of 0.19 corresponds to a p-value of 0.01 for the difference between each subject's distribution of ROI values and the yNC group's distribution), and group level histograms are shown in figure 3. This approach reveals a rightward shift in the distribution of PIB ROI values in Ambig oNC, PIB+ oNC and AD groups, reflecting a greater number of elevated PIB ROIs in these subjects.

A final measure of PIB uptake that simultaneously combined aspects of focal DVR magnitude and extent is plotted in figure 2C. In this analysis, the number of ROIs with values at least 2 standard deviations above the yNC ROI-specific mean was tallied for each subject. This analysis shows a clear stepwise increase across groups. Interestingly, this analysis reveals that many PIB- oNC subjects show substantial numbers of ROIs (>10) with high PIB uptake, suggestive of amyloid accumulation in this group.

Table 2: yNC derived cutoff values

Hemi	Freesurfer ROI	YNC Mean	YNC SD	Cutoff (above)	Cutoff (below)	PIB+ oNC, N=11		Ambig oNC, N=15		PIB- oNC, N=49	
						# High	# Low	# High	# Low	# High	# Low
Right	bankssts	1.1230	0.0593	1.24	1.00	11	0	9	0	6	0
Left	bankssts	1.1557	0.0592	1.27	1.04	10	0	7	0	5	0
Right	caudalanteriorcingulate	1.0790	0.0352	1.15	1.01	11	0	5	1	5	12
Left	caudalanteriorcingulate	1.1400	0.1057	1.35	0.93	9	0	0	0	0	3
Right	caudalmiddlefrontal	1.0791	0.0418	1.16	1.00	10	0	5	0	3	6
Left	caudalmiddlefrontal	1.0577	0.0309	1.12	1.00	11	0	13	0	10	6
Right	cuneus	1.1363	0.0510	1.24	1.03	8	1	0	1	0	8
Left	cuneus	1.0909	0.0588	1.21	0.97	7	0	3	0	0	2
Right	entorhinal	0.9461	0.0433	1.03	0.86	6	0	4	1	6	5
Left	entorhinal	0.9600	0.0646	1.09	0.83	2	0	2	2	1	3
Right	frontalpole	0.7526	0.0518	0.86	0.65	8	1	1	0	4	3
Left	frontalpole	0.7883	0.0652	0.92	0.66	6	1	2	0	1	3
Right	fusiform	1.0339	0.0379	1.11	0.96	9	0	2	0	1	4
Left	fusiform	1.0447	0.0448	1.13	0.96	8	0	1	0	1	5
Right	inferiorparietal	1.0589	0.0354	1.13	0.99	11	0	11	0	8	1
Left	inferiorparietal	1.0459	0.0248	1.10	1.00	11	0	13	0	14	5
Right	inferiortemporal	0.9541	0.0281	1.01	0.90	11	0	5	0	1	1
Left	inferiortemporal	0.9634	0.0345	1.03	0.89	9	0	4	0	1	3
Right	insula	1.0978	0.0473	1.19	1.00	10	0	2	0	1	3
Left	insula	1.0895	0.0469	1.18	1.00	10	0	4	0	1	3
Right	isthmuscingulate	1.0902	0.0560	1.20	0.98	11	0	6	0	4	0
Left	isthmuscingulate	1.1005	0.0846	1.27	0.93	10	0	1	0	0	1
Right	lateraloccipital	1.0569	0.0239	1.10	1.01	9	0	10	1	9	7
Left	lateraloccipital	1.0389	0.0317	1.10	0.98	9	1	5	1	5	10
Right	lateralorbitofrontal	0.9919	0.0445	1.08	0.90	11	0	0	0	0	5
Left	lateralorbitofrontal	0.9761	0.0395	1.06	0.90	11	0	6	0	2	3
Right	lingual	1.0739	0.0405	1.15	0.99	4	0	0	2	0	15
Left	lingual	1.0298	0.0522	1.13	0.93	4	0	1	1	0	2
Right	medialorbitofrontal	0.9565	0.0446	1.05	0.87	11	0	8	1	10	2
Left	medialorbitofrontal	0.9936	0.0495	1.09	0.89	10	0	8	0	5	4
Right	middletemporal	0.9635	0.0216	1.01	0.92	11	0	8	0	8	4
Left	middletemporal	0.9607	0.0270	1.01	0.91	9	0	4	0	8	4
Right	paracentral	1.0830	0.0602	1.20	0.96	9	0	5	1	1	3
Left	paracentral	1.0864	0.0690	1.22	0.95	8	0	3	0	0	6
Right	parahippocampal	0.9815	0.0344	1.05	0.91	7	0	4	1	5	9
Left	parahippocampal	0.9884	0.0535	1.10	0.88	7	0	1	1	0	6
Right	parsopercularis	1.0700	0.0436	1.16	0.98	10	0	2	0	1	5
Left	parsopercularis	1.0355	0.0315	1.10	0.97	11	0	9	0	4	8
Right	parsorbitalis	0.9347	0.0534	1.04	0.83	11	0	0	0	1	6
Left	parsorbitalis	0.9092	0.0675	1.04	0.77	10	0	1	0	0	1
Right	parstriangularis	1.0135	0.0448	1.10	0.92	11	0	5	0	5	2
Left	parstriangularis	0.9845	0.0412	1.07	0.90	11	0	9	0	6	4
Right	pericalcarine	1.1294	0.0467	1.22	1.04	7	1	3	1	1	4
Left	pericalcarine	1.0845	0.0772	1.24	0.93	6	0	1	0	2	0
Right	postcentral	1.0353	0.0415	1.12	0.95	9	0	1	0	0	10
Left	postcentral	1.0115	0.0340	1.08	0.94	9	0	3	0	1	7
Right	posteriorcingulate	1.1162	0.0440	1.20	1.03	11	0	7	0	4	5
Left	posteriorcingulate	1.1335	0.0561	1.25	1.02	11	0	1	0	0	3
Right	precentral	1.0631	0.0505	1.16	0.96	9	0	3	0	2	3
Left	precentral	1.0628	0.0404	1.14	0.98	10	0	4	0	1	5
Right	precuneus	1.0826	0.0428	1.17	1.00	11	0	7	0	0	7
Left	precuneus	1.0532	0.0538	1.16	0.95	10	0	7	0	5	1
Right	rostralanteriorcingulate	1.0670	0.0630	1.19	0.94	11	0	5	0	2	4
Left	rostralanteriorcingulate	1.0971	0.0642	1.23	0.97	10	0	6	0	2	4
Right	rostralmiddlefrontal	0.9820	0.0422	1.07	0.90	11	0	6	0	3	2
Left	rostralmiddlefrontal	0.9750	0.0290	1.03	0.92	11	0	8	0	7	2
Right	superiorfrontal	1.0074	0.0309	1.07	0.95	11	0	7	0	4	6
Left	superiorfrontal	1.0316	0.0373	1.11	0.96	11	0	5	0	0	11
Right	superiorparietal	1.0586	0.0493	1.16	0.96	9	0	4	0	0	3
Left	superiorparietal	1.0317	0.0471	1.13	0.94	9	0	6	0	2	3
Right	superiortemporal	1.0039	0.0169	1.04	0.97	11	0	4	0	10	8
Left	superiortemporal	1.0259	0.0333	1.09	0.96	10	0	1	0	2	5
Right	supramarginal	1.0329	0.0300	1.09	0.97	11	0	8	0	6	2
Left	supramarginal	1.0290	0.0262	1.08	0.98	11	0	13	0	6	3
Right	temporalpole	0.8440	0.0616	0.97	0.72	6	0	0	0	1	4
Left	temporalpole	0.8534	0.0434	0.94	0.77	3	1	1	3	1	12
Right	transversetemporal	1.1055	0.0768	1.26	0.95	8	0	2	0	3	1
Left	transversetemporal	1.1724	0.0612	1.29	1.05	6	0	2	0	0	1

Table 2: Means, standard deviations (SD) and cutoffs are listed for all FreeSurfer ROIs (68 total). Cutoffs were defined as 2 SDs above the yNC mean. An analogous "below" cutoff was also examined (2 SDs below the yNC mean). The number of ROIs classified as low and high based on these 2 cut offs is listed for PIB+ oNC, Ambig oNC and PIB- oNC groups separately.

Figure 2: Secondary measures of PIB uptake

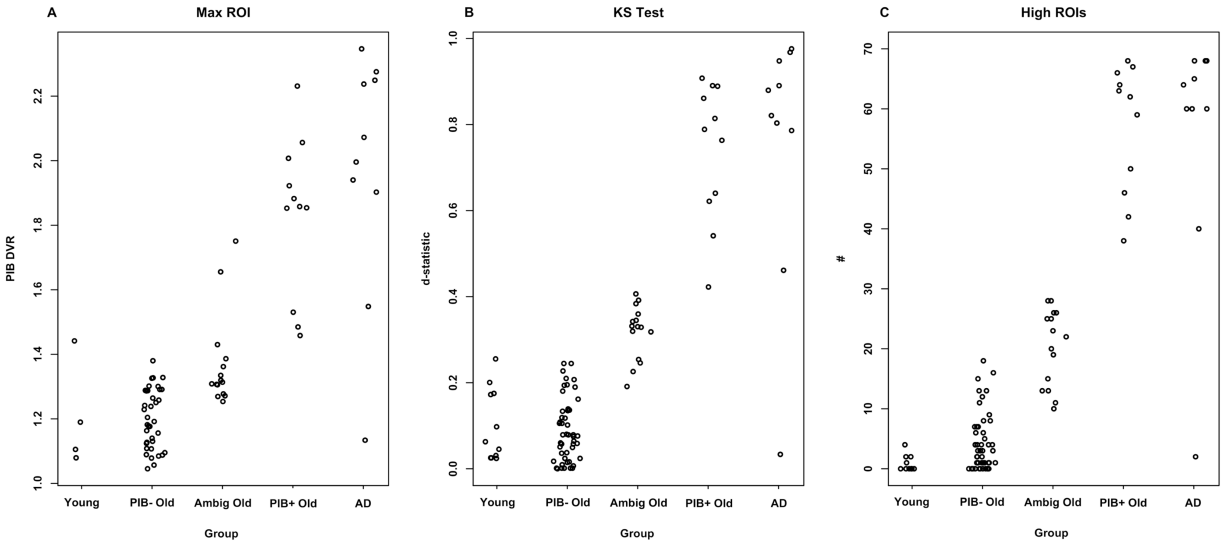

Figure 2: (A) Focal PIB DVR magnitude was examined by plotting the maximum ROI value for each subject. (B) Extent of elevated PIB DVR values was assessed using Kolmogorov–Smirnov (K-S) tests. (C) High ROIs were tallied for each subject (as defined by yNC-derived cut off values). For consistency, oNC are plotted using group classification as defined by PIB index cut offs. Across these approaches, Ambig oNC subjects reside between PIB- and PIB+ oNC groups, and the PIB+ oNC group is similar to the AD group.

Figure 3: Qualitative examination of group level distributions

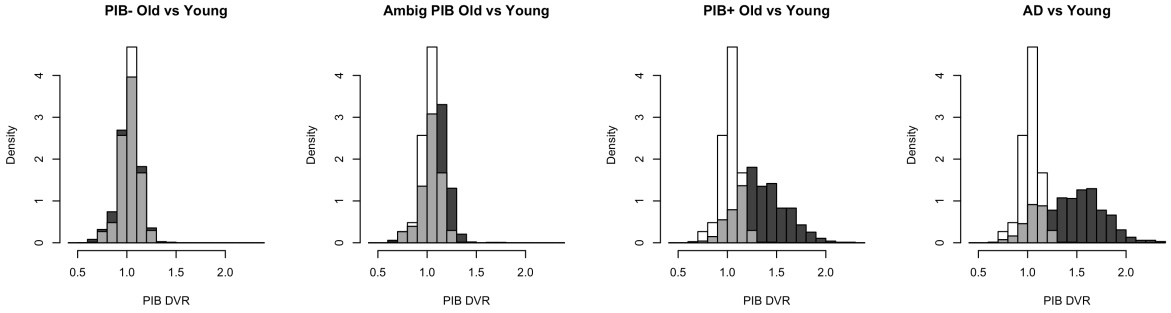

Figure 3: oNC and AD group histograms are overlaid on the yNC group's histogram. Density is plotted on the y-axis rather than frequency to account for different subject number in each group. White portions exclusively reflect yNC subjects, dark grey reflects the group under comparison, and light grey reflects the overlap between histograms. A rightward shift in the distribution of PIB DVR ROIs values is present in Ambig oNC, PIB+ oNC and AD groups, reflecting a greater quantity of elevated PIB DVR ROI values in these subjects.

<u>Ambiguous elevations versus analogous decreases</u>

Instances of ambiguously elevated PIB values were compared to analogous reductions for (1) PIB Index (the number of subjects falling above 1.08 versus below 0.99), (2) KS-test d-statistics (the number of subjects showing significant deviation from the young distribution ($p<0.01/d>0.19$) in each direction) and (3) high versus low ROIs (the total number of ROIs above and below yNC ROI-specific cutoffs). This analysis was

restricted to data from Ambig oNC and PIB- oNC subjects, since these data contain the ambiguous signals under investigation. Chi-squared tests were used to compare the number of subjects with high versus low PIB index values, as well as the number of subjects showing a significant distribution shifts. A paired t-test was used to contrast the number of high and low ROIs across subjects.

There were significantly more oNC with ambiguously high PIB indices than ambiguously low (15 versus 4 subjects; $\chi^2 = 6.37$, df = 1, p = 0.01; figure 1), a greater number of subjects with a significant rightward than leftward shift in PIB ROI values (23 versus 10 subjects; $\chi^2 = 5.12$, df = 1, p= 0.024) and a trend for more high than low ROIs across subjects (a mean of 8 high ROIs compared to 5 low ROIs per subject; t = 1.69, df = 63, p-value = 0.096).

Spatial distribution of high ROIs

To investigate the spatial pattern of elevated PIB values, the percentage of oNC with high values for each ROI was plotted on a schematic brain for the entire oNC group, as well as within PIB+, Ambig, and PIB- oNC groups. This analysis revealed that elevated ROIs were most common in association cortices, most notably medial orbital, dorsolateral prefrontal, and temporoparietal cortices (figure 4). Repeating this analysis within groups revealed diffuse elevations in PIB+ oNC subjects and more focal deposition in Ambig oNC subjects (in prefrontal, precuneus and temporoparietal cortices, figure 5A-B). Furthermore, the PIB- oNC group showed evidence for elevated ROIs in dorsolateral prefrontal, medial orbital and temporoparietal cortices (figure 5C). Conversely, low ROIs were diffusely spread across the examined regions and did not reveal a consistent pattern (table 2 and figure 6).

Figure 4: Spatial distribution of elevated PIB values

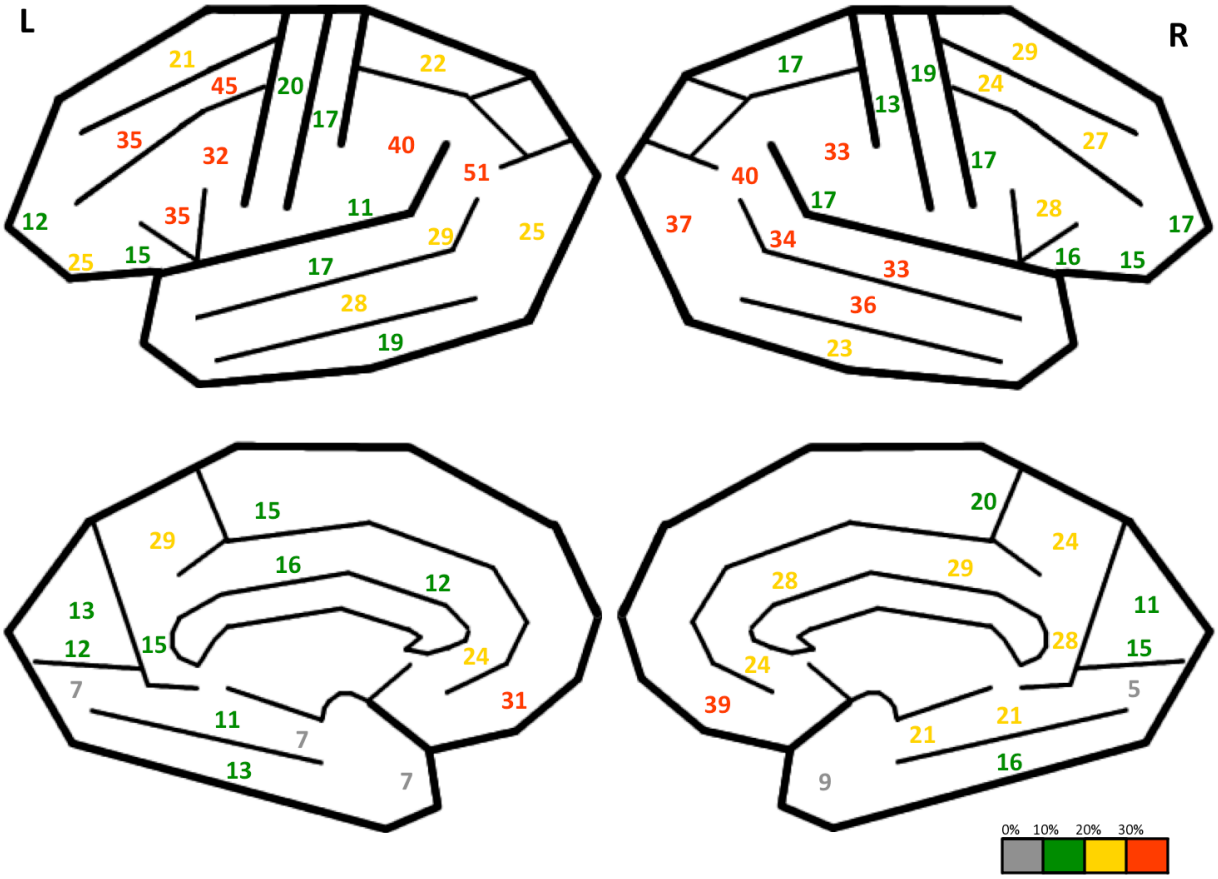

Figure 4: Schematic showing the percentage of oNC subjects with high PIB values for each cortical ROI. Many subjects have elevated ROI values in association cortices, with the largest percentages present in medial orbital, dorsolateral prefrontal, and temporoparietal cortices. All ROIs listed in supplemental table 1 are represented other than the insula. Text color scheme: red=greater than 30%, yellow=21-30%, green=11-20%, gray=0-10%.

Figure 5: Within group spatial distributions

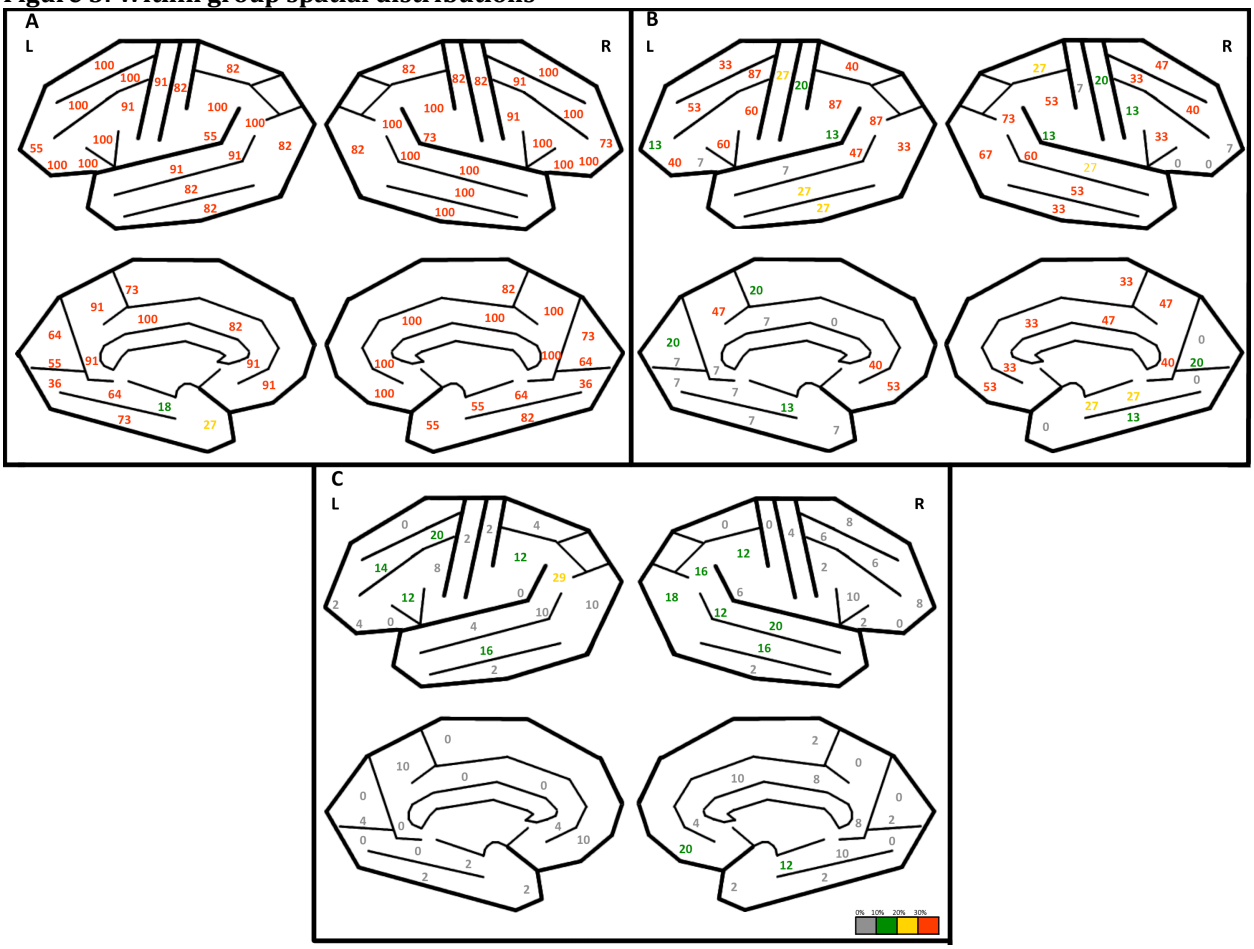

Figure 5: Percentage of subjects with high ROIs plotted separately for (A) PIB+, (B) Ambig and (C) PIB- oNC groups. Elevated ROIs are present across all regions in PIB+ oNC subjects, whereas Ambig oNC subjects show a pattern of restricted elevation, albeit in areas known to show high levels of amyloid deposition (prefrontal, precuneus and temporoparietal cortices). Interestingly, even the PIB- oNC group shows some evidence of focal deposition in dorsolateral prefrontal, medial orbital and temporoparietal cortices. All ROIs listed in supplemental table 1 are represented other than the insula. Text color scheme: red=greater than 30%, yellow=21-30%, green=11-20%, gray=0-10%.

Figure 6: Prevalence of high and low subjects per ROI

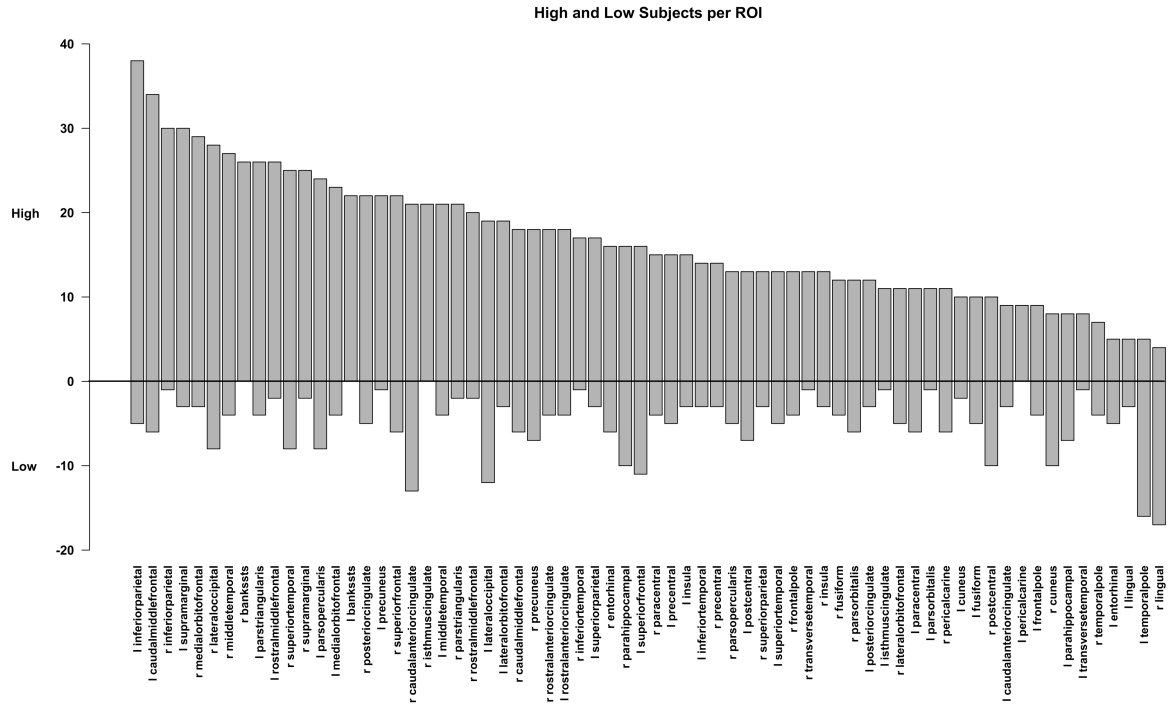

Figure 6: Total number of oNC subjects with high and low ROIs are plotted for each ROI. The number of subjects with high values is depicted by the upper edge of each bar, whereas the number of subjects with low values is depicted by the lower edge of each bar. ROIs are ordered along the x-axis by number of subjects with high ROIs. There is a lack of relationship between the number of subjects with high and low values within each ROI.

Discussion

In this study we employed two approaches to classify oNC subjects based on PIB index values. An iterative outlier approach using index values from the oNC group yielded a cutoff value of 1.16 (IO-cutoff). An approach using data from a sample of yNC subjects (age range 20-30, who are likely to lack Aβ deposition and hence provide a good estimate of PIB negativity), revealed a lower cutoff value of 1.08 (yNC-cutoff). oNC subjects falling above the IO-cutoff (PIB+ oNC; 11/75) showed substantial overlap with AD subjects across all examined measures of PIB uptake. Subjects falling between the 2 cutoffs were less obvious and labeled as ambiguous (Ambig oNC; 15/75), and the remaining subjects were considered PIB- oNCs (49/75). Further examination of these oNC groups across different PIB quantification measures consistently confirmed the intermediate status of Ambig oNC subjects, suggesting that this categorization was not merely an artifact of the employed classification approach. Furthermore, ambiguously elevated values were consistently more prevalent than analogous decreases and present in regions known to show amyloid deposition, suggesting that slightly elevated values do not solely reflect noise. Interestingly, a number of PIB- subjects showed evidence of elevation across the different measures, suggesting that a subset of PIB- subjects may also have elevated Aβ burden. Overall, the

analyses presented in this manuscript, in conjunction with recently published pathological data, suggest a biological relevance of slight PIB elevations in oNCs.

An approach that combines magnitude and extent may be most sensitive

Qualitative comparison across the measures used to quantify PIB reveals that the number of high ROIs has the clearest stepwise progression from young NC to PIB-/Ambig/PIB+ oNC groups and AD, perhaps because the combination of magnitude and extent makes this measure less inherently noisy than the other measures examined. For instance, the maximum ROI approach identified a yNC subject whose value was much higher than all yNC and PIB- oNC subjects, as well as the majority of Ambig oNC subjects (1.44 in the left caudal anterior cingulate). However, the variance in the yNC group was substantially decreased using the total high ROI approach, and this subject's tally fell below all Ambig oNC as well as many PIB- oNC subjects. Therefore, it is possible that multiple ROIs should be considered to reduce noise in PIB classification. On the other hand, a global approach—such as the PIB index approach—may lose sensitivity by averaging too many regions. Overall, it will be necessary to apply these methods to independent cohorts to determine the generalizability of these approaches.

Slight elevations outnumber slight decreases

An obvious possibility is that slight elevations simply reflect noise amongst subjects lacking Aβ deposition. Noise within PIB-PET scans may be caused by bleed-in effects of nonspecific white matter binding, wash-out effects of neighboring cerebrospinal fluid, co-registration errors between MRI-defined ROIs and PIB PET scans, inaccurate labeling of gray matter ROIs, subject motion and errors during PET acquisition/reconstruction. It is difficult to predict how these factors will interact to affect signal, but one possibility is that these factors would simply produce noise without any bias towards higher or lower values. Thus, a higher prevalence of slight increases compared to slight decreases would support the claim that slightly elevated values reflect a biologically relevant signal. To this end, we contrasted the number of instances of slight elevations to the instances of analogous decreases. We excluded PIB+ oNC subjects to focus on the ambiguous signals present in Ambig and PIB- oNC. Across all 3 measures examined (high versus low PIB index values, right versus leftward shift in ROI distributions, and the total number of high versus low ROIs), there were greater numbers of ambiguous elevations compared to analogous reductions. This asymmetry argues that these slight elevations contain a meaningful signal rather than merely reflecting noise in the data.

Spatial distribution of elevated regions follows known pattern of amyloid deposition

It is also possible, however, that the noise in the PIB signal is positively biased towards higher cortical uptake because high white matter binding of the tracer is the predominant factor. Thus, we investigated the spatial pattern of elevated regions amongst oNCs by computing the percentage of subjects with high ROIs for the 68 FreeSurfer regions investigated. These percentages were plotted for the entire oNC group, and also separately for PIB+, Ambig and PIB- oNC subjects. This analysis revealed a pattern consistent with known patterns of amyloid deposition as measured with PIB-PET imaging (Fripp et al., 2008; Mintun et al., 2006) and postmortem staining (Braak and Braak, 1991; Thal et al., 2002). This regional specificity is difficult to explain by elevated white matter binding.

Specifically, elevated PIB across subjects was seen across multiple association cortices, with the highest percentages in medial orbital, dorsolateral prefrontal, and temporoparietal cortices. Within-group examination revealed diffuse elevation in PIB+ oNC, with a more restricted pattern in Ambig oNC subjects. Elevated uptake was even present for a subset of PIB- oNC subjects (dorsolateral prefrontal, medial orbital and temporoparietal cortices), suggesting the presence of amyloid deposition in PIB- oNC subjects. Importantly, the pattern of regional elevation across these 3 levels of PIB uptake resembles the stages of amyloid deposition described by postmortem staining studies (Braak and Braak, 1991; Thal et al., 2002). Specifically, our analysis revealed the greatest vulnerability to Aβ burden in neocortical heteromodal regions (prefrontal and temporoparietal cortices), followed by the cingulate gyrus and medial temporal cortex whereas the least vulnerable cortical regions were unimodal sensory cortices. Overall, concordance between the spatial distribution of elevated PIB in this study and established patterns of Aβ deposition further strengthens the claim that these slight elevations are indicative of Aβ deposition.

Slightly elevated PIB values and postmortem data

Recent research from the Baltimore Longitudinal Study of Aging suggests that slightly elevated PIB indices may correspond to Aβ deposition measured at postmortem examination (Sojkova et al., 2011). The authors describe a series of 6 oNC subjects that underwent both PIB imaging and postmortem examination. Although the PIB values are not directly comparable to the values reported in our study (due to inter-scanner differences, data processing methods, etc), the pattern presented in their research parallels the findings presented in our manuscript. Three cases in the Sojkova series had low to slightly elevated PIB index DVR values (1.01, 1.06 and 1.09; cases B, C and D respectively), as well as postmortem evidence of plaque deposition (all had a CERAD rating of moderate). In contrast, case A had a PIB index of 0.96 and no evidence of plaques at postmortem examination. In addition to reporting global PIB index values, PIB values for 9 ROIs were also examined. Interestingly, the maximum ROI value for the "Aβ -negative" case A was 1.03, whereas the maximum values for "Aβ-ambiguous" cases B-D were 1.16, 1.24, and 1.21 respectively. The PIB profile seen in cases B-D is reminiscent of the Ambig oNC reported in our study. The observation that these 3 ambiguous cases have postmortem confirmation for the presence of amyloid deposition greatly strengthens the argument that slightly elevated PIB values in oNC may reflect a biologically relevant signal.

Future approaches are needed to establish the relevance of ambiguous cases

The results presented in this manuscript are largely descriptive—it is clear that follow up studies are needed to determine whether ambiguously elevated PIB values represent a biologically meaningful signal. Future studies that directly compare PIB to post-mortem measurements of Aβ in slightly elevated cases are of utmost importance in determining the sensitivity of PIB imaging. It is likely that these studies will primarily draw from patient populations with low levels of Aβ since this type of data are extremely difficult to obtain in cognitively normal individuals. Longitudinal PIB-PET imaging in oNCs will also offer insight into the relevance of Ambig cases. For instance, longitudinal examination of regions showing high uptake will reconcile whether these regional elevations reflect noise or meaningful signal. It is also likely that Ambig oNCs are at risk for transitioning to PIB+,

and longitudinal PIB imaging will be able to confirm or refute this speculation. More immediately, it is possible that interpretation of Ambig oNC subjects as PIB- may lead researchers to falsely accept a lack of difference between PIB+ and PIB- oNC. Overall, the potential relevance of these slightly elevated oNC subjects may help guide future studies examining PIB uptake in oNC populations.

Atrophy correction

A limitation in this study is the lack of atrophy correction to PIB-PET data. In previous publications our group has employed a 2-compartmental atrophy correction procedure to PIB data (Mormino et al., 2009; Rabinovici et al., 2010), however we choose to refrain from this procedure for suspicion that some older subjects may have high levels of atrophy without any amyloid deposition (for instance, atrophy may be due to vascular etiologies (Raz et al., 2007)). During an initial analysis of this data we applied atrophy correction to yNC and oNC PIB scans, and found that the majority of oNC subjects were above the yNC PIB index cutoff (data not shown), and have assumed that this result represents overcorrection. Consequently, the lack of atrophy correction in this manuscript may in fact underestimate the prevalence of slightly elevated levels of amyloid in oNC (ie. the signal from amyloid must first overcome the washout effects of atrophy). Interestingly, this point may be applicable to the PIB- AD case presented in this manuscript (PIB index=1.03). Although this PIB index value falls amongst yNC and PIB- oNC values, this subject has cortical atrophy comparable to the 4 oNC subjects with the lowest PIB index values (0.88, 0.93, 0.96 and 0.98). Thus, it is unclear whether this PIB- AD case is truly Aβ negative, or has evidence for elevated uptake compared to "atrophy-matched" PIB- oNC subjects. The strategy of "atrophy matching" cases to assess slight elevations amongst oNC and patients against subjects with high atrophy that are confirmed to be amyloid-free (via postmortem examination, cerebrospinal fluid, etc) may be a promising alternative to traditional atrophy correction techniques. Nevertheless, the lack of atrophy correction in this manuscript is likely to underestimate the quantity of elevated PIB values amongst oNCs.

Conclusions

By applying two distinct cutoff approaches, we indentified 3 groups of oNC subjects with varying levels of PIB uptake. Although the interpretation of this classification scheme is debatable, investigation of Aβ levels in oNCs is of utmost importance in understanding the temporal course of Aβ deposition in AD development, and perhaps will afford an ideal window in which anti-Aβ treatments may be most effective (before widespread amyloid deposition has occurred). Overall, the data presented in this manuscript supports the biological relevance of slightly elevated PIB values in oNC subjects, and future studies of aging and preclinical AD will be able to directly test these claims.

References

Aizenstein HJ, Nebes RD, Saxton JA, Price JC, Mathis CA, Tsopelas ND, et al. Frequent amyloid deposition without significant cognitive impairment among the elderly. Arch Neurol 2008; 65: 1509-17.

Alzheimer A. Über eine eigenartige Erkrankung der Hirnrinde. Allg Zeitschr Psychiatr Psychiatr-Gerichtl Med 1907; 109: 146-148.

Andrews-Hanna JR, Reidler JS, Sepulcre J, Poulin R, Buckner RL. Functional-anatomic fractionation of the brain's default network. Neuron 2010; 65: 550-62.

Apostolova LG, Dutton RA, Dinov ID, Hayashi KM, Toga AW, Cummings JL, et al. Conversion of mild cognitive impairment to Alzheimer disease predicted by hippocampal atrophy maps. Arch Neurol 2006; 63: 693-9.

Arnold SE, Hyman BT, Flory J, Damasio AR, Van Hoesen GW. The topographical and neuroanatomical distribution of neurofibrillary tangles and neuritic plaques in the cerebral cortex of patients with Alzheimer's disease. Cereb Cortex 1991; 1: 103-16.

Bacskai BJ, Frosch MP, Freeman SH, Raymond SB, Augustinack JC, Johnson KA, et al. Molecular imaging with Pittsburgh Compound B confirmed at autopsy: a case report. Arch Neurol 2007; 64: 431-4.

Baron RM, Kenny DA. The moderator-mediator variable distinction in social psychological research: conceptual, strategic, and statistical considerations. J Pers Soc Psychol 1986; 51: 1173-82.

Becker JA, Hedden T, Carmasin J, Maye J, Rentz DM, Putcha D, et al. Amyloid-beta associated cortical thinning in clinically normal elderly. Ann Neurol 2011.

Beckmann CF, Smith SM. Probabilistic independent component analysis for functional magnetic resonance imaging. IEEE Trans Med Imaging 2004; 23: 137-52.

Bennett DA, Schneider JA, Arvanitakis Z, Kelly JF, Aggarwal NT, Shah RC, et al. Neuropathology of older persons without cognitive impairment from two community-based studies. Neurology 2006; 66: 1837-44.

Bennett DA, Schneider JA, Wilson RS, Bienias JL, Arnold SE. Neurofibrillary tangles mediate the association of amyloid load with clinical Alzheimer disease and level of cognitive function. Arch Neurol 2004; 61: 378-84.

Bentahir M, Nyabi O, Verhamme J, Tolia A, Horre K, Wiltfang J, et al. Presenilin clinical mutations can affect gamma-secretase activity by different mechanisms. J Neurochem 2006; 96: 732-42.

Blumenfeld RS, Ranganath C. Prefrontal cortex and long-term memory encoding: an integrative review of findings from neuropsychology and neuroimaging. Neuroscientist 2007; 13: 280-91.

Bookheimer SY, Strojwas MH, Cohen MS, Saunders AM, Pericak-Vance MA, Mazziotta JC, et al. Patterns of brain activation in people at risk for Alzheimer's disease. N Engl J Med 2000; 343: 450-6.

Bourgeat P, Chetelat G, Villemagne VL, Fripp J, Raniga P, Pike K, et al. Beta-amyloid burden in the temporal neocortex is related to hippocampal atrophy in elderly subjects without dementia. Neurology 2010; 74: 121-7.

Braak H, Braak E. Neuropathological stageing of Alzheimer-related changes. Acta Neuropathol 1991; 82: 239-59.
Braak H, Braak E. Frequency of stages of Alzheimer-related lesions in different age categories. Neurobiol Aging 1997; 18: 351-7.
Braak H, Del Tredici K. The pathological process underlying Alzheimer's disease in individuals under thirty. Acta Neuropathol 2011; 121: 171-81.
Braskie MN, Landau SM, Wilcox CE, Taylor SD, O'Neil JP, Baker SL, et al. Correlations of striatal dopamine synthesis with default network deactivations during working memory in younger adults. Hum Brain Mapp 2010.
Bredesen DE. Neurodegeneration in Alzheimer's disease: caspases and synaptic element interdependence. Mol Neurodegener 2009; 4: 27.
Brewer JB, Zhao Z, Desmond JE, Glover GH, Gabrieli JD. Making memories: brain activity that predicts how well visual experience will be remembered. Science 1998; 281: 1185-7.
Buckner RL, Andrews-Hanna JR, Schacter DL. The brain's default network: anatomy, function, and relevance to disease. Ann N Y Acad Sci 2008; 1124: 1-38.
Buckner RL, Head D, Parker J, Fotenos AF, Marcus D, Morris JC, et al. A unified approach for morphometric and functional data analysis in young, old, and demented adults using automated atlas-based head size normalization: reliability and validation against manual measurement of total intracranial volume. Neuroimage 2004; 23: 724-38.
Buckner RL, Sepulcre J, Talukdar T, Krienen FM, Liu H, Hedden T, et al. Cortical hubs revealed by intrinsic functional connectivity: mapping, assessment of stability, and relation to Alzheimer's disease. J Neurosci 2009; 29: 1860-73.
Buckner RL, Snyder AZ, Shannon BJ, LaRossa G, Sachs R, Fotenos AF, et al. Molecular, structural, and functional characterization of Alzheimer's disease: evidence for a relationship between default activity, amyloid, and memory. J Neurosci 2005; 25: 7709-17.
Buckner RL, Vincent JL. Unrest at rest: default activity and spontaneous network correlations. Neuroimage 2007; 37: 1091-6; discussion 1097-9.
Burt C, Thomson GH. The factorial analysis of human ability [Bk Rev.]. Br J Educ Psychol 1947; 17: 40-8.
Cabeza R, Anderson ND, Locantore JK, McIntosh AR. Aging gracefully: compensatory brain activity in high-performing older adults. Neuroimage 2002; 17: 1394-402.
Cairns NJ, Ikonomovic MD, Benzinger T, Storandt M, Fagan AM, Shah AR, et al. Absence of Pittsburgh compound B detection of cerebral amyloid beta in a patient with clinical, cognitive, and cerebrospinal fluid markers of Alzheimer disease: a case report. Arch Neurol 2009; 66: 1557-62.
Chetelat G, Villemagne VL, Bourgeat P, Pike KE, Jones G, Ames D, et al. Relationship between atrophy and beta-amyloid deposition in Alzheimer disease. Ann Neurol 2010a; 67: 317-24.
Chetelat G, Villemagne VL, Pike KE, Baron JC, Bourgeat P, Jones G, et al. Larger temporal volume in elderly with high versus low beta-amyloid deposition. Brain 2010b; 133: 3349-58.
Cirrito JR, Yamada KA, Finn MB, Sloviter RS, Bales KR, May PC, et al. Synaptic activity regulates interstitial fluid amyloid-beta levels in vivo. Neuron 2005; 48: 913-22.

Citron M, Oltersdorf T, Haass C, McConlogue L, Hung AY, Seubert P, et al. Mutation of the beta-amyloid precursor protein in familial Alzheimer's disease increases beta-protein production. Nature 1992; 360: 672-4.
D'Esposito M, Zarahn E, Aguirre GK, Rypma B. The effect of normal aging on the coupling of neural activity to the bold hemodynamic response. Neuroimage 1999; 10: 6-14.
Dale AM. Optimal experimental design for event-related fMRI. Hum Brain Mapp 1999; 8: 109-14.
Dale AM, Fischl B, Sereno MI. Cortical surface-based analysis. I. Segmentation and surface reconstruction. Neuroimage 1999; 9: 179-94.
Damoiseaux JS, Beckmann CF, Arigita EJ, Barkhof F, Scheltens P, Stam CJ, et al. Reduced resting-state brain activity in the "default network" in normal aging. Cereb Cortex 2008; 18: 1856-64.
Damoiseaux JS, Rombouts SA, Barkhof F, Scheltens P, Stam CJ, Smith SM, et al. Consistent resting-state networks across healthy subjects. Proc Natl Acad Sci U S A 2006; 103: 13848-53.
Daselaar SM, Prince SE, Cabeza R. When less means more: deactivations during encoding that predict subsequent memory. Neuroimage 2004; 23: 921-7.
Davies CA, Mann DM, Sumpter PQ, Yates PO. A quantitative morphometric analysis of the neuronal and synaptic content of the frontal and temporal cortex in patients with Alzheimer's disease. J Neurol Sci 1987; 78: 151-64.
Davis DG, Schmitt FA, Wekstein DR, Markesbery WR. Alzheimer neuropathologic alterations in aged cognitively normal subjects. J Neuropathol Exp Neurol 1999; 58: 376-88.
de Chastelaine M, Wang TH, Minton B, Muftuler LT, Rugg MD. The Effects of Age, Memory Performance, and Callosal Integrity on the Neural Correlates of Successful Associative Encoding. Cereb Cortex 2011.
de Leon MJ, Convit A, George AE, Golomb J, de Santi S, Tarshish C, et al. In vivo structural studies of the hippocampus in normal aging and in incipient Alzheimer's disease. Ann N Y Acad Sci 1996; 777: 1-13.
de Leon MJ, Convit A, Wolf OT, Tarshish CY, DeSanti S, Rusinek H, et al. Prediction of cognitive decline in normal elderly subjects with 2-[(18)F]fluoro-2-deoxy-D-glucose/poitron-emission tomography (FDG/PET). Proc Natl Acad Sci U S A 2001; 98: 10966-71.
Delis D, Kramer J, Kaplan E, Ober B. California Verbal Learning Test. San Antonio: The Psychological Corporation, 2000.
Desikan RS, Segonne F, Fischl B, Quinn BT, Dickerson BC, Blacker D, et al. An automated labeling system for subdividing the human cerebral cortex on MRI scans into gyral based regions of interest. Neuroimage 2006; 31: 968-80.
Dickerson BC, Bakkour A, Salat DH, Feczko E, Pacheco J, Greve DN, et al. The cortical signature of Alzheimer's disease: regionally specific cortical thinning relates to symptom severity in very mild to mild AD dementia and is detectable in asymptomatic amyloid-positive individuals. Cereb Cortex 2009; 19: 497-510.
Dickerson BC, Salat DH, Greve DN, Chua EF, Rand-Giovannetti E, Rentz DM, et al. Increased hippocampal activation in mild cognitive impairment compared to normal aging and AD. Neurology 2005; 65: 404-11.

Dodart JC, Bales KR, Gannon KS, Greene SJ, DeMattos RB, Mathis C, et al. Immunization reverses memory deficits without reducing brain Abeta burden in Alzheimer's disease model. Nat Neurosci 2002; 5: 452-7.
Driscoll I, Zhou Y, An Y, Sojkova J, Davatzikos C, Kraut MA, et al. Lack of association between (11)C-PiB and longitudinal brain atrophy in non-demented older individuals. Neurobiol Aging 2010.
Duverne S, Motamedinia S, Rugg MD. The relationship between aging, performance, and the neural correlates of successful memory encoding. Cereb Cortex 2009; 19: 733-44.
Eichenbaum H, Yonelinas AP, Ranganath C. The medial temporal lobe and recognition memory. Annu Rev Neurosci 2007; 30: 123-52.
Engler H, Forsberg A, Almkvist O, Blomquist G, Larsson E, Savitcheva I, et al. Two-year follow-up of amyloid deposition in patients with Alzheimer's disease. Brain 2006; 129: 2856-66.
Filippini N, MacIntosh BJ, Hough MG, Goodwin GM, Frisoni GB, Smith SM, et al. Distinct patterns of brain activity in young carriers of the APOE-epsilon4 allele. Proc Natl Acad Sci U S A 2009; 106: 7209-14.
Fischl B, Liu A, Dale AM. Automated manifold surgery: constructing geometrically accurate and topologically correct models of the human cerebral cortex. IEEE Trans Med Imaging 2001; 20: 70-80.
Fischl B, Salat DH, Busa E, Albert M, Dieterich M, Haselgrove C, et al. Whole brain segmentation: automated labeling of neuroanatomical structures in the human brain. Neuron 2002; 33: 341-55.
Forsberg A, Engler H, Almkvist O, Blomquist G, Hagman G, Wall A, et al. PET imaging of amyloid deposition in patients with mild cognitive impairment. Neurobiol Aging 2007.
Foster ER, Campbell MC, Burack MA, Hartlein J, Flores HP, Cairns NJ, et al. Amyloid imaging of Lewy body-associated disorders. Mov Disord 2010; 25: 2516-23.
Fotenos AF, Mintun MA, Snyder AZ, Morris JC, Buckner RL. Brain volume decline in aging: evidence for a relation between socioeconomic status, preclinical Alzheimer disease, and reserve. Arch Neurol 2008; 65: 113-20.
Fox MD, Raichle ME. Spontaneous fluctuations in brain activity observed with functional magnetic resonance imaging. Nat Rev Neurosci 2007; 8: 700-11.
Fox MD, Snyder AZ, Vincent JL, Corbetta M, Van Essen DC, Raichle ME. The human brain is intrinsically organized into dynamic, anticorrelated functional networks. Proc Natl Acad Sci U S A 2005; 102: 9673-8.
Fripp J, Bourgeat P, Acosta O, Raniga P, Modat M, Pike KE, et al. Appearance modeling of 11C PiB PET images: characterizing amyloid deposition in Alzheimer's disease, mild cognitive impairment and healthy aging. Neuroimage 2008; 43: 430-9.
Goldman WP, Price JL, Storandt M, Grant EA, McKeel DW, Jr., Rubin EH, et al. Absence of cognitive impairment or decline in preclinical Alzheimer's disease. Neurology 2001; 56: 361-7.
Gould RL, Brown RG, Owen AM, Bullmore ET, Howard RJ. Task-induced deactivations during successful paired associates learning: an effect of age but not Alzheimer's disease. Neuroimage 2006; 31: 818-31.

Grady CL, McIntosh AR, Beig S, Keightley ML, Burian H, Black SE. Evidence from functional neuroimaging of a compensatory prefrontal network in Alzheimer's disease. J Neurosci 2003; 23: 986-93.
Greicius MD, Krasnow B, Reiss AL, Menon V. Functional connectivity in the resting brain: a network analysis of the default mode hypothesis. Proc Natl Acad Sci U S A 2003; 100: 253-8.
Greicius MD, Srivastava G, Reiss AL, Menon V. Default-mode network activity distinguishes Alzheimer's disease from healthy aging: evidence from functional MRI. Proc Natl Acad Sci U S A 2004; 101: 4637-42.
Greicius MD, Supekar K, Menon V, Dougherty RF. Resting-state functional connectivity reflects structural connectivity in the default mode network. Cereb Cortex 2009; 19: 72-8.
Grober E, Hall CB, Lipton RB, Zonderman AB, Resnick SM, Kawas C. Memory impairment, executive dysfunction, and intellectual decline in preclinical Alzheimer's disease. J Int Neuropsychol Soc 2008; 14: 266-78.
Gutchess AH, Welsh RC, Hedden T, Bangert A, Minear M, Liu LL, et al. Aging and the neural correlates of successful picture encoding: frontal activations compensate for decreased medial-temporal activity. J Cogn Neurosci 2005; 17: 84-96.
Hagmann P, Cammoun L, Gigandet X, Meuli R, Honey CJ, Wedeen VJ, et al. Mapping the structural core of human cerebral cortex. PLoS Biol 2008; 6: e159.
Hardy J, Selkoe DJ. The amyloid hypothesis of Alzheimer's disease: progress and problems on the road to therapeutics. Science 2002; 297: 353-6.
Hedden T, Van Dijk KR, Becker JA, Mehta A, Sperling RA, Johnson KA, et al. Disruption of functional connectivity in clinically normal older adults harboring amyloid burden. J Neurosci 2009; 29: 12686-94.
Hulette CM, Welsh-Bohmer KA, Murray MG, Saunders AM, Mash DC, McIntyre LM. Neuropathological and neuropsychological changes in "normal" aging: evidence for preclinical Alzheimer disease in cognitively normal individuals. J Neuropathol Exp Neurol 1998; 57: 1168-74.
Ikonomovic MD, Klunk WE, Abrahamson EE, Mathis CA, Price JC, Tsopelas ND, et al. Post-mortem correlates of in vivo PiB-PET amyloid imaging in a typical case of Alzheimer's disease. Brain 2008; 131: 1630-45.
Jack CR, Jr., Dickson DW, Parisi JE, Xu YC, Cha RH, O'Brien PC, et al. Antemortem MRI findings correlate with hippocampal neuropathology in typical aging and dementia. Neurology 2002; 58: 750-7.
Jack CR, Jr., Knopman DS, Jagust WJ, Shaw LM, Aisen PS, Weiner MW, et al. Hypothetical model of dynamic biomarkers of the Alzheimer's pathological cascade. Lancet Neurol 2010a; 9: 119-28.
Jack CR, Jr., Lowe VJ, Senjem ML, Weigand SD, Kemp BJ, Shiung MM, et al. 11C PiB and structural MRI provide complementary information in imaging of Alzheimer's disease and amnestic mild cognitive impairment. Brain 2008; 131: 665-80.
Jack CR, Jr., Lowe VJ, Weigand SD, Wiste HJ, Senjem ML, Knopman DS, et al. Serial PIB and MRI in normal, mild cognitive impairment and Alzheimer's disease: implications for sequence of pathological events in Alzheimer's disease. Brain 2009; 132: 1355-65.

Jack CR, Jr., Petersen RC, Xu YC, O'Brien PC, Smith GE, Ivnik RJ, et al. Prediction of AD with MRI-based hippocampal volume in mild cognitive impairment. Neurology 1999; 52: 1397-403.
Jack CR, Jr., Wiste HJ, Vemuri P, Weigand SD, Senjem ML, Zeng G, et al. Brain beta-amyloid measures and magnetic resonance imaging atrophy both predict time-to-progression from mild cognitive impairment to Alzheimer's disease. Brain 2010b; 133: 3336-48.
Jicha GA, Parisi JE, Dickson DW, Johnson K, Cha R, Ivnik RJ, et al. Neuropathologic outcome of mild cognitive impairment following progression to clinical dementia. Arch Neurol 2006; 63: 674-81.
Kaplan E, Goodglass H, Weintraub S. Boston Naming Test. Philadelphia: Lea and Febiger, 1983.
Katzman R, Terry R, DeTeresa R, Brown T, Davies P, Fuld P, et al. Clinical, pathological, and neurochemical changes in dementia: a subgroup with preserved mental status and numerous neocortical plaques. Ann Neurol 1988; 23: 138-44.
Kemppainen NM, Aalto S, Karrasch M, Nagren K, Savisto N, Oikonen V, et al. Cognitive reserve hypothesis: Pittsburgh Compound B and fluorodeoxyglucose positron emission tomography in relation to education in mild Alzheimer's disease. Ann Neurol 2008; 63: 112-8.
Kemppainen NM, Aalto S, Wilson IA, Nagren K, Helin S, Bruck A, et al. Voxel-based analysis of PET amyloid ligand [11C]PIB uptake in Alzheimer disease. Neurology 2006; 67: 1575-80.
Killiany RJ, Hyman BT, Gomez-Isla T, Moss MB, Kikinis R, Jolesz F, et al. MRI measures of entorhinal cortex vs hippocampus in preclinical AD. Neurology 2002; 58: 1188-96.
Klunk WE, Engler H, Nordberg A, Wang Y, Blomqvist G, Holt DP, et al. Imaging brain amyloid in Alzheimer's disease with Pittsburgh Compound-B. Ann Neurol 2004; 55: 306-19.
Knopman DS, Parisi JE, Salviati A, Floriach-Robert M, Boeve BF, Ivnik RJ, et al. Neuropathology of cognitively normal elderly. J Neuropathol Exp Neurol 2003; 62: 1087-95.
Kok E, Haikonen S, Luoto T, Huhtala H, Goebeler S, Haapasalo H, et al. Apolipoprotein E-dependent accumulation of Alzheimer disease-related lesions begins in middle age. Ann Neurol 2009; 65: 650-7.
Kramer JH, Jurik J, Sha SJ, Rankin KP, Rosen HJ, Johnson JK, et al. Distinctive neuropsychological patterns in frontotemporal dementia, semantic dementia, and Alzheimer disease. Cogn Behav Neurol 2003; 16: 211-8.
Kukolja J, Thiel CM, Wilms M, Mirzazade S, Fink GR. Ageing-related changes of neural activity associated with spatial contextual memory. Neurobiol Aging 2009; 30: 630-45.
Langbaum JB, Chen K, Lee W, Reschke C, Bandy D, Fleisher AS, et al. Categorical and correlational analyses of baseline fluorodeoxyglucose positron emission tomography images from the Alzheimer's Disease Neuroimaging Initiative (ADNI). Neuroimage 2009; 45: 1107-16.
Langstrom B, Antoni G, Gullberg P, Halldin C, Malmborg P, Nagren K, et al. Synthesis of L- and D-[methyl-11C]methionine. J Nucl Med 1987; 28: 1037-40.

Leinonen V, Alafuzoff I, Aalto S, Suotunen T, Savolainen S, Nagren K, et al. Assessment of beta-amyloid in a frontal cortical brain biopsy specimen and by positron emission tomography with carbon 11-labeled Pittsburgh Compound B. Arch Neurol 2008; 65: 1304-9.
Lezak M. Neuropsychological Assessment. Second ed. New York, Oxford: Oxford University Press, Inc., 1995.
Link JM, Krohn KA, Clark JC. Production of [11C]CH3I by single pass reaction of [11C]CH4 with I2. Nucl Med Biol 1997; 24: 93-7.
Lockhart A, Lamb JR, Osredkar T, Sue LI, Joyce JN, Ye L, et al. PIB is a non-specific imaging marker of amyloid-beta (Abeta) peptide-related cerebral amyloidosis. Brain 2007; 130: 2607-15.
Logan J, Fowler JS, Volkow ND, Wang GJ, Ding YS, Alexoff DL. Distribution volume ratios without blood sampling from graphical analysis of PET data. J Cereb Blood Flow Metab 1996; 16: 834-40.
Lott IT, Head E, Doran E, Busciglio J. Beta-amyloid, oxidative stress and down syndrome. Curr Alzheimer Res 2006; 3: 521-8.
Lustig C, Snyder AZ, Bhakta M, O'Brien KC, McAvoy M, Raichle ME, et al. Functional deactivations: change with age and dementia of the Alzheimer type. Proc Natl Acad Sci U S A 2003; 100: 14504-9.
Mathalon DH, Sullivan EV, Rawles JM, Pfefferbaum A. Correction for head size in brain-imaging measurements. Psychiatry Res 1993; 50: 121-39.
Mathis CA, Wang Y, Holt DP, Huang GF, Debnath ML, Klunk WE. Synthesis and evaluation of 11C-labeled 6-substituted 2-arylbenzothiazoles as amyloid imaging agents. J Med Chem 2003; 46: 2740-54.
McKhann G, Drachman D, Folstein M, Katzman R, Price D, Stadlan EM. Clinical diagnosis of Alzheimer's disease: report of the NINCDS-ADRDA Work Group under the auspices of Department of Health and Human Services Task Force on Alzheimer's Disease. Neurology 1984; 34: 939-44.
Meltzer CC, Kinahan PE, Greer PJ, Nichols TE, Comtat C, Cantwell MN, et al. Comparative evaluation of MR-based partial-volume correction schemes for PET. J Nucl Med 1999; 40: 2053-65.
Meyer-Luehmann M, Spires-Jones TL, Prada C, Garcia-Alloza M, de Calignon A, Rozkalne A, et al. Rapid appearance and local toxicity of amyloid-beta plaques in a mouse model of Alzheimer's disease. Nature 2008; 451: 720-4.
Miller SL, Celone K, DePeau K, Diamond E, Dickerson BC, Rentz D, et al. Age-related memory impairment associated with loss of parietal deactivation but preserved hippocampal activation. Proc Natl Acad Sci U S A 2008; 105: 2181-6.
Minoshima S, Giordani B, Berent S, Frey KA, Foster NL, Kuhl DE. Metabolic reduction in the posterior cingulate cortex in very early Alzheimer's disease. Ann Neurol 1997; 42: 85-94.
Mintun MA, Larossa GN, Sheline YI, Dence CS, Lee SY, Mach RH, et al. [11C]PIB in a nondemented population: potential antecedent marker of Alzheimer disease. Neurology 2006; 67: 446-52.
Mirra SS, Heyman A, McKeel D, Sumi SM, Crain BJ, Brownlee LM, et al. The Consortium to Establish a Registry for Alzheimer's Disease (CERAD). Part II. Standardization of the neuropathologic assessment of Alzheimer's disease. Neurology 1991; 41: 479-86.

Morcom AM, Good CD, Frackowiak RS, Rugg MD. Age effects on the neural correlates of successful memory encoding. Brain 2003; 126: 213-29.
Mormino EC, Kluth JT, Madison CM, Rabinovici GD, Baker SL, Miller BL, et al. Episodic memory loss is related to hippocampal-mediated beta-amyloid deposition in elderly subjects. Brain 2009; 132: 1310-23.
Mormino EC, Smiljic A, Hayenga AO, S HO, Greicius MD, Rabinovici GD, et al. Relationships between Beta-Amyloid and Functional Connectivity in Different Components of the Default Mode Network in Aging. Cereb Cortex 2011.
Morris JC. The Clinical Dementia Rating (CDR): current version and scoring rules. Neurology 1993; 43: 2412-4.
Morris JC, Roe CM, Grant EA, Head D, Storandt M, Goate AM, et al. Pittsburgh Compound B imaging and prediction of progression from cognitive normality to symptomatic Alzheimer disease. Arch Neurol 2009; 66: 1469-75.
Morris JC, Roe CM, Xiong C, Fagan AM, Goate AM, Holtzman DM, et al. APOE predicts amyloid-beta but not tau Alzheimer pathology in cognitively normal aging. Ann Neurol 2010; 67: 122-31.
O'Brien JL, O'Keefe KM, LaViolette PS, DeLuca AN, Blacker D, Dickerson BC, et al. Longitudinal fMRI in elderly reveals loss of hippocampal activation with clinical decline. Neurology 2010; 74: 1969-76.
Oh H, Mormino EC, Madison C, Hayenga A, Smiljic A, Jagust WJ. beta-Amyloid affects frontal and posterior brain networks in normal aging. Neuroimage 2010; 54: 1887-95.
Okello A, Koivunen J, Edison P, Archer HA, Turkheimer FE, Nagren K, et al. Conversion of amyloid positive and negative MCI to AD over 3 years: an 11C-PIB PET study. Neurology 2009; 73: 754-60.
Palop JJ, Chin J, Roberson ED, Wang J, Thwin MT, Bien-Ly N, et al. Aberrant excitatory neuronal activity and compensatory remodeling of inhibitory hippocampal circuits in mouse models of Alzheimer's disease. Neuron 2007; 55: 697-711.
Park DC, Reuter-Lorenz P. The adaptive brain: aging and neurocognitive scaffolding. Annu Rev Psychol 2009; 60: 173-96.
Petrella JR, Prince SE, Wang L, Hellegers C, Doraiswamy PM. Prognostic value of posteromedial cortex deactivation in mild cognitive impairment. PLoS One 2007; 2: e1104.
Pike KE, Savage G, Villemagne VL, Ng S, Moss SA, Maruff P, et al. Beta-amyloid imaging and memory in non-demented individuals: evidence for preclinical Alzheimer's disease. Brain 2007; 130: 2837-44.
Price JC, Klunk WE, Lopresti BJ, Lu X, Hoge JA, Ziolko SK, et al. Kinetic modeling of amyloid binding in humans using PET imaging and Pittsburgh Compound-B. J Cereb Blood Flow Metab 2005; 25: 1528-47.
Price JL, Morris JC. Tangles and plaques in nondemented aging and "preclinical" Alzheimer's disease. Ann Neurol 1999; 45: 358-68.
Qi Z, Wu X, Wang Z, Zhang N, Dong H, Yao L, et al. Impairment and compensation coexist in amnestic MCI default mode network. Neuroimage 2009.
Rabinovici GD, Furst AJ, Alkalay A, Racine CA, O'Neil JP, Janabi M, et al. Increased metabolic vulnerability in early-onset Alzheimer's disease is not related to amyloid burden. Brain 2010; 133: 512-28.

Rabinovici GD, Furst AJ, O'Neil JP, Racine CA, Mormino EC, Baker SL, et al. 11C-PIB PET imaging in Alzheimer disease and frontotemporal lobar degeneration. Neurology 2007; 68: 1205-12.
Rabinovici GD, Jagust WJ. Amyloid imaging in aging and dementia: testing the amyloid hypothesis in vivo. Behav Neurol 2009; 21: 117-28.
Rabinovici GD, Jagust WJ, Furst AJ, Ogar JM, Racine CA, Mormino EC, et al. Abeta amyloid and glucose metabolism in three variants of primary progressive aphasia. Ann Neurol 2008; 64: 388-401.
Raichle ME, Snyder AZ. A default mode of brain function: a brief history of an evolving idea. Neuroimage 2007; 37: 1083-90; discussion 1097-9.
Ranganath C, Heller A, Cohen MX, Brozinsky CJ, Rissman J. Functional connectivity with the hippocampus during successful memory formation. Hippocampus 2005; 15: 997-1005.
Raz N, Rodrigue KM. Differential aging of the brain: patterns, cognitive correlates and modifiers. Neurosci Biobehav Rev 2006; 30: 730-48.
Raz N, Rodrigue KM, Haacke EM. Brain aging and its modifiers: insights from in vivo neuromorphometry and susceptibility weighted imaging. Ann N Y Acad Sci 2007; 1097: 84-93.
Reitan R. Validity of the Trailmaking Test as an indication of organic brain damage. Perceptual and motor skills 1958; 8: 271-276.
Rentz DM, Locascio JJ, Becker JA, Moran EK, Eng E, Buckner RL, et al. Cognition, reserve, and amyloid deposition in normal aging. Ann Neurol 2010; 67: 353-64.
Reuter-Lorenz P. New visions of the aging mind and brain. Trends Cogn Sci 2002; 6: 394.
Riecker A, Grodd W, Klose U, Schulz JB, Groschel K, Erb M, et al. Relation between regional functional MRI activation and vascular reactivity to carbon dioxide during normal aging. J Cereb Blood Flow Metab 2003; 23: 565-73.
Rosen AC, Prull MW, O'Hara R, Race EA, Desmond JE, Glover GH, et al. Variable effects of aging on frontal lobe contributions to memory. Neuroreport 2002; 13: 2425-8.
Rowe CC, Ellis KA, Rimajova M, Bourgeat P, Pike KE, Jones G, et al. Amyloid imaging results from the Australian Imaging, Biomarkers and Lifestyle (AIBL) study of aging. Neurobiol Aging 2010; 31: 1275-83.
Rowe CC, Ng S, Ackermann U, Gong SJ, Pike K, Savage G, et al. Imaging beta-amyloid burden in aging and dementia. Neurology 2007; 68: 1718-25.
Salthouse TA, Babcock RL, Shaw RJ. Effects of adult age on structural and operational capacities in working memory. Psychol Aging 1991; 6: 118-27.
Savva GM, Wharton SB, Ince PG, Forster G, Matthews FE, Brayne C. Age, neuropathology, and dementia. N Engl J Med 2009; 360: 2302-9.
Schmitt FA, Davis DG, Wekstein DR, Smith CD, Ashford JW, Markesbery WR. "Preclinical" AD revisited: neuropathology of cognitively normal older adults. Neurology 2000; 55: 370-6.
Segonne F, Dale AM, Busa E, Glessner M, Salat D, Hahn HK, et al. A hybrid approach to the skull stripping problem in MRI. Neuroimage 2004; 22: 1060-75.
Selkoe DJ. Normal and abnormal biology of the beta-amyloid precursor protein. Annu Rev Neurosci 1994; 17: 489-517.
Shankar GM, Bloodgood BL, Townsend M, Walsh DM, Selkoe DJ, Sabatini BL. Natural oligomers of the Alzheimer amyloid-beta protein induce reversible synapse loss by

modulating an NMDA-type glutamate receptor-dependent signaling pathway. J Neurosci 2007; 27: 2866-75.
Sheline YI, Raichle ME, Snyder AZ, Morris JC, Head D, Wang S, et al. Amyloid Plaques Disrupt Resting State Default Mode Network Connectivity in Cognitively Normal Elderly. Biol Psychiatry 2009.
Small BJ, Fratiglioni L, Viitanen M, Winblad B, Backman L. The course of cognitive impairment in preclinical Alzheimer disease: three- and 6-year follow-up of a population-based sample. Arch Neurol 2000; 57: 839-44.
Small SA, Stern Y, Tang M, Mayeux R. Selective decline in memory function among healthy elderly. Neurology 1999; 52: 1392-6.
Smith CD, Chebrolu H, Wekstein DR, Schmitt FA, Jicha GA, Cooper G, et al. Brain structural alterations before mild cognitive impairment. Neurology 2007; 68: 1268-73.
Sojkova J, Driscoll I, Iacono D, Zhou Y, Codispoti KE, Kraut MA, et al. In Vivo Fibrillar {beta}-Amyloid Detected Using [11C]PiB Positron Emission Tomography and Neuropathologic Assessment in Older Adults. Arch Neurol 2011; 68: 232-40.
Sorg C, Riedl V, Muhlau M, Calhoun VD, Eichele T, Laer L, et al. Selective changes of resting-state networks in individuals at risk for Alzheimer's disease. Proc Natl Acad Sci U S A 2007; 104: 18760-5.
Sperling RA, Laviolette PS, O'Keefe K, O'Brien J, Rentz DM, Pihlajamaki M, et al. Amyloid deposition is associated with impaired default network function in older persons without dementia. Neuron 2009; 63: 178-88.
Spreng RN, Wojtowicz M, Grady CL. Reliable differences in brain activity between young and old adults: a quantitative meta-analysis across multiple cognitive domains. Neurosci Biobehav Rev 2010; 34: 1178-94.
Stern Y. Cognitive reserve and Alzheimer disease. Alzheimer Dis Assoc Disord 2006; 20: S69-74.
Storandt M, Mintun MA, Head D, Morris JC. Cognitive decline and brain volume loss as signatures of cerebral amyloid-beta peptide deposition identified with Pittsburgh compound B: cognitive decline associated with Abeta deposition. Arch Neurol 2009; 66: 1476-81.
Thal DR, Rub U, Orantes M, Braak H. Phases of A beta-deposition in the human brain and its relevance for the development of AD. Neurology 2002; 58: 1791-800.
Thompson PM, Hayashi KM, Dutton RA, Chiang MC, Leow AD, Sowell ER, et al. Tracking Alzheimer's disease. Ann N Y Acad Sci 2007; 1097: 183-214.
Tomlinson BE, Blessed G, Roth M. Observations on the brains of non-demented old people. J Neurol Sci 1968; 7: 331-56.
Trivedi MA, Murphy CM, Goetz C, Shah RC, Gabrieli JD, Whitfield-Gabrieli S, et al. fMRI activation changes during successful episodic memory encoding and recognition in amnestic mild cognitive impairment relative to cognitively healthy older adults. Dement Geriatr Cogn Disord 2008; 26: 123-37.
Vannini P, Hedden T, Becker JA, Sullivan C, Putcha D, Rentz D, et al. Age and amyloid-related alterations in default network habituation to stimulus repetition. Neurobiol Aging 2011.
Villemagne VL, Pike KE, Chetelat G, Ellis KA, Mulligan RS, Bourgeat P, et al. Longitudinal assessment of Abeta and cognition in aging and Alzheimer disease. Ann Neurol 2011; 69: 181-92.

Villemagne VL, Pike KE, Darby D, Maruff P, Savage G, Ng S, et al. Abeta deposits in older non-demented individuals with cognitive decline are indicative of preclinical Alzheimer's disease. Neuropsychologia 2008.
Wagner AD, Koutstaal W, Schacter DL. When encoding yields remembering: insights from event-related neuroimaging. Philos Trans R Soc Lond B Biol Sci 1999; 354: 1307-24.
Wagner AD, Schacter DL, Rotte M, Koutstaal W, Maril A, Dale AM, et al. Building memories: remembering and forgetting of verbal experiences as predicted by brain activity. Science 1998; 281: 1188-91.
Walsh DM, Klyubin I, Fadeeva JV, Cullen WK, Anwyl R, Wolfe MS, et al. Naturally secreted oligomers of amyloid beta protein potently inhibit hippocampal long-term potentiation in vivo. Nature 2002; 416: 535-9.
Walsh DM, Selkoe DJ. A beta oligomers - a decade of discovery. J Neurochem 2007; 101: 1172-84.
Wang L, Zang Y, He Y, Liang M, Zhang X, Tian L, et al. Changes in hippocampal connectivity in the early stages of Alzheimer's disease: evidence from resting state fMRI. Neuroimage 2006; 31: 496-504.
Wechsler D. Wechsler Adult Intelligence Scale-Revised. San Antonio: The Psychological Corporation, 1987a.
Wechsler D. Wechsler Memory Scale-Revised. San Antonio: The Psychological Corporation, 1987b.
Weis S, Leube D, Erb M, Heun R, Grodd W, Kircher T. Functional Neuroanatomy of Sustained Memory Encoding Performance in Healthy Aging and in Alzheimer's Disease. Int J Neurosci 2011.
Wilson AA, Garcia A, Chestakova A, Kung H, Houle S. A rapid one-step radiosynthesis of the beta-amyloid imaging radiotracer N-methyl-[^1^1C]2-(4'-methylaminophenyl)-6-hydroxybenzothiazole ([^1^1C]-6-OH-BTA-1). J Labelled Compounds and Radiopharmaceuticals 2004; 47: 679-682.
Wolk DA, Price JC, Saxton JA, Snitz BE, James JA, Lopez OL, et al. Amyloid imaging in mild cognitive impairment subtypes. Ann Neurol 2009; 65: 557-68.
Zaidi H, Ruest T, Schoenahl F, Montandon ML. Comparative assessment of statistical brain MR image segmentation algorithms and their impact on partial volume correction in PET. Neuroimage 2006; 32: 1591-607.
Zec R. The stroop color-word test: A paradigm for procedural learning. Arch Clin Neuropsychol 1986; 1: 274-275.
Zhou J, Greicius MD, Gennatas ED, Growdon ME, Jang JY, Rabinovici GD, et al. Divergent network connectivity changes in behavioural variant frontotemporal dementia and Alzheimer's disease. Brain 2010; 133: 1352-67.